WILEY

KINETIC PECULIARITIES OF SOLID PHASE REACTIONS

E. Ya. Davydov • A. P. Vorotnikov
G. B. Pariyskii • G. E. Zaikov

INTRODUCTION

Elementary chemical reactions in condensed and gas phases have radical qualitative distinctions. Neighbouring molecules generally do not affect chemical reactions in gases and the reactivity of particles in gas-phase reactions is primarily conditioned by the structure of their electronic shells. The opposite applies in the condensed phase, where the surrounding molecules exert a decisive influence on all chemical reactions ranging from the approach of the reacting particle through the reaction with the medium to the actual chemical transformation. The kinetic regularity depends on how rapidly the local properties, which affect the particle reactivity, are changed. In the general case, the rate constants of the reactions in the condensed phase are the effective functions of some structural-physical parameters which characterize the local molecular organization of the medium at that time. As a result for the simplest monomolecular reaction, an exponential kinetic law is obeyed only when the local properties are changed much faster than the chemical transformation rate. This situation, as a rule, applies to liquids. In the solid phase, however, the time of passage through all feasible states for a reacting particle is much greater than the characteristic time of the chemical reaction. As a consequence of the interference with molecular motion, particles are in states with different reactivity, that is, they are kinetically non-equivalent. Under these conditions, the rate observed depends on how the particles are initially distributed in the solids by kinetic parameters, and how this distribution changes with time. In view of the fact that the elementary reaction rate in the solid phase is determined by the rate constants, the kinetics are often called 'polychronal'. The influence of local structural-physical properties is one reason for the peculiar kind of structural 'memory' connected with the initial distribution of particles in reactivity. In other words, for given experimental conditions, the dependence of the kinetics on the sample preparation as well as the initiation methods, is typical for reactions in solids.

As a rule, simple kinetic laws do not describe the macroscopic concentration changes in solids, and the Arrhenius law for the effective rate constants is not obeyed over a rather wide temperature range. However, kinetic research into processes in the solid phase are of great theoretical and practical interest despite the many factors which prevent analysis of experimental data. It is this research which provides the unique possibility of estimating the physical structure characteristics at the cage level. This is evident from the discovery that kinetic equations of processes exhibit an initial state and a change in the particle distribution density over local conditions, which reflects the structural organization of the medium. For example, kinetic research at low temperatures allows the tunnel effects in reactions to be studied. It is well known that the determination of the tunnelling probability from kinetic data, is acutely sensitive to the solid matrix microstructure [1].

The actual simulation of kinetics in the solid phase, however, presents difficulties. On the one hand, we require the local properties of the matrix to remain unchanged, while on the other, a chemical process might be caused by the physical structure realignment of the nearest surroundings of the reacting particles, or even by their mutual approach. It is obvious, then, why the kinetics of reactions with a distribution of particles over their reactivity has originally been studied using the example of heterogeneous catalytic reactions [2]. The kinetic non-equivalence in these processes is immediately apparent from the non-homogeneity of the catalyst surface, which results from disruptions in the crystal lattice. These disruptions display different catalytic properties, and can change the properties of the surface. The concept of the distribution of particles by their activation energies was first introduced in this work. The mathematical treatment was proposed by Roginskii [2] to describe the kinetics of processes characterized by distribution functions of different analytical forms. The manner in which the distribution of reagents over the kinetic parameters can affect a process was demonstrated as well as how to estimate the distribution form from kinetic data.

More recently, a similar approach has been carried out using the homogeneous processes in solids to describe the kinetics of radiation damage annealing [3,4] and the low-temperature decay of free radicals in γ-irradiated organic substances [5,6]. A large body of research, dealing with the free radical recombination processes in crystals and amorphous substances, as well as in polymers [7], has

revealed their distinctive features, namely, the stepwise form of their kinetic curves. Several hypotheses, providing an explanation for the nature of these common phenomena, were proposed on the basis of the structural organizational peculiarities of solids. The kinetic regularities observed have been associated with structural non-homogeneity, the stabilization of free radicals in pairs for different distances [8], an increased local concentration of radicals in structural defects [9], the chain-heat mechanism of recombination [10,11], and the free volume model [12].

The radical decay in a solid matrix was found to be sufficiently complicated to enable the study of the nature of kinetic non-equivalence, because this process involves the approach of free radicals in addition to cage recombination. For example, the physical diffusion mechanism of macroradicals is difficult to imagine in polymers below the glass temperature. To explain the free valence migration in the solid media, the relay transfer reaction mechanism must be considered [13]. In that case kinetic regularities observed can serve only as indirect evidence of the kinetic non-equivalence occurring in macroscopic homogeneous media.

The immediate proof of these concepts were obtained only when the cage monomolecular reactions were investigated, and when the possibility arose of changing the distribution of the reactivity of particles without a chemical composition change in the reacting systems. The decay of radial pairs at low temperatures in polycrystals, organic glasses and polymers was first considered in some detail as a cage process of this type [14]. Taking into account the small distances between radicals in pairs, one can conclude that kinetic peculiarities of this process are uniquely representative of the structure effect of the surroundings. A large amount of kinetic research has been performed on the other model cage reaction connected with the hydrogen atom abstraction by methyl radicals in frozen organic matrices [1]. It was shown in these works that elementary chemical processes really could take place in conditions of kinetic non-equivalence of particles, when the correlation time over all states with different reactivity is vastly greater than that for the chemical interaction.

For an understanding of the reaction mechanism in the solid phase, kinetic investigations of carbene reactions are of special interest. The distinctive feature of this cage process is a formation of short-living intermediate radical pairs resulting from the hydrogen atom transfer reaction to carbenes [15]. In this connection, the influence of the

surroundings on the carbene conversion can be traced both to the hydrogen atom transfer stage and to the radical pair recombination.

This book is not intended to be an exhaustive treatise of experimental and theoretical data currently accumulated on the kinetics of reactions in the solid phase. Rather, the emphasis is on the consideration of elementary reactions from the viewpoint of existing concepts of the influence of the molecular organization of media on the kinetic features of these processes. The experimental kinetic data obtained can be used in a number of cases to evaluate the structural and molecular dynamic characteristics of the solid state.

References

1. Goldanskii V.I., Trakhtenberg L.I. and Flerov V.N. (1989) *Tunnelling Phenomena in Chemical Physics*. N.Y., L.: Gordon and Breach Science Publ.
2. Roginskii S.Z. (1948) *Adsorption and Catalysis on Inhomogeneous Surfaces*, Moscow: Akademiya Nauk.
3. Waite T.R. (1957) *Phys. Rev.*, **107**, 471.
4. Primack W. (1955) *Phys. Rev.*, **100**, 1677.
5. Mikhailov A.I., Lebedev Ya.S. and Buben N.Ya. (1964) *Kinetika i Kataliz.*, **5**, 1020.
6. Mikhailov A.I., Lebedev Ya.S. and Buben N.Ya. (1965) *Kinetika i Kataliz.*, **6**, 48.
7. Emanuel N.M. and Buchachenko A.L. (1987) *Chemical Physics of Polymer Degradation and Stabilization*, Utrecht: Science Press.
8. Campbell T.D. and Lonney F.D. (1962) *Austr. J. Chem.*, **15**, 642.
9. Cracco F., Ariva A. and Dole M.J. (1962) *Chem. Phys.*, **37**, 2449.
10. Jackson J.L. and Montrol E.W. (1958) *J. Chem. Phys.*, **28**, 1101.
11. Vasil'ev G.K. and Tal'roze V.A. (1963) *Kinetika i Kataliz.*, **4**, 497.
12. Burshtein A.I. (1978) *Uspekhi Khimii.*, **47**, 212.
13. Loy B.R. (1961) *J. Phys. Chem.*, **65**, 58.
14. Yakimchenko O.E. and Lebedev Ya.S. (1978) *Uspekhi Khimii*, **47**, 1018.
15. Platz M.S. (1989) *Acc. Chem. Res.*, **21**, 236.

1 FORMALLY KINETIC DESCRIPTION OF REACTIONS WITH DISPERSION IN REACTIVITY

Contents

The kinetic non-equivalence of reacting particles in the solid phase is one of their general characteristics. However, we now consider the kinetic regularity of 'stepwise' reactions. We need to discover in which cases a spread in the rate constants can be seen and experimentally investigated. In this chapter, we will investigate the various possible methods of describing reactions kinetically.

1.1 Kinetics of reactions with a wide spread in reactivity

Dispersion of reactivity can occur for a number of reasons: the variability of the configuration state of the reacting particles; the structure

of the surroundings; or the different spatial arrangement of the particles. This can cause a slowing in the intra- and intermolecular realignments in the solid phase. An exchange between states with different reactivities can also be retarded. So all reacting systems can be separated into ensembles with different rate constants [1]. The simple kinetic laws are obeyed in the closed region within each ensemble, and concentrations of particles must be added at each moment of time. For the open system, a number of particles with a distinct rate constant are constantly restored, then the rates of conversion in the ensembles are added. Integrating, we obtain for the closed system [1]

$$N(t) = N_0 \int_{k_{\min}}^{k_{\max}} f(kt)\varphi(k)\mathrm{d}k \tag{1.1}$$

and for the open system

$$V(N) = \int_{k_{\min}}^{k_{\max}} V(k, N)\varphi(k)\mathrm{d}k \tag{1.2}$$

where $f(kt)$ is the kinetic function at the given rate constant k, that is, the fraction of particles which had not reacted by the time t, N_0 is the initial concentration of 'distributed' particles, $\varphi(k)\mathrm{d}k \equiv N(k)/N_0$ is the fraction of particles reacting with the definite rate constant ($\int \varphi(k)\mathrm{d}k = 1$), $k_{\min}$ and $k_{\max}$ are border rate constants.

Data available in the literature are concerned only with closed systems. Let us consider a simple method of the stepwise reaction description for the widespread reactivity of particles used in the examination of heterogeneous reactions [2], reactions of the free radical recombination and oxidation in organic glasses and polymers [3–5] and the long lifetime phosphorescence decay [6,7]. Replacing in (1.1) the distribution function $\varphi(k)$ by $\varphi(E) = \varphi(k)\mathrm{d}k/\mathrm{d}E$, where E is the activation energy. Then

$$N(t) = N_0 \int_{E_{\min}}^{E_{\max}} f[k_0 t \exp(-E/RT)]\varphi(E)\mathrm{d}E, \tag{1.3}$$

where $E_{\max}$ and $E_{\min}$ are limiting values of the activation energy. With the variations in E spread over wide limits at a given time, the expression $[k_0 t \exp(-E/RT)]$ changes quickly from $k_0 t \gg 1$ to 0. Also, the share of unreacted species $f(kt)$ for any kinetic law is changed from 0 to 1, during which a 'leap' takes place in the region of $kt = 1$, that is at $E^* = RT \ln(k_0 t)$. This means that integrating (1.3)

can be conducted, in practice, from E^* to E_{max}. It is suggested that the distribution of E is rather widespread, so $E_{min} < E^* < E_{max}$. At $E > E^*$, it is believed that $f(kt) \approx 1$. Then approximately

$$N(t) = N_0 \int_{E^*}^{E_{max}} \varphi(E)\mathrm{d}E \tag{1.4}$$

From (1.4), plotting experimental data in coordinates $N(t)/N_0$, $\ln t$, we can obtain the integral law of distribution in E, and the derivative of $\mathrm{d}N/\mathrm{d}\ln t$ gives $\varphi(E)$ directly. Actually,

$$\frac{\mathrm{d}N}{\mathrm{d}\ln t} = -\varphi(E)\frac{\mathrm{d}E}{\mathrm{d}\ln t} = -RT\varphi(E) \tag{1.5}$$

A typical example of stepwise kinetics is shown in Fig. 1.1 for the decomposition of polymethylmethacrylic acid macroradicals with the main chain breaking [8].

$$\sim CH_2C^{\bullet}(CH_3)CH_2C(CH_3)(COOH)\sim\!\!\rightarrow\sim CH_2C(CH_3)=CH_2+ C^{\bullet}(CH_3)(COOH)CH_2\sim \tag{1.6}$$

It is evident from the figure, that kinetic curves, which in coordinates $N(t)/N_0$, t are tending to some limit, become straightened-out in coordinates $N(t)/N_0$, $\ln t$. In accordance with (1.4) this means that the distribution $\varphi(E)$ is of the right-angled type

$$\varphi(E) = \begin{cases} (E_{max} - E_{min})^{-1} & \text{for} \quad E_{min} \leqslant E \leqslant E_{max} \\ 0 \quad \text{for} \quad E > E_{max}, & E < E_{min} \end{cases} \tag{1.7}$$

Hence the equation for the distribution function of the rate constants is obtained in the form:

$$\begin{aligned} \varphi(k) &= \varphi(E)\frac{\mathrm{d}E}{\mathrm{d}t} \\ \varphi(k) &= [k\ln(k_{max}/k_{max})]^{-1} \end{aligned} \tag{1.8}$$

The fulfilling of (1.6) was observed in the vast majority of experiments when the stepwise kinetics was studied over a reasonable time range [9,10]. This fact can be used as an empirical basis of the distribution for effective reactivity in the form of (1.7) and (1.8).

In order to investigate the temperature dependence of the unreacted particle concentrations during the same time we note that the annealing curves obtained can also define $\varphi(E)$

$$(\mathrm{d}N/\mathrm{d}T)_{t=\mathrm{const}} = -N_0 R\ln(k_0 t)\varphi(E) \tag{1.9}$$

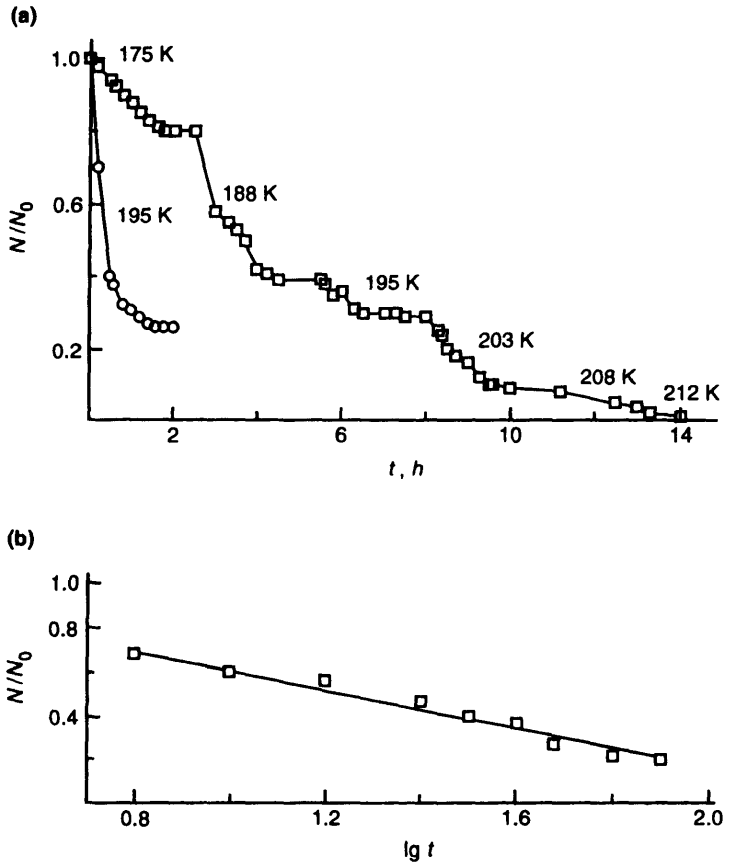

Figure 1.1 The decay kinetics of macroradicals of polymethacrylic acid (a) and its anamorphosis at 195 K (b).

In most cases the experimental dependence (1.9) is close to linear [4,8–10]. The $\varphi(E)$ function can be approximated therefore by the right-angled form, and $\varphi(k)$ is described by (1.8). The deviations observed from (1.9) are due both to the phase and structure transitions in a matrix.

Therefore, step-like kinetics studies allow us to establish the approximate value of $\varphi(k)$. After substitution of (1.7) into (1.1) and (1.2), the kinetic dependency has the value

$$N(t) = N_0[k \ln (k_{max}/k_{min})]^{-1} \int_{k_{min}}^{k_{max}} f(kt)\mathrm{d}k \qquad (1.10)$$

In this case the reaction rate is determined as follows

$$-dN/dt = N_0[t \ln (k_{max}/k_{min})]^{-1}[f(k_{min}t) - f(k_{max}t)] \quad (1.11)$$

From (1.8) one can conveniently consider the kinetic peculiarities of the stepwise reactions. If k_{min} and k_{max} are very different, then the experimental measurements are performed in conditions when $f(k_{max}t) = 0$. In other words, the most active particles react completely in a time compared with the measurement time, and $f(k_{min}t) = 1$, i.e., the most inactive centres still do not react.

The condition $f(k_{max}t) = 0$ is not realized in the initial portion of a kinetic curve, and the condition $f(k_{min}t) = 1$ is not true at $N(t)/N_0 \to 1$. The analysis of kinetic regularities for the right-angled distribution (1.7) was performed in many works [4,8–11]. For a wide enough distribution at $1/k_{max} \leqslant t \leqslant k_{min}$ one can obtain, from (1.4)

$$N(t)/N_0 = (E_{max} - E_{min})^{-1}[E_{max} - RT \ln (k_0 t)] \quad (1.12)$$

On the basis of equation (1.12) the values of $\lg k_0(s^{-1}) = 13.7 \pm 1$, $E_{min} = 13.0 \pm 1$ kcal/mol, $E_{max} = 16.1 \pm 1$ kcal/mol were obtained for the polymethylmethacrylic acid macroradical decomposition (1.6) at low temperatures [8]. From a physical standpoint, these distributions may be caused by various conformational states of macroradicals. Because of this, the macroradical decomposition results from the different initial energetic states, and therefore the energy of the reaction will be variable. Equation (1.10) can be presented as

$$N(t)/N_0 = -\ln (k_{min}t)[\ln (k_{max}/k_{min})]^{-1} \quad (1.13)$$

To explain the origin of right-angled distribution in activation energies (1.7) it should be taken that E includes the local environment reorganization term [1]: $E = E_{chem} + E_{reorg}$. Furthermore, it would appear natural that the nearest environment of the reacting centre can be in different structural states, so that distinct values of E_{reorg} are required in order to create favourable conditions for the reactions. On the other hand, all forms of the cage structure cannot have the same probability. For example, the least E_{reorg} corresponds to the most tolerant configurations of the reacting cage. Therefore, it should be assumed that the correlation between the cage state energy and E_{reorg} is absent in the limits $E_{max} - E_{min}$, and $\varphi(E)$ can be approximated by the right-angled function (1.7).

In a similar manner one can consider the case of the rate constant distribution by pre-exponents [5]. Let $k(\Delta S) = k_0 \exp(-\Delta S/R - E/RT)$, where ΔS is the activation entropy with the distribution $\varphi\Delta S : \Delta S_{min} \ll \Delta S_{max}$. Suppose that E is constant. From the preceding, one can obtain in much the same manner as (1.4)

$$N(t) = N_0 \int_{\Delta S^*}^{\Delta S_{max}} \varphi(\Delta S^*) d\Delta S, \qquad (1.14)$$

where $\Delta S^*/R = -E/RT + \ln k_0 t$.

For the right-angled distribution $\varphi(\Delta S) = (\Delta S_{max} - \Delta S_{min})^{-1}$ we have

$$N(t) = N_0(\Delta S_{max} - \Delta S_{min})^{-1}(\Delta S_{max} + E/RT - \ln k_0 t) \qquad (1.15)$$

By this means, as for (1.12), kinetic curves will be straightened out into coordinates $N(t)/N_0$, $\ln t$. Such independence of the T parameter of the distribution can be realized, for instance, at the spatial hindrances for particles as well as during the tunnel processes of electron transfer [12]. From (1.14) the equation for annealing curves is obtained:

$$dN(t)/dT = N_0(\Delta S_{max} - \Delta S_{min})^{-1} E/RT^2 \qquad (1.16)$$

A comparison of equations (1.12) and (1.14) indicates that the slope of the straight lines depends on the temperature during distribution by the activation energy, and is independent of it for $\varphi(\Delta S)$. This criterion allows the two distributions to be distinguished.

It is worth considering the general case for distribution in the rate constants, when the reacting species differ in both activation energies and pre-exponential factors. The main formula for the kinetic analysis is (1.12). The method covered in reference [13] may be used to determine the distributions in E and k_0. The kinetic curve set obtained at different temperatures is dissected by horizontal lines at different degrees of conversion $\theta(t, T)$, and values of the rate constants $k(\theta, T) = t^{-1}(\theta, T)$, determining the reactivity of given kinetic ensembles, are found. Then the temperature dependencies of $k(\theta, T)$ are plotted in Arrhenius coordinates, and activation energies and pre-exponents are determined for the different kinetic ensembles. The $\theta(E)$ and $\theta(k_0)$ plots are integral functions of the distribution by corresponding parameters. As an example these distributions are shown in Fig. 1.2 for the reaction of biradical formation in clusters of

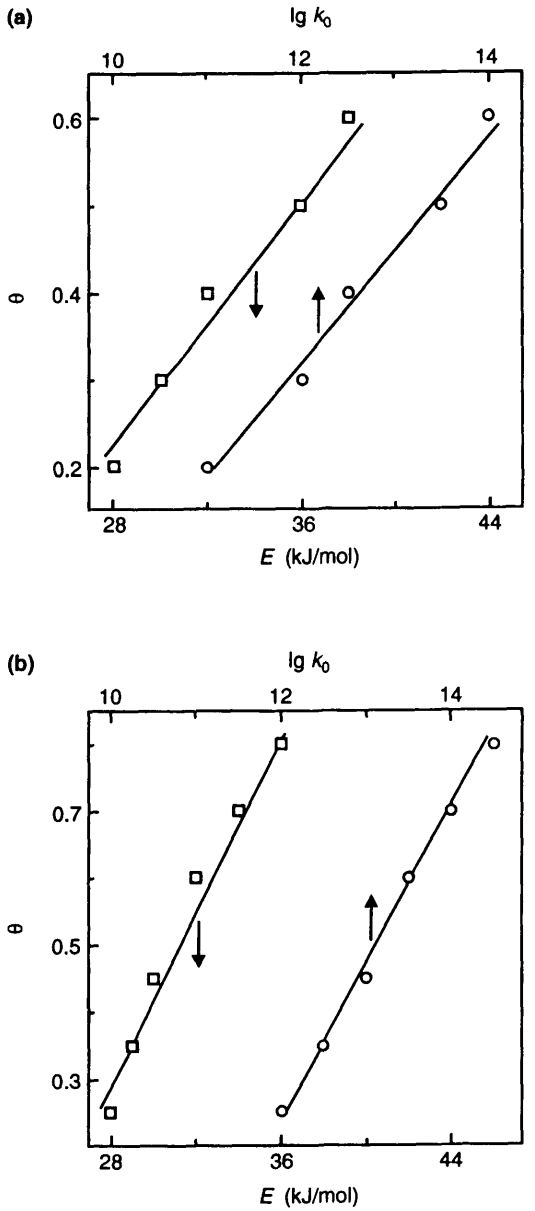

Figure 1.2 Distribution functions of diphenylcarbene by Arrhenius parameters of BR formation in PMMA (a) and PC (b).

triplet diphenylcarbenes at 77–120 K in polymers (PMMA, polycarbonate (PC)) [14,15]:

(1.17)

The plots in Fig. 1.2 are essentially linear and the functions $\varphi(E)$ and $\varphi(\lg k_0)$ may be considered to be of the right-angled type.

1.2 Kinetics of reactions with a narrow spread in reactivity

Previous work has established that the kinetics of the hydrogen atom abstraction by methyl radicals, at low temperatures in solids, is of the non-stationary type [16,17] and can be presented by the equation

$$N(t) = N_0 \exp(-at^{1/2}), \tag{1.18}$$

where a is the parameter depending on the temperature and nature of the matrix. The explanation of this regularity was based on differences in the cage distance between radicals and molecules of the matrix, which result in distinctions in the hydrogen atom transfer probability. Equation (1.17), however, can be used to describe the kinetics of the radical reactions by other mechanisms. In particular, the dissociate decay of XeF and KrF radicals can also be described by this formula [18]. It would appear reasonable that the kinetic law observed is sufficiently common to the solid-phase reactions and is caused by the dispersion of particles in reactivity.

To find the distribution for the rate constants of processes with such kinetics, the following procedure was performed in reference [18]. The experimental law of the concentration change was substituted into equation (1.1). It is expected that the exponential law governs the reaction for equivalence conditions.

$$\exp(-at^{1/2}) = \int_{k_{\min}}^{k_{\max}} \varphi(k) \exp(-kt)\mathrm{d}k \tag{1.19}$$

A related method was used in reference [19]. The kinetic dependence (1.17) is the Laplace transform [20] of the function

$$\varphi(k) = (a/k^{3/2}) \exp(-a^2/4k) \tag{1.20}$$

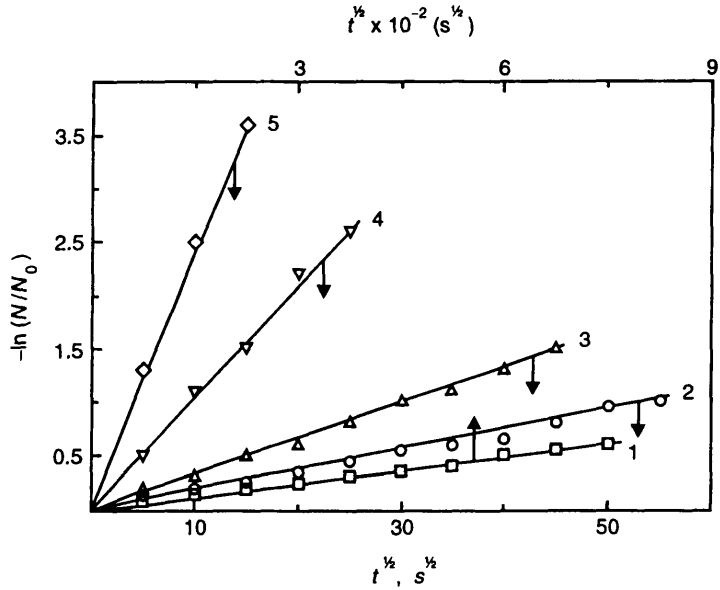

Figure 1.3 Kinetics of CHC decay in PMMA in coordinates of (1.18): (1) 77 K; (2) 113 K; (3) 128 K; (4) 148 K; (5) 161 K.

Next it was assumed that $\varphi(k)$ is a fraction of the wide distribution. We need to ascertain in what conditions the function (1.19) can approximate (1.8). The most probable value of the rate constant in (1.19) corresponds to $k^* = a^2/6$. At $k > 2k^*$ the function (1.8) is practically coincident with (1.19) for the narrow right-angled distribution at $E_{max} - E_{min} \approx 3.3\,RT$ and $k_{min} \approx k^*$. The k_{max} value of the narrow distribution can be found from the initial reaction rates. In this way one can estimate the k_{min} and k_{max} values for a non-wide distribution using the proximity of (1.19) and (1.8).

Approximations of kinetics of the triplet cyclohexadienone carbene (CHC) decay are shown in Fig. 1.3 in coordinates of equation (1.17). This process is associated at low temperatures with the hydrogen atom transfer from the matrix molecules by a simplified scheme [21,22]

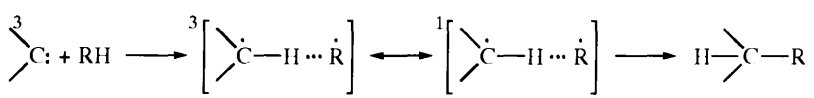

(1.21)

The distribution width in rate constants $[\ln(k_{max}/k_{min})]$ of the CHC decay in PMMA, calculated from experimental data, does not exceed five for the temperature range studied [23]. This fact substantiates the use of the above-mentioned approximation.

1.3 Kinetics of relaxation in the reactivity of particles in solids

The kinetics of chemical reactions in the solid phase are determined both by the distribution of particles in their reactivity, and by relaxation processes. The separate study of these two factors has been possible due to a detection of kinetic non-equivalence in the photochemical reactions. So, the kinetics of the low-temperature decay of diphenylcarbenes by reaction (1.21) in organic glasses depends on the technique of carbene photogeneration [24]. Carbene decay has been investigated at 98 K. It was established that the effective rate constant of the carbene decay decreases regularly after repeated photolysis of frozen samples. If frozen sample photolysis is carried out after prior melting, then the decay rate does not change. The explanation of this phenomenon was made in the context of the carbene reactivity distribution. The successive depletion of the distribution of active particles occurs in the frozen matrix, and this distribution is not restored, owing to the small molecular mobility. In contrast, a total restoration of the initial distribution takes place in melting samples, and the decay rate of carbene is kept constant.

An investigation of the relaxation effect on the reactivity has been carried out in detail with the photo-oxidation of aromatic hydrocarbons (naphthacene, anthracene, and rubrene) in solid polymers [9,24–29]. The mechanism of photo-oxidation includes reactions involving the singlet oxygen [30]. Considering the non-equivalence of oxidized molecules in their reactivity, kinetics can be described by an equation similar to (1.1)

$$N(t) = N_0 \varphi_0(k) e^{-kt} dk, \tag{1.22}$$

where $\varphi_0(k)$ is the distribution function density at the initial instant of time. To investigate the kinetics of relaxation, samples were initially irradiated by light at room temperature for the extent of the conversion P (time t_p). Under these conditions the efficiency of the relaxation processes is negligible. As this takes place, the molecular

distribution has the following density [29]

$$\varphi(k) = \frac{\varphi_0(k)\mathrm{e}^{-kt_p}}{\int \varphi_0(k)\mathrm{e}^{-kt_p}\mathrm{d}k} \tag{1.23}$$

enriched by molecules with a small reactivity compared with the initial one. Subsequently, the system was activated by heating the sample in the dark at the given temperature $T(60^\circ - 80\ ^\circ\mathrm{C})$ for some time η. The new distribution obtained was investigated by a second photo-oxidation for a time τ. The sequence of the distribution changes is presented by the scheme:

$$\varphi_0(k) \xrightarrow{\text{initial photolysis}} \frac{\varphi_0(k)\mathrm{e}^{-kt}P}{\int \varphi_0(k)\mathrm{e}^{-kt}P\,\mathrm{d}k} \xrightarrow{\text{heating}} \varphi(k,\eta,T) \xrightarrow{\text{second photolysis}}$$

$$\rightarrow C(\tau,\eta,T) = \int \varphi(k,\eta,T)\mathrm{e}^{-kt}\mathrm{d}k, \tag{1.24}$$

where $C(\tau,\eta,T)$ is the molecular concentration.

Under this investigation scheme, three processes are separated in time. It has been found that relaxation proceeds most efficiently with a small heating time. Subsequently, retardation of the process is observed. The simplest explanation of this phenomenon lies in the varied equilibrium distributions of the molecules achieved at various T. Suppose that all molecules have an equal probability of changing their reactivity in a unit of time r and acquire a reactivity k with a probability $q(k)$ as a result of this act. Then the kinetics of the relaxation processes can be written as

$$\partial\varphi(k,\eta)/\partial\eta = -r\varphi(k,\eta) + q(k)r\int \varphi(k,\eta)\mathrm{d}k, \tag{1.25}$$

where $\int \varphi(k,\eta)\mathrm{d}k = 1$. In this case, based on the non-equilibrium distribution (1.22), the equation for the relaxation process kinetics may be written as

$$\varphi(k,\eta) = \frac{\varphi_0(k)\mathrm{e}^{-kt_p}}{\int \varphi_0(k)\mathrm{e}^{-kt_p}}\mathrm{e}^{-r\eta} + \varphi_0(k)(1-\mathrm{e}^{-r\eta}) \tag{1.26}$$

The curve set obtained under thermal activation takes the form

$$C(\tau,\eta) = C_n(\tau)\mathrm{e}^{-r\eta} + C_0(\tau)(1-\mathrm{e}^{-r\eta}), \tag{1.27}$$

where $C_n(\tau)$ is the non-activated molecular concentration. The fraction of the non-activated molecules in time η, is determined in

accordance with (1.26) as

$$S(\tau, \eta) = \frac{C(\tau, \eta) - C_0(\tau)}{C_n(\tau) - C_0(\tau)} = e^{-r\eta} \tag{1.28}$$

The relationship $(1 - e^{-r\eta})$ quantitatively defines the degree of relaxation.

Thus, the model of the equivalent particle considered with reference to the relaxation processes, makes it possible to characterize the kinetics accurately by the relaxation timer r^{-1}. But this approach does not permit us to describe the experimental kinetic end of relaxation. The experimental dependence is approximated to the kinetic curve $C_0(\tau)$ much more slowly than is required for equation (1.26). Because of this, consideration must be given to the non-equivalence of molecules in the relaxation processes. For this purpose, all molecules should be broken down into ensembles with the reactivity change probability r. Equations (1.25–1.28) will be considered true for each ensemble. Let $g(r)$ be the fraction of particles with the given value of r, then equations (1.27) and (1.28) can be rewritten as

$$C(\tau, \eta) = C_\eta(\tau) \int e^{-r\eta} g(r) dr + C_0(\tau) \left(1 - \int g(r) e^{-r\eta} dr \right) \tag{1.29}$$

$$S(\tau, \eta) = \int g(r) e^{-r\eta} dr \tag{1.30}$$

By this means the kinetics of the relaxation processes can be characterized by a degree of restoration of the equilibrium distribution $(1 - e^{-r\eta})$. One can also consider the quantitative parameters determining the efficiency and kinetics of the particle relaxation in reactivity. Estimation of the parameters sought was achieved by approximations of the experimental plots of S on η using the following analytical equation [29]

$$S(\tau, \eta) = (1 + nQ_0 \eta)^{-1/n} \tag{1.31}$$

The dependence of (1.30) type encloses a wide category of the monotonically decreasing functions from the exponential at $n \to 0$ to the plots with a kinetic end (1.13) at $n \to \infty$. In this case

$$Q_0 = \left. \frac{\partial S(\tau, \eta)}{\partial \eta} \right|_{\eta=0} = \int r g(r) dr \tag{1.32}$$

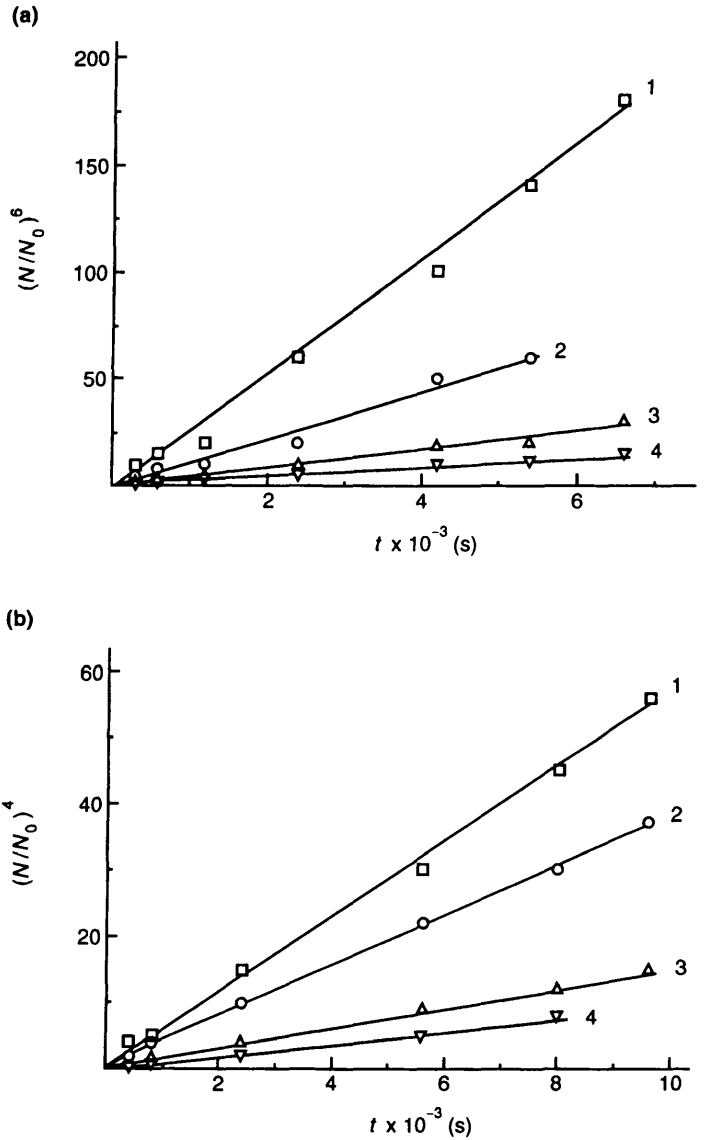

Figure 1.4 The decay kinetics of carbenes in filled PMMA (a) and AC (b) at 100 K in coordinates of (1.31) with: (1) 1; (2) 25; (3) 40; (4) 65% of aerosil.

is the average probability of the molecule reactivity change and can be interpreted as the parameter determining the relaxation process efficiency, whereas, n is a characteristic of the relaxation handicap.

An example of the stepwise kinetic curve treatment in coordinates of (1.31) is shown in Fig. 1.4. In this figure the corresponding anamorphoses are presented for the 2,6-di-t-butylcyclohexadienone carbene decay in PMMA and acetylcellulose (AC) filled by aerosil. Here, the Q_0 parameter means the average effective rate constant $Q_0 \equiv k_{av}$ defined on the basis of the distribution in the effective rate constant $\varphi(k_{eff})$: $k_{av} = \int k_{eff}\,\varphi(k_{eff})\mathrm{d}k_{eff}$, and n is the parameter of this distribution width. As indicated in the figure, k_{av} decreases with an increase in the filler content in polymers, and yet all curves are approximated by the same straight lines irrespective of the filler content, suggesting that the width of the carbene distribution in the decay rate constant is invariable at the given temperature [31].

1.4 On the limits of approximate methods for the description of non-equivalent kinetics

The description of chemical reaction kinetics under conditions of non-equivalence in reactivity requires knowledge of the appropriate distribution density $\varphi(k, T)$ as well as the mechanism and intensity of the relaxation processes which result in the reactivity change. The inverse problem of chemical kinetics consists in the determination of the particle distribution from experimental kinetic dependencies. Generally, the problem of distribution function determination represents a mathematical problem of the inverse Laplace transform [18,19] because the following integral equation needs to be solved (for monomolecular reactions)

$$N(t) = \int_0^\infty \varphi(k)\mathrm{e}^{-kt}\mathrm{d}k \qquad (1.33)$$

The problem of numerical solution (1.33) falls into the category of incorrectly posed problems [32], that is, an error in the $\varphi(k)$ determination can be made as large as required when an error in the left-hand side term of (1.33) approaches zero [33]. This means that we must use extreme care in the $\varphi(k)$ interpretation if the approximation, for example (1.8), is applied to the distribution function. This is true despite the fact that the kinetic dependence, determined by the

Laplace transform, describes the experimental data well. Some further limitations are required for $\varphi(k)$ which provides the solution for a decrease in the error in the left-hand side term of (1.33). In the simplest case, the experimental dependence obtained is extrapolated by a function for which the inverse Laplace transform could be found in analytic form. For example, the aromatic hydrocarbon photo-oxidation in polymers at $T < T_g$ [29] as well as the triplet carbene decay in filled polymers [31] are adequately straightened in coordinates $[N_0/N(t)]^n$, t (Fig. 1.4). The inverse Laplace transform from the function $(1 + \alpha t)^{-1/n}$ gives the distribution of particles in reactivity as follows [33]:

$$\varphi(k) = [\alpha^{1/n}\Gamma(1/n)^{-1}\exp(-k/\alpha)]k^{1/n-1},$$

where Γ is gamma function, $k > 0, n > 0$. If the extrapolating function does not come from experimental error, then one of the possible descriptions of the process is realized. The ambiguity of the description disappears because $\varphi(k)$ is automatically determined by choosing the extrapolating function.

The most often used method of the $\varphi(k)$ determination is a replacement of the integral equation (1.33) kernel by the function $G(k,t)$ [1]. Instead of (1.33), the following equation should be solved

$$N(t) = \int_0^\infty \varphi^*(k)G(k,t)\mathrm{d}k, \tag{1.34}$$

where

$$G(k,t) = \{1 \text{ at } 0 \leqslant kt \leqslant 1, \qquad 0 \text{ at } kt > 1\}.$$

It is believed that $\varphi^*(k)$ and $\varphi(k)$ are close together. This approximation is a better, and more generally true $\varphi(k)$. The solution of (1.33) gives a reasonable approximation for $\varphi(k)$ in the form of (1.8) when a kinetic curve becomes straightened out in coordinates of $N(t)/N_0$, $\ln t$. The distribution $\varphi^*(k)$ is defined in the region of $1/t_2 \leqslant k \leqslant 1/t_1$, where t_1 and t_2 are correspondingly first and final experimental points in the kinetic curve. In this case a fraction of the k values for which we can determine $\varphi^*(k)$ is

$$N(t_1) - N(t_2) = \int_{1/t_2}^{1/t_1} \varphi^*(k)\mathrm{d}k \tag{1.35}$$

In practice, $N(t_1) - N(t_2)$ is commonly ~ 0.5 [11], while the time region (t_1, t_2) can be very significant. This is because the k value fraction, for which $\varphi^*(k)$ is unknown, is quite large. This brings us to the problem of the $\varphi^*(k)$ extrapolation for the essential fraction of k. This problem is also an incorrectly formulated problem. However, if $\varphi^*(k)$ is close to (1.8), then it may be considered as a 'good' approximation for the true particle distribution in a reactivity. The function (1.8) is generally extrapolated to the k value, which is outside the region of $(1/t_2, 1/t_1)$: $k_{\min} > 0$ and $k_{\max} < \infty$ [1]. It is generally believed that condition $k_{\min} t \leqslant 1$ and $k_{\max} t \geqslant 1$ are valid for $t_1 < t < t_2$.

It should be pointed out, however, [33] that the kinetic curve, plotted in coordinates $N(t)/N_0$ versus $\ln t$, has an inflection point. Taking into consideration experimental errors, one can recognize the straight-line portion in the neighbourhood of this point. Its extension will be determined by the magnitude of these errors. In addition, the distribution function (1.8) with a length $(1/t_2, 1/t_1)$ cannot be extended into the remaining region of its definition at insignificant conversion $N(t_1) - N(t_2)$, even with a very significant length of the straight-line portion. This remaining region appears to be excessively wide in this case, and such as extrapolation is basically equal to an arbitrary assumption of the $\varphi(k)$ form. Finally, the values of $k_{\max}$ and $k_{\min}$ appear from condition $\int_0^\infty \varphi^*(k)\mathrm{d}k = 1$; minor changes of $\varphi(k)$ can cause limitless variations in $k_{\max}$ and $k_{\min}$. For example, $k_{\max}$ may be considered as infinity for $\varphi(k) = ak^{-(1+\varepsilon)}$, where $\epsilon > 0$ is reasonably small. A cautionary note is appropriate, therefore, in reference to the $k_{\max}$ and $k_{\min}$ interpretation.

There are some objective limitations for the numerical determination of $\varphi(k)$ because the dependence $N(t)$ is given over a time range $0 - t_2$ and with some error σ. As a consequence, the value of the portion of $\varphi(k)$ with $k < k_1$, where $\int_0^{k_1} \varphi(k)(1 - \mathrm{e}^{-kt_1})\mathrm{d}k = \sigma$, will be uncertain. The portion with $k > k_2$, where $\int_{k_2}^\infty \varphi(k)\mathrm{e}^{-kt_1}\mathrm{d}k = \sigma$, is also a possibility (t_1 is the first point on the experimental curve after 0). The method, using equation (1.33) and replacing the kernel by the $G(k, T)$ function (1.34), is also being used for bimolecular reactions. One can show [33] that this method leads us to the same results, for a reaction of any order, as it does for the monomolecular reactions.

1.5 Possible methods for the description of reactions with distributed kinetic parameters

A large body of reserach into chemical reactions in solids shows the need for a prediction of kinetic behaviour of systems with a wide distribution of parameters under different experimental conditions [34]. This quotation is associated, as noted above, with the solution of the incorrectly formulated mathematical problem [33]. Efforts were made in recent years to devise methods for an approximate solution of these problems with an effective assessment of the solution errors [35–37]. Consider the common principles of kinetic behaviour prediction in experimental conditions. Suppose the availability of some distribution in the activation energy and pre-exponent $\varphi(E, k_0)$ of the rate constant, $k(E, k_0, U)$, where $U = 1000/RT$ is the modified Arrhenius temperature. The description of the reaction kinetics takes the form:

$$N[t, U(j)] = \int_{k_i} \int_{E} \exp\{-k_0 \exp[-EU(j)]t\} \mathrm{d}\varphi(E, k_0), j = 1, \ldots, n, \tag{1.36}$$

where $U(1), \ldots, U(n)$ are the values of experimental conditions (e.g., temperature). The independence of $\varphi(E, k_0)$ on temperature suggests that the Arrhenius law is applicable for the particle ensembles with located kinetic parameters, and that the interaction of media and particles is not changed by a variation in temperature. This generalized Arrhenius law under given experimental conditions, is obeyed only in the case when equation (1.36) has a solution for $\varphi(E, k_0)$ in the considered temperature region. Thus we can assert that experiment confirms the adequacy of a kinetic description by equation (1.36).

Formulation of the problem of the predicted kinetic description at a point in time t_{pr} at given temperature U_{pr} assumes the form:

$$N(t_{pr}, U_{pr}) = \int_{k_i} \int_{E} \exp\{-k_0 \exp(-EU_{pr})t_{pr}\} \mathrm{d}\varphi(E, k_0) \tag{1.37}$$

if (1.36) is taken into account, that is

$$N[t(i, j), U(j)] = \int_{k_i} \int_{E} \exp\{-k_0 \exp[-EU(j)]t(i, j)\} \mathrm{d}\varphi(E, k_0) \tag{1.38}$$

$j = 1, \ldots, n$ and $i = 0, 1, \ldots, m$, where $\varphi(E, k_0)$ is an unknown initial state of the reacting system and $t(i,j)$ is an i-instant of time of the measurement at $U(j)$. The problem (1.37) can be solved by two ways. The first one consists in the search for $\varphi(E, k_0)$ on the basis of (1.36) with its subsequent replacement into (1.37). The second way includes creating a computer program in quest of the maximum and minimum values of $N(t_{pr}, U_{pr})$ from (1.37). These extreme values determine the correct interval for a true solution of the prediction problem.

The mathematical problem posed in (1.37), like the $\varphi(E, k_0)$ search from equation (1.36), represents a category of incorrect problems. The new correct methods of solution for the (1.37) type were proposed in references [35] and [36]. These methods provide an accurate method of estimating errors for an approximate solution in similar kinds of problems. It is expected that some reacting particles are involved in the set of parallel processes, each being characterized by the Arrhenius parameters k_0, E. In addition, the number of parallel pathways of the chemical reaction is unknown, and $\mathrm{d}\varphi(E, k_0) = \varphi(E, k_0)\mathrm{d}k_0\,\mathrm{d}E$ is the unknown density of the reaction pathway probability with parameters E, k_0. In this case the Arrhenius plot of the rate constant is represented as follows:

$$k(\varphi, U) = \int_{k_i} \int_{E} k_0 \exp(-EU)\mathrm{d}\varphi(E, k_0) \tag{1.39}$$

The Arrhenius dependence (1.39) at E and k_0 is not rectilinear. The related violation of the classical temperature dependence in the solid phase reactions has come to be known as the compensation effect (CEF) [38] which was explained by the temperature realignment of the medium structural organization. The model data were designed for the temperature dependence of the rate constant [35]. Rate constants at $T_1 = 373\,K, T_2 = 363\,K, T_3 = 353\,K, T_4 = 343\,K$ are of the form

$$k(j) = k_0 \exp[-E_0 U(j)][1 + D(j)], j = 1, \ldots, 4, \tag{1.40}$$

where $\lg k_0 = 6$, $E_0 = 6\,\mathrm{kcal/mol}$ and $D(j)$ is the experimental error. The computer program solved the problem of the $k(U_{pr}, k_0, E)$ prediction at T_{pr}.

References [35–37] may be considered as a development of formal methods of the kinetic description of solid phase processes. They give the generalized analytic equations of the kinetic non-equivalence, conditioned by the local molecular organization of solids.

References

1. Lebedev Ya.S (1978) *Kinetika i kataliz*, **19**, 1367.
2. Roginskii S.Z. (1949) *Adsorption and catalysis on inhomogeneous surfaces*, Ed. AN SSSR.
3. Mikhailov A.I., Lebedev Ya.S. and Buben N.A. (1964) *Kinetika i Kataliz*, **5**, 1020.
4. Mikhailov A.I., Lebedev Ya.S. and Buben N.A. (1965) *Kinetika i Kataliz*, **6**, 48.
5. Mikhailov A.I., Bol'shakov A.U., Lebedev Ya.S. and Gol'danskii V.I. (1972) *Fizika tverdogo tela.*, **14**, 1172.
6. Primak W. (1955) *Phys. Rev.*, **100**, 1677.
7. Honig J.M. (1954) *J. Chem. Phys.*, **22**, 1689.
8. Davydov E.Ya., Pariyskii G.B. and Toptygin D.Ya. (1977) *Vysocomolek. Soed.*, **A 19**, 977.
9. Karpukhin O.N. (1978) *Uspekhikhimii*, **47**, 1119.
10. Gaponova I.S., Goldberg V.N., Pariyskii G.B., Toptygin D.Ya., and Lebedev Ya.S. (1974) *Izvestiya Acad. Nauk SSSR, ser. Khimich.*, 3533.
11. Radsig V.A. (1976) *Vysocomolek. Soed.*, **A**, 1899.
12. Zamaraev K.I., Khairutdinov R., Mikhailov A.I. and Gol'danskii V.I. (1971) *Doklady Acad. Nauk SSSR*, **199**, 640.
13. Kuzina S.N. and Mikhailov A.I. (1976) *Doklady Acad. Nauk SSSR*, **231**, 1160.
14. Davydov E.Ya., Vorotnikov A.P. and Pustoshnyi V.P. (1995) *Oxidation Communications*, **18**, 230.
15. Vorotnikov A.P. and Davydov E.Ya. (1991) *Khimich. Fizika*, **10**, 1475.
16. Vyazovkin V.L., Bol'shakov B.V. and Tolkatchev V.A. (1983) *Chem. Phys.*, **75**, 11.
17. Siebrand W. and Wildman T.A. (1986) *Acc. Chem. Res.*, **19**, 238.
18. Yakimchenko O.E. and Degtyarev E.N. (1980) *Khimiya Vysok. Energii.* **14**, 239.
19. Doba T., Ingold K.U. and Siebrand W. (1984) *Chem. Phys. Lett.*, **103**, 399.
20. Abramovitz M. and Stegun I.A. (1994) *Handbook of mathematical functions*, Natl. Bur. St. Washington, p. 1026.
21. Wright B.B. (1985) *Tetrahedron*, **42**, 1517.
22. Platz M.S (1989) *Acc. Chem. Res.*, **21**, 236.
23. Vorotnikov A.P., Davydov E.Ya. and Toptygin D.Ya. (1984) *Vysocomolek. Soed.*, **B26**, 664.
24. Senthilnathan V.P. and Platz M.S. (1980) *J. Am. Chem. Soc.*, **102**, 7637.
25. Anisimov V.M. and Karpukhin O.N. (1973) *Izvestiya Akad. Nauk SSSR, ser. Khimich.*, 1914.
26. Anisimov V.M., Karpukhin O.N. and Mattuchi A.M. (1974) *Doklady Akad. Nauk SSSR*, **214**, 828.

27. Savinov E.N., Anisimov V.M. and Karpukhin O.N. (1977) *Doklady Akad. Nauk SSSR*, **233**, 164.
28. Savinov E.N., Anisimov V.M. and Karpukhin O.N. (1979) *Vysocomolek. Soed.*, **B21**, 834.
29. Mardaleyshvili I.R., Kutyrkin V.A., Karpukhin O.N. and Anisimov V.M. (1984) *Vysocomolek. Soed.*, **B26**, 1513.
30. Young R., Werkly K. and Martin R. J. (1971) *Am. Chem. Soc.*, **93**, 5774.
31. Davydov E.Ya., Vorotnikov A.P. and Toptygin D.Ya. (1989) *Izvestiya Akad. Nauk SSSR, ser. Khimich.*, 2453.
32. Tikhonov A.N. and Arsenin V.Ya. (1979) *Solutions of the Non-Correct Problems*, Moscow, Nauka.
33. Kutyrkin V.A., Mardaleyshvili I.R., Karpukhin O.N. and Anisimov V.M. (1984) *Kinetika i Kataliz*, **25**, 1310.
34. Emanuel N.M. and Buchachenko A.L. (1987) *Chemical Physics of Polymer Degradation and stabilization*, Utrecht. VNU Science Press.
35. Kutyrkin V.A. and Anisimov V.M. (1994) *Khimich. Fizika*, **13**, 97.
36. Kutyrkin V.A. (1995) *Khimich. Fizika*, **14**, 71.
37. Kutyrkin V.A. (1995) *Khimich. Fizika*, **14**, 90.
38. Lebedev Ya.S., Tsvetkov Yu.D. and Voevodskii V.V. (1960) *Kinetika i Kataliz*, **1**, 496.

2 INFLUENCE OF SPACE-ORIENTATION FACTORS ON REACTIVITY IN SOLIDS

Contents

A distinctive feature of chemical reactions in the solid phase is the limited mobility of the particles participating in the reaction. To a good approximation, therefore, the solid medium can be considered as a series of 'cages' which include the nearest neighbouring molecules. These cages do not interact with each other and do not possess the usual properties of a reacting system. In fact, all the peculiarities of the solid phase reactions are exhibited in the cages.

The orientations of the reacting particles are acknowledged to be the main controlling factor of the reaction mechanism and kinetics. As a result, the related substances exhibit essential differences in their reactivity. This phenomenon is interpreted from the standpoint of the topochemical postulate [1] whereby the solid phase reactions are

associated with the minimum of molecular motion. This postulate suggests that reactions in solids are controlled by fixed distances and orientations, which are determined in turn by the physical structure of the different media. Reaction takes place when reacting centres are aligned with the reaction coordinate and come within distances of 0.3–0.4 nm [2,3]. Bimolecular reactions take place between neighbouring particles, resulting in the dependence of the product composition on the spatial consistency of the reacting particles in the matrix.

This topochemical concept was confirmed in practice and used successfully in the solid phase photopolymerization of divinyl monomers [4] and phenyldiacryl acid [5]. The relative yields of products in the solid phase reactions are determined by the efficiency of the local environmental rearrangement, due to rotational and translational diffusion. These processes give favourable mutual orientations of reactants [6,7]. Reactions of radical pairs (RP) and triplet carbenes are ideal subjects for investigating the space-orientation factor effects on kinetics.

2.1 Geometry of radical pairs

Radical pairs play an important role in the reactions of different organic substances, such as processes involving the formation of radicals and their recombination and decay. An interest in examining the RP structure and mechanism of reactions had its origins in the possibility of detecting these particles by the ESR technique [8,9].

The ESR spectrum of RPs is defined by the splitting attributed to the dipole–dipole interaction of non-pair electrons [10]. In the general case the splitting value depends on the distance r between non-pair electrons and the angle θ between the magnetic field direction and a vector connecting non-pair electrons:

$$D = 3g\beta(1 - 3\cos^2\theta)/2r^3 \tag{2.1}$$

The ESR spectra constitute a two-signal superposition. In this case the spectrum splittings $D_\perp$ and $D_\parallel = 2D_\perp$ are determined only by the magnitude of the average distance:

$$D_\perp = 3g\beta/2r_{\text{av}}^3 \tag{2.2}$$

As an illustration, the RP spectrum, obtained by the low-temperature (77 K) photolysis of diphenyldiazomethane in polypiperylene [12],

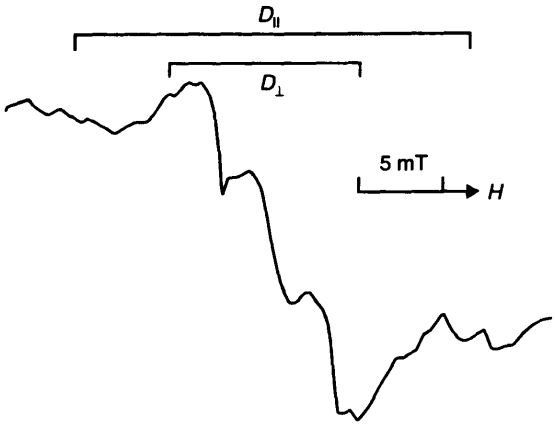

Figure 2.1 ESR spectrum of radical pairs in polypiperylene with diphenyldiazomethane irradiated by light with $\lambda \geqslant 500$ nm at 77 K.

is shown in Fig. 2.1. This RP incorporates allylic macroradicals $\sim CH_2CH = CH\,^{\bullet}C(CH_3)CH_2 \sim$ and diphenylmethyl radicals $Ph_2\,^{\bullet}CH$ resulting from the hydrogen atom transfer to diphenylcarbene from allylic C–H bonds of macromolecules. The average distance in such RPs, defined by formula (2.2), is 0.52 nm.

Two RP with $r_{av} = 0.54$ nm and 0.63 nm were detected during photoreduction of space-hindered 3,6-di-tert-butyl-o-benzoquinone and 2,4,6-tri-tert-butylphenol in vaseline at 77 K [13,14]. The effects of the different radiofrequency power were used in these works to separate individual signals from a combined spectrum. A concurrent formation of the two types of RPs was explained by the initial existence of the phenol and quinone sandwich complexes of two configurations, which are rigidly fixed in the glassed solution. The radical pairs of phenoxy and oxiphenoxy radicals arise as a result of the hydrogen atom transfer. The spectral detection of RPs, differing in the electronic structure of oxiphenoxy radicals, resulted in an accurate knowledge of the mechanism of H atom transfer in cages.

2.2. Kinetics of the formation and decay of radical pairs

In most cases RPs are formed by low-temperature photolysis and γ-irradiation of frozen solutions or polymers. RPs resulting during radiolysis are generally stable at the initiation temperature, and one

can study their recombination, substitution and rearrangement processes by annealing. RPs resulting from photolysis recombine predominantly in cages, and the simplified reaction scheme appears as follows [15]

$$M \xrightarrow{k_0} [R_1 \cdots R_2] \begin{array}{l} \xrightarrow{k_2} R_1 + R_2 \\ \xrightarrow{k_1} M' \end{array} \tag{2.3}$$

A kinetic study of the RP formation under photodecomposition of unstable compounds is useful for understanding the initiation mechanism in solids. These experiments were performed on AIBN [16,17], azobis-2-phenyl-3-methylbutane [18], tetraphenylhydrazine [19,20] and acyl peroxides [21]. The ESR spectra of RPs can be observed at low temperatures (77–100 K) in crystal substances and frozen solutions.

The distance change in RPs was immediately observed by ESR in the course of the photolysis of *o*-quinone and diphenylanilin in chlorbenzene [22]. The average distance changes from 0.62 nm in the initial stage to 0.64 nm. Consequently, molecular complexes from which RPs are formed under the action of light, are kinetically non-equivalent and differed in geometric size. Based on (2.3), the RP formation kinetics at the initial concentration of complexes C_0 can be described by the simple equation

$$C = C_0 k_1 \{1 - \exp[-(k_1 + k_2)\tau]\}/(k_1 + k_2), \tag{2.4}$$

where k_1 and k_2 are respectively the RP formation and decay rate constants. At the same time, the r_{av} change during the RP photogeneration suggests that (2.4) should be averaged by the distribution function $\varphi(k)$:

$$\tilde{C} = \int_{k_{min}}^{k_{max}} C(k\tau)\varphi(k)\mathrm{d}k \tag{2.5}$$

The distribution in k_1 may be neglected when $k_2 \gg k_1$. Based on the $\varphi(k)$ approximation (1.8), one can obtain

$$\tilde{C} = [k_1 C_0/\ln(k_{2max}/k_{2min})] \cdot \int_{k_{2min}}^{k_{2max}} k_2^{-2}[1 - \exp(-k_2\tau)]\mathrm{d}k_2 \tag{2.6}$$

The marked dispersion of the rate constants was observed at the RP annealing [22] which is supported by the stepwise kinetic curves and

the linearization in coordinates $\tilde{C}/C_0$, $\ln \tau$. In accordance with (2.5) and (1.8), it can be shown that

$$C/\tilde{C}_0 = [\ln (k_{max}/k_{min})]^{-1} \int_{k_{min}}^{k_{max}} k^{-1} \exp(-k\tau) dk \qquad (2.7)$$

The approximated equation, by analogy with (1.12), is true for $\ln (k_{max}/k_{min}) \gg 1$, whence E_{max} and E_{min} for the RP decay can be determined. It was shown [23] that $E_{max} - E_{min} \sim \Delta r$ if the rate constant change is due to a dispersion by distances between radicals in RPs. In the case of [22] it was obtained that $\Delta r/r_{av} \approx \Delta E/E \approx 0.3 \pm 0.1$, whereas the initial distance spread is much smaller: $\Delta r/r_{av} \approx 0.03 - 0.06$.

The dispersion in distances is not the only reason for the existence of the rate constant set for the cage reaction. The stepwise kinetics is not accompanied by the D parameter change. This means that the kinetic non-equivalence is due to the structural distinctions of the environment of RPs [24,25]. The kinetics of the RP decay in oriented polyethylene is non-exponential, whereas the average distance is not changed ($r_{av} = 0.53$ nm).

The regularity observed was sequentially traced in experiments with tetraphenylhydrazine. The decay kinetics of RPs, formed by the low-temperature photolysis (77 K) of mono-and polycrystal samples of tetraphenylhydrazine in toluene, has been studied in detail in [26,27]. ESR detected the four kinds of RPs in monocrystals of this compound. These RPs are formed by the decomposition of molecules, variously oriented in the magnetic field. RPs in polycrystals have equivalent magnetic properties, but the kinetics of their decay is characterized by the different rate constants [26]. By this means ESR spectra permit it to recognize the kinetic non-equivalent states of RPs with fixed inter-radial distances.

2.3 Reactions for substitution with participation of radical pairs

The cage migration of free valency is important in radical reactions at low temperatures when the molecular mobility is frozen. Measurements of kinetic constants in the cage reaction of the hydrogen atom were originally accomplished using photochemical conversions of RPs. The rate constants, kinetic isotope effect, direction of the free valency migration and distance of the hydrogen atom transfer were

determined in γ-irradiated dimethylglyoxime and dimethylglyoxime–D_2 from the kinetics of the RP transformation [29]. It was established that the characteristic feature of the migration reactions is their stereospecifity. Another interesting feature is the sensitivity of this reaction to weak molecular interactions. It was found in [29] that the intramolecular hydrogen migration takes place at low temperatures (77–120 K) by two ways, which are equivalent in direction, distance and radical chemical structure. This is because the iminoxyl radicals of RP are capable of hydrogen bond formation with the surrounding molecules or to one another. Dynamic equilibrium between two positions of active centres is observed when such interactions are unavailable. This equilibrium state exists at high temperatures (270–320 K). The hydrogen atom in this case is probably localized in two positions, resulting in the appearance of two ESR spectra by analogy with the hydrogen atom transfer in the o-quinone-phenol complex [22,28].

Free valence migration was noted in the dimethylglyoxime γ-irradiated crystals under the action of UV light at 77 K [30]. This process, connected with RP conversions of the RPs occurs, however, unstereospecifically and concurrently in several directions. In this case light irradiation results in electronic excitation of radicals which react either with neighbouring molecules or recombine.

2.4 Influence of spatial orientations on carbene chemistry

Skell's postulates [31,32] suppose that the carbene reactivity is determined by the spin state. The singlet carbene can be inserted into ordinary chemical bonds by the one-step process. The spin retention rule for triplet carbene forbids the one-step interaction. The reaction of triplet carbenes with C–H bonds results in an RP formation that can recombine by conversion in the singlet state (1.21). If the carbene ground state is a triplet, the composition of the carbene reaction products will be governed by the ratio of the rates of the carbene intersystem crossing into the ground state and the reaction in the excited singlet state. In this case, the equilibrium population of the carbene spin states, determined from the energy of the singlet-triplet splitting ΔE, is also of considerable importance [33]. Transition to the glass matrices by a decrease in temperature must also be of assistance in the carbene relaxation from the excited singlet to the ground triplet state. In addition, the phase state change can radically alter the

effectiveness of the carbene conversion by the singlet and triplet mechanisms.

The works of Tomioka and co-workers best demonstrate the influence of topochemical factors on the carbene chemistry in solids. The photolysis of the phenylcarbene precursor 2,3-diphenyloxirane in isopropanol at 273 K results predominantly in the formation of benzylisopropyl ester and some quantity products of the phenylcarbene insertion into C–H bonds [34]. The insertion products are identical with those obtained from another carbene precursor—phenyldiazomethane. A substantial increase in the yield of the carbene insertion products into C–H bonds was observed during photolysis at 77 K. Under these conditions the selectivity of the insertion into different C–H bonds of isopropanol is sensitive to the nature of the carbene precursor: phenylcarbenes generated from oxiranes show higher selectivity than those from phenyldiazomethane. A similar dependence of the insertion reaction selectivity on the carbene precursor has been seen in the 2,2-dimethylbutane matrix at 77 K while this characteristic is independent of the precursor nature in the liquid phase [35,36]. The dependence of the reaction selectivity on the carbene source structure is inherent for diphenylcarbenes in solids [37].

It must be exphasized that the triplet arylcarbenes, generated in organic matrices at 77 K from different precursors, have no differences in their ESR spectra [38], suggesting that they are identical in configuration in spite of the different reactivity. The spatial-configurational compatibility between the carbene precursors and the matrix molecules of relative sizes is responsible for differences in the product yield. The concept of configurational compatibility in the solid phase also extends to the intramolecular carbene reactions. A sharp decrease in the 3-phenylhydrazo-benzofurane yield from 99% to 60% occurs in cyclohexane for the alcoxy diphenylcarbene intramolecular reaction at 77 K by comparison with liquid solutions [39,40].

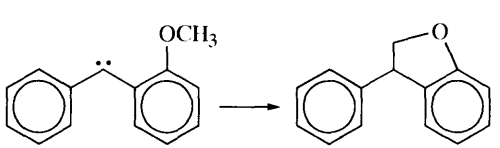

(2.8)

The rotational isomerization of alcoxy groups occurs effectively in singlet carbenes with trans-configuration of the substitute, generated by photolysis in liquid solution, and the favourable orientation arises

in the C–H bond of the substitute for the intramolecular reaction of insertion. The rotational isomerization process, however, becomes slower in the solid matrix at low temperatures, resulting in the decreasing of the indicated product yield. As this takes place, the yield of the intermolecular reaction product grows from 1–40%, when triplet carbenes react with the matrix by the abstraction–recombination mechanism (1.21).

One can trace the matrix effect on the typical monomolecular process in solids using the example of the carbene intramolecular rearrangement. Irradiation of 1,2-diphenyl-1-diazopropane by UV light in methylcyclohexane leads to formation of the three products in much the same proportions at room temperature [41].

$$\begin{aligned} \mathrm{PhC(=N_2)CH(CH_3)Ph} &\xrightarrow[-N_2]{kv} \mathrm{PhCH{=}CPh(CH_3)} \\ &+ \mathrm{PhCH{=}C(CH_3)Ph} + \mathrm{Ph_2C{=}CH(CH_3)} \end{aligned} \tag{2.9}$$

As the temperature decreases, the yield of the phenyl migration product increases as long as a solution in kept liquid (81% at 163 K). When a solution is frozen, the yield of this product is suppressed (2% at 77 K). The predominance of the phenyl group migration over the hydrogen atom migration with decreasing temperature suggests that the activation energy of the hydrogen 1,2-migration is greater than the corresponding parameter for the phenyl migration. It seems likely that this effect is related to a difference in the rehybridization energy of the carbon atom from sp^3 to sp^2, which must occur with the valent angle change. Migration of the hydrogen atom requires relaxation of a larger volume of CH_3 and Ph groups. This requirement gives rise to the relaxation process delay relative to the hydrogen atom migration at sufficiently low temperatures ($\sim$ 163 K) even in the liquid solution. In turn, this delay can result in a situation where the hydrogen migration process has a higher activation barrier as against the phenyl migration. The depression of Ph migration, caused by the solution freezing in spite of an increase in energy, is due to the molecular motion being strongly inhibited and to the dense packing of the environment when the volume phenyl group migration over the distance of the C–C bond becomes unfeasible. Migration of the small size hydrogen atom is significant even at 77 K. By this means the phase-state influence on the molecular relaxation and the effectiveness of the concurrent spatial transfer of atoms and functional groups

determines the composition of the carbene intramolecular rearrangement.

2.5 Space-orientation effects in kinetics of low-temperature decay of carbenes

Investigations of the carbene chemistry in the solid phase provide a way of explaining the nature of the matrix effect on a qualitative level. The determination of the quantitative characteristics of the structural-physical influence of the medium is possible on the basis of kinetic research into carbene reactions with their surrounding molecules. The characteristic peculiarity of these reactions, connected with the hydrogen atom transfer in cages, is the kinetic inequivalence of the particles. This, in addition to the deviation from the first-order law, is strikingly illustrated by the dependence of the carbene decay rate on the duration of the photogeneration stage [42,43]. The kinetics of the diphenylcarbene and diphenylmethylene decay has been studied in propanol at 77 K after a prior photolysis of samples. When the sample had been exposed at 98 K for some time the irradiation was repeated. These operations were conducted many times. In this case the effective rate constant of the carbene decay decreases by 10–15%. The carbene decay at 98 K is characterized by a single rate constant if the samples are irradiated by light at 77 K after prior warming to room temperature. It was found in [42,43] that the effective rate constant of the carbene decay decreases with an increase in the duration of the prior photolysis.

The results of kinetic studies can be explained in the context of structural inhomogeneity of the reaction cages of the matrix. The reactivity of carbenes depends on the located orientations in cages, where each orientation corresponds to the distinct rate constant. In the reacting system the distribution by the rate constants is steadily changed as the disappearance of the most favourable orientations for reaction takes place. Because of the impeding of molecular movements at low temperatures the favourable carbene orientations are not regenerated and the distribution becomes less and less active. The decrease in the rate constant values in relation to the photolysis time, is a consequence of such structural-physical inhomogeneity of the cages. The situation changes profoundly when the frozen solution melts. A total spatial stirring of the carbene precursors occurs as a result of the intense molecular mobility in a liquid, and the initial

carbene distribution in reactivity is re-established at the following stage of photolysis.

Restoration of the reactant distribution by thermoactivation is the common characteristic feature of the solid phase reactions both in organic glasses and polymers, for example, the photo-oxidation of aromatic hydrocarbons [44,45]. The distinctions lay in the temperature region of activation. The special feature of the environmental influence results from a two-step mechanism of the carbene conversion (1.21). In this case the structural peculiarities of cages can have an effect on both the kinetics of the hydrogen atom transfer and the intermediate RP reactions. The dynamics of the steps of one process can be affected by the local surroundings in different ways. Actually, an approach to within 0.3–0.4 nm between the carbene and C–H bond is required for the hydrogen atom transfer. As a result of this step the primary triplet RP is formed, which can recombine only by the singlet state conversion. The frequency of singlet–triplet transforms in RP is 10^8 s^{-1} [46]. Thus the RP spin dynamics is on the same scale as molecular dynamics which is capable of providing transfers and minor movements in the radicals to effect recombination. At the same time, the experimentally determined rate constants of the triplet carbene decay are very small (10^{-3}–10^{-4} s^{-1}) at 77 K in different organic matrices.

It must be emphasized that there are principal differences between the RPs which result in active intermediates during carbene decay and the RPs which are stabilized in organic glasses [26,48–50] and polymers [51,52] and those registered by the characteristic spectra of ESR [8,9]. The first type represent RPs with a lifetime in the cage which is short compared with the spin evolution time. The high recombination rate of such RPs is probably due to two reasons: the small distance between radicals (0.3 nm) and the time delay of the chemical bond rearrangements relative to the hydrogen atom transfer [53]. The RPs of the second type are compared with isolated free radicals by their thermal stability. For them, the distance between radicals is 0.5–0.8 nm. Their formation may be connected with the molecular relaxation of RPs of the first type.

The results of reference [54] can serve as a theoretical basis to account for the controlling influence of spatial orientations on the kinetic inequivalence of carbenes in reactions with C–H bonds. The authors worked out the ideal geometric configuration of the classic transition state corresponding to a minimum potential barrier for the

reaction of triplet methylene with H_2 and CH_4 from the path lying in the methylene plane and lengthwise to the angle HCH bisector. In these conditions the potential barrier for the reaction with H_2 is 103 kJ/mol. The deflection of the migrating hydrogen atom from this path by 20°–40° increases the potential barrier by as much as 110 kJ/mol.

The considerations outlined do not preclude other possible reasons for the kinetic inequivalence of carbenes in solids, specifically associated with the relaxation processes. A matrix is ordinarily regarded as a thermostat with equilibrium properties unchanged in the course of the solid phase reaction. The physical peculiarities of the solid matrix include an excess of the lattice free energy stored, for example, during the glass hardening [55,56]. In general, the slow relaxation processes at low temperatures must be taken into account in descriptions of the solid phase kinetics. Relaxation ensures that the particle orientation is suitable for the reaction [57–59]. The reaction does not take place until this orientation is realized and, consequently, relaxation may be considered to be the controlling process. In this case the concentration dependence on time is described by the following equation.

$$N(t) = N_0 \exp\left(-\int_0^t k(t)\mathrm{d}k\right), \tag{2.10}$$

where $k(t)$ is the time dependent kinetic parameter. The kinetics of the solid phase reaction can be described generally by equations (1.1) or (2.10). They are equivalent, and the $k(t)$ parameter is connected with the distribution $\varphi(k)$ by the following relationship [60]

$$k(t) = \int_0^\infty k\varphi(k)\exp(-kt)\mathrm{d}k \Big/ \int_0^\infty \varphi(k)\exp(-kt)\mathrm{d}k \tag{2.11}$$

Various relations are possible between the rates of the matrix relaxation and the chemical reaction in real conditions. The $N(t)$ measurements, alone, therefore do not permit unambiguous conclusions about kinetic inequivalence [60], because both the rate constant distribution and the matrix relaxation result in the same kinetic dependencies. In this connection, special experiments are required to clarify the reasons for 'polychronal' kinetics in cage reactions. Experiments of this sort have been described in references [61] and [62] referring to kinetics of the low-temperature decay of triplet carbenes in PMMA. The rather narrow distribution in rate constants was observed for cyclohexadienone carbenes (CHC) at 77–160 K:

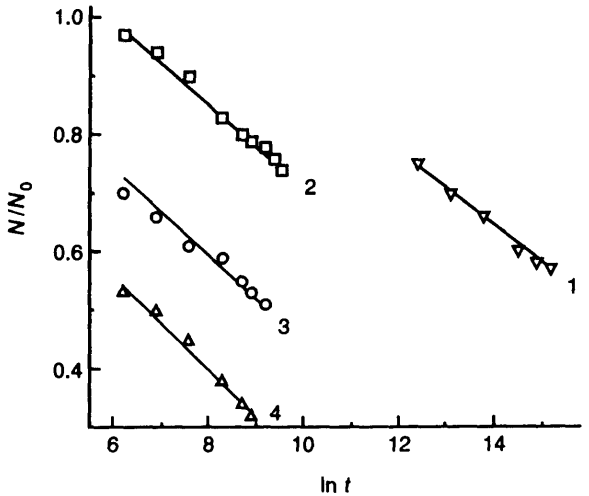

Figure 2.2 Kinetics of TBCHC decay in PMMA at: (1) 77 K; (2) 100 K; (3) 115 K; and (4) 131 K.

$\lg(k_{max}/k_{min}) \leqslant 5$. The carbene decay kinetics we well described by coordinates $N/N_0 - t^{0.5}$ (Fig. 1.3). Other regularities have been noticed in the decay of these carbenes containing tert-butyl substitutes (TBCHC). The kinetic curves are satisfactorily straightened out in the coordinates of equation (1.12) (Fig. 2.2). This result may be attributed to a wider distribution in reactivity for the hydrogen atom abstraction by tert-butyl-substituted carbenes. The rate constant scatter is 2–3 times as large as that for unsubstituted carbenes at the same temperature interval: $\lg(k_{max}/k_{min}) = 9-13$. Most likely tert-butyl groups are responsible for a wide set of mutual arrangements of the carbene centre and C–H bonds of macromolecules, characterized by the respective rate constant.

2.6 Influence of space-orientation factors on the spin and chemical dynamics of radical pairs

The unique information about the kinetic peculiarities of the solid phase reactions with RP involvement is obtainable from the magnetic field effect (MFE) owing to the determination of the cage structural-physical characteristics. The MFE on the kinetics of RP reactions is associated in kinetic models with a change in the intersystem crossing probability [63,64]. This effect is of interest in the elucidation of the

mechanism of radical reactions, along with the structural behaviour of media [65].

The kinetic curves of the TBCHC decay in ethylacetate (EA) and hexaethyldisiloxane (ES) in magnetic fields of different strength are shown in Fig. 2.3 (a,b). Since the highest degree of conversion had not

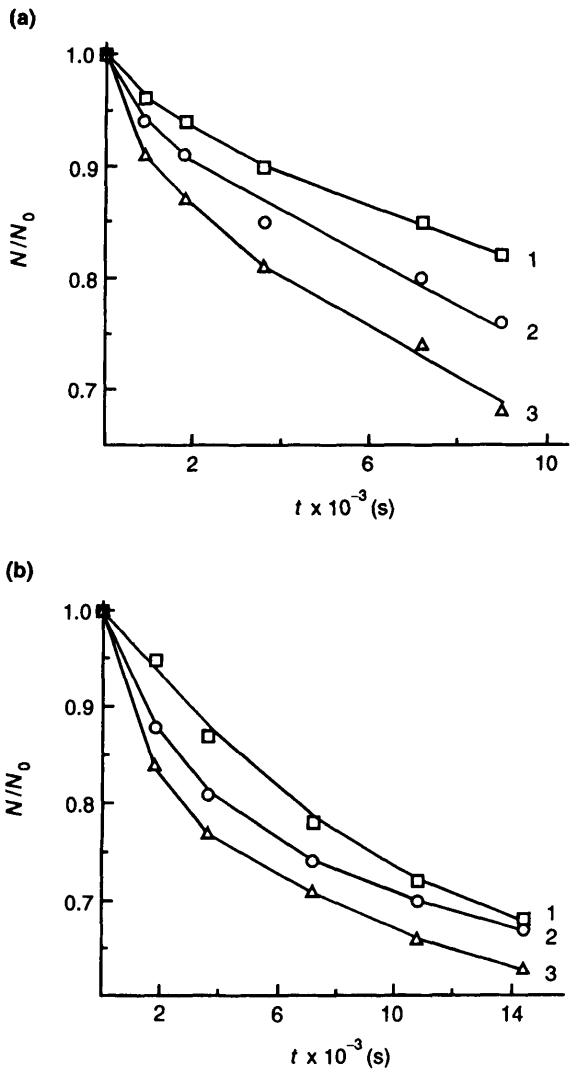

Figure 2.3 Kinetics of TBCHC decay (77 K) at magnetic fields: (1) 0; (2) 300; (3) 160 mT in EA (a) and: (1) 0; (2) 300; (3) 30 mT in ES (b).

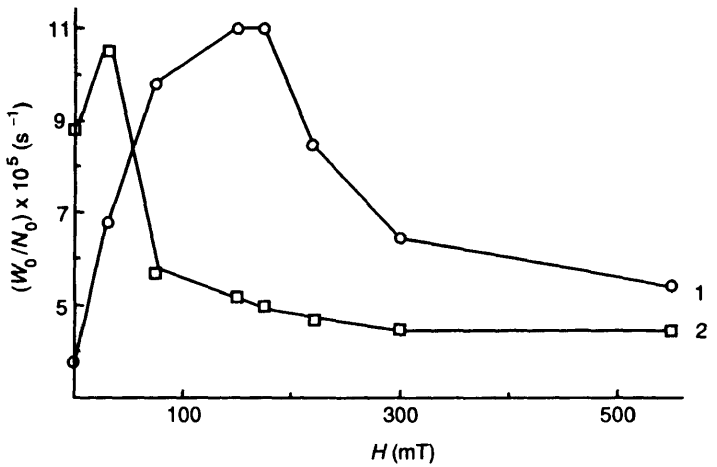

Figure 2.4 Magnetic field effect on TBCHC rate decay (77 K) in (1) EA; and (2) ES.

exceeded 20% at 77 K, the initial rates W_0 were chosen as experimental parameters undergoing the magnetic field influence [66]. The dependencies obtained are given in Fig. 2.4. It is seen that these rates change as a function of the field with maxima in both glasses. The rate is also affected by the magnetic field in solid polymers (Fig. 2.5). In this case magnetic dependencies vary unmonotonically [67]. The abrupt changes, amounting to 40% in PMMA and 50% in acetylcellulose (AC), take place within the ranges of field 200–300 mT.

The fact that MFE on the triplet carbene decay at 77 K results from the hydrogen atom transfer, causes us to conclude that this process is reversible. To explain MFE, the following mechanism can be proposed:

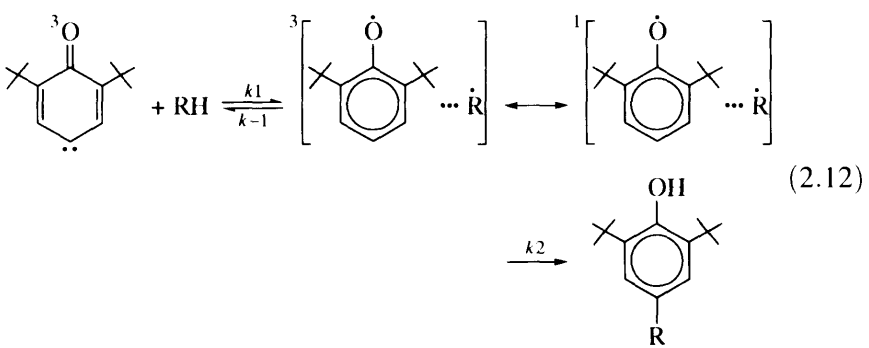

(2.12)

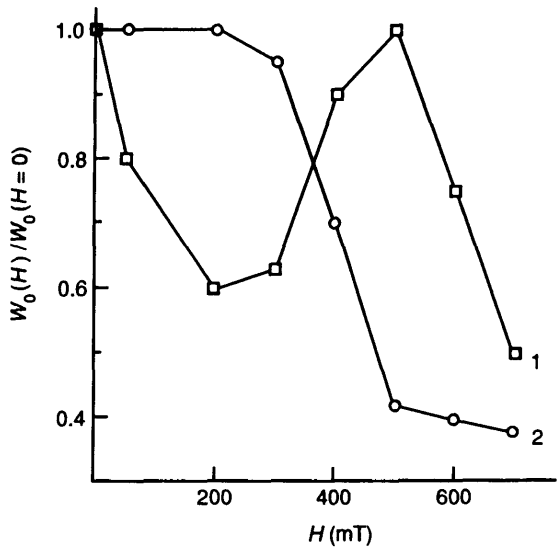

Figure 2.5 Magnetic field effect on TBCHC decay (77 K) in (1) PMMA; and (2) AC.

The triplet RP is formed in the first stage. This RP undergoes singlet–triplet evolution. The RP in the triplet state is converted into original triplet carbene by the back hydrogen atom transfer, but in the singlet state the RP is recombined. The efficiency of recombination is dependent on the relative population of the triplet and singlet levels of RP (P_T/P_S). From (2.12) it follows that the effective rate constant of TBCHC decay in zero field is expressed as

$$k_{ef} = \frac{k_1}{(k_{-1}P_T/k_2P_S) + 1} \tag{2.13}$$

It will be noted that k_{ef} at 77 K is about 10^{-4} s^{-1} whereas the characteristic time of spin dynamics is $\sim 10^{-8}$ s. For MFE initiation, k_2 and k_{-1} should be comparable to the spin evolution frequency. In this connection one can conclude that the limiting step of the low-temperature decay of carbenes is the formation of primary triplet RP. This stage defined by k_1 includes the cage reorganization for favourable mutual orientations of C–H bonds and carbenes to create the tunnel transfer of the hydrogen atom [68]. The slow process of the cage reorganization ($\sim 10^4$ s) seems to be due to the levelling of two potential wells in energy needed to produce forward and back atom

tunnelling. Fluctuations of the polarization forces as a result of the polar group movements can induce changes in the potential well configurations with time. Consequently, the two energy levels are varied and can coincide for a while with the subsequent atom transfer.

The magnetic field splits the triplet level of RP into three sublevels T_0, T_+ and T_- with the result that the probability of the triplet–singlet conversions decrease. In a sufficiently high field, the mixture of T_0 and T_+, T_- by the HFI mechanism [63,64] may be neglected. Then the effective rate constant is averaged over the rate constants of RP arising initially on all T_0, T_+ and T_- levels. Equation (2.13) becomes

$$k_{ef} = k_1 \varphi(H),$$

where

$$\varphi(H) = \frac{1}{3}\left(\frac{1}{(k_{-1}P_{T_+}/k_2P_S) + 1} + \frac{1}{(k_{-1}P_{T_+}/k_2P_S) + 1} + \frac{1}{(k_{-1}P_{T_-}/k_2P_S) + 1}\right) \tag{2.14}$$

In (2.14) the relative populations P_{T+}/P_{T-} and P_{T+}/P_{T-} are functions of the magnetic field. From Figs. 2.4 and 2.5, the plots of MFE observed can be assumed to result from the exchange interactions J of non-pair electrons in intermediate, short-lived RP. The exchange interaction, splitting triplet and singlet levels of RP, can lower the probability of the spin evolution for zero field. Within some interval of magnetic field the mixture of $T-$ and S levels makes it possible to increase abruptly the population of the RP singlet level (Fig. 2.6). As a consequence, the fraction of primary RP disappearing in the triplet state by the back transfer of the H atom with the formation of the starting carbene, is reduced and accordingly the fraction of RP decaying by recombination, is increased. This rate of TBCHC decay builds up to a maximum of the field strength complying with the resonance condition

$$2J = -a/8 + g\beta H/\hbar, \tag{2.15}$$

where a is the effective HFI constant of the RP non-pair electrons.

The question of the J significance in magnetic effects is dealt with in the literature in some detail [64]. It follows, from available data, that MFE with the dependence of the kinetic constants observed in the field strength, can occur under specific conditions. The exchange

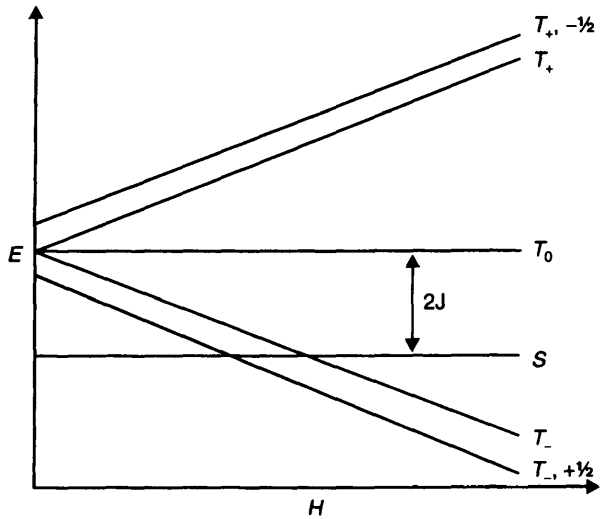

Figure 2.6 Energetic levels of RP (one magnetic nucleus) in magnetic field with strong exchange interaction.

interaction, as a function of distance, usually takes the form of the exponential law [69]

$$J(r) = J_0 \exp(-\alpha r), \tag{2.16}$$

where $J_0 = -0.446 \cdot 10^{19}$ rad/s and $\alpha = 27\,\text{nm}^{-1}$. The average spacing in RP must be consistent with J, exceeding in energy other interactions mixing S and T levels (spin–orbital, dipole–dipole, HFI). The exchange interaction of non-pair electrons does not, as a rule, play an important part in liquid phase reactions. This situation corresponds to a model in which $S-T$ transitions take place, not at the instant of direct contact of the radicals, but at the spacing between their two repeat collisions when the distance between non-pair electrons is reasonably large [63]. The exchange interaction, however, can be essential for spin dynamics. In particular, this is realized in biradicals. The resonance type MFE was first discovered during the cyclic ketone photolysis by the kinetics of the chemically induced dynamic nuclear spin polarization signal [70]. The MFE on the intersystem crossing rate constant of this type was noted for alkylacylbiradicals [71,72]. All dependencies obtained are similar in appearance, and there are grounds for believing that they resulted from a common phenomenon: the T_- and S level mixing at the

specific magnetic field strength. Exchange interactions are evidently of considerable importance not only for biradical reactions when the resonance conditions of S and T_- (or T_+) levels (2.15) can be retained throughout the whole lifetime of the biradicals. The MFE of the resonance type was also shown in some distinctive liquid phase reactions with the participation of RPs: for instance, the dimethylcadmium autooxidation [73]. A clearly defined MFE on the rate of this reaction is derived from the linkage of RP, resulting in an initial reaction with the dimethylcadmium molecule for some time. The strong exchange interaction splitting between the S and T levels of RP arises, in this case, between radicals fixed on a small molecule. The S–T transitions, the efficiency of which determine the probability of the radical exit from cages, are suppressed by J in non-resonance fields. The exit of radicals from RP is maximized in the magnetic field corresponding to (2.15).

From examples outlined in literature, it follows that the resonance MFE with an extreme dependence of the kinetic constants on the external magnetic field strength, may be expected under particular conditions. The average distance between non-pair electrons in RP must accord with the exchange energy which exceeds that of the magnetic interactions mixing S and T levels ($r < 0.8$ nm); the duration of stay for radicals in location of the S, T–level intersection in the magnetic field must be enough for the intersystem crossing modulated by the Zeeman interaction. In all likelihood, the low-temperature decay of triplet carbenes in polymers [67] and organic glasses [66] corresponds to such conditions. RPs are formed in these reactions through the hydrogen atom transfer between the carbon atoms over small distances (~ 0.3 nm), and strong restrictions of the molecular mobility in the solid matrix significantly increase the RP lifetime in distinct conformations.

All points of the experimental plots in Figs. 2.4 and 2.5 were obtained under similiar conditions to when the theory of the RP spin dynamics in high magnetic fields can be used to analyze MFE. It should be pointed out that equation (2.14) was derived assuming that triplet RPs are formed equally probably in T_0, T_+ and T_- without transitions between triplet levels [66]. Consequently, different channels of the singlet–triplet transitions are displayed. The complete analysis of MFE was accomplished for RP with only one magnetic nucleus of spin 1/2. However, approximations can be applied for a more complex case when the RP contains several protons. Then the

root-mean-square constant of MFE with all protons may be introduced into the treatment. It is believed that the hyperfine interaction with two equal protons takes place in RPs which are produced in EA, ES, PMMA and AC during the carbene decay. Then $a = (\sum a_{1k}^2 + \sum a_{2n}^2)^{0.5}$, a_{1k} and a_{2n} are HFI constants.

The Kaptein model [74–76], in which radical distances are fixed, was used to deal with the spin evolution of RP [66,67]. The singlet state populations of RP are deduced by this model as

$$P_{S(T_0)} = \frac{a^2\tau^2/8}{1 + (a^2/4 + 4J^2)\tau^2} \tag{2.17}$$

$$P_{S(T_{+,-})} = \frac{a^2\tau^2/4}{1 + [a^2/2 + (2J + a/4 \pm g\beta H/\hbar)^2]\tau^2}, \tag{2.18}$$

where τ is the lifetime of RP. RP is formed at the initial stage in T_0, T_+ and T_-. The relative populations of the singlet and triplet levels in the magnetic field $P_T/P_S = (1-P_S)/P_S$ are estimated from (2.17) and (2.18).

In all systems studied the HFI effective constants amount to 3–4 mT ($5.2\text{–}6.9 \cdot 10^8$ rad/s). If $\tau \approx 10^{-8}$ s and $a^2\tau \gg 1$ then

$$P_{T_0}/P_S \approx [8(2J)^2/a^2] + 1 \tag{2.19}$$

$$P_{T_{+,-}}/P_S \approx [4(2J + a/4 \pm g\beta H/\hbar)^2/a^2] + 1 \tag{2.20}$$

The dependencies of the probabilities of RP recombination on the magnetic field can be plotted from Equations (2.14, 2.19 and 2.20) [67]. The form of $\varphi(H)$ is determined by J and k_{-1}/k_2 (Fig. 2.7). At J comparable to the effective HFI constants, $\varphi(H)$ decreases steadily to a plateau, and $\varphi(H = 0) \approx 3\varphi(H_\infty)$ in accordance with numbers of the intersystem crossing channels working effectively in zero and high magnetic fields. The magnetic dependence has a maximum at $H = 2J\hbar/g\beta$.

The comparison of estimated plots of Fig. 2.7 with the experimental ones shows that MFE observed in PMMA and AC is approximated by the set of $\varphi(H)$ with different values of J. So the two types of RP can be resolved in PMMA with $J \approx 0$ and $J \approx 4.4 \times 10^{10}$ rad/s. The availability of the five types of RP with J from 0 to 3.5×10^{10} rad/s may be detected for MFE in AC. The cages in low-molecular glasses of EA and ES are more uniform relative to the exchange energies in the RPs. This is evident from the pronounced extreme changes of the

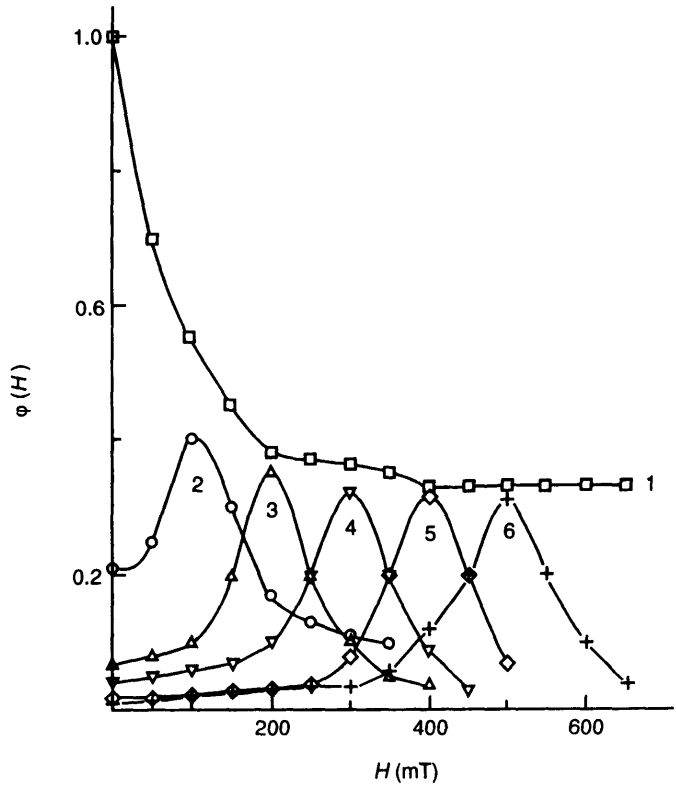

Figure 2.7 Probabilities of the radical pair recombination in magnetic field at : (1) $2J = 0$; (2) 1.7×10^{10}; (3) 3.5×10^{10}; (4) 5.2×10^{10}; (5) 7×10^{10} and (6) 8.8×10^{10} rad/s; $k_{-1}/k_2 = 1.8 \times 10^{-3}$.

reaction rate in the magnetic field. The J values are 1.3×10^{10} rad/s and 2.7×10^{9} rad/s in ES [66]. The estimation of k_{-1}/k_2 in EA and ES gives a value of 3×10^{-3}.

The MFE character found in references [66] and [67] is conditioned by special features of the RP dynamics in the solid phase. It should be mentioned that the influence of factors inessential to liquids is possible in this case. Apart from the exchange interaction, which is of importance in the singlet–triplet evolution at a reasonable lifetime for RPs ($\tau \gg 10^{-9}$ s), one would expect the magnetic dipole–dipole interactions to influence the RP non-pair electrons. These interactions are not averaged in solids on account of the small molecular mobility [77]. The estimation of the dipole–dipole interaction energy in RPs

with inter-radial distances of 0.35–0.4 nm by (2.2) gives the value $D \approx 5 \times 10^9$ rad/s comparable with the exchange energy.

Taking into consideration the unisotropic dipole–dipole interaction, the triplet state energy can be expressed as follows

$$E_{T_0} = 2J + D/3(1-3\cos^2\theta) \tag{2.21}$$

$$E_{T_{\pm}} = 2J - D/6(1-3\cos^2\theta) \pm g\beta H/\hbar, \tag{2.22}$$

where θ is the angle between the magnetic field direction and the RP axis. Then the relative populations of singlet and triplet levels are obtained by integration over all possible orientations of RP

$$\frac{P_{T_0}}{P_S} = \int_0^{\pi/2} \left\{ \frac{8[2J + D/3(1-3\cos^2\theta)]^2}{a^2\hbar^2} + 1 \right\} \sin\theta \mathrm{d}\theta \tag{2.23}$$

$$\frac{P_{T_{\pm}}}{P_S} = \int_0^{\pi/2} \left\{ \frac{8[2J - D/6(1-3\cos^2\theta) \pm g\beta H]^2}{a^2\hbar^2} + 1 \right\} \sin\theta \mathrm{d}\theta \tag{2.24}$$

as a result of integration we obtain

$$\frac{P_{T_0}}{P_S} = \frac{32}{a^2\hbar^2}\left(\frac{D^2}{45} + J^2\right) + 1 \tag{2.25}$$

$$\frac{P_{T_{\pm}}}{P_S} = \frac{8}{a^2\hbar^2}\left(\frac{D^2}{45} + (2J \pm g\beta H)^2\right) + 1 \tag{2.26}$$

A comparison of (2.25, 2.26) and (2.19, 2.20) shows that the dipole–dipole interaction cannot change relative populations or the MFE character.

An alternative mechanism of the magnetic field influence on the carbene reaction rate is connected with the electron spin paramagnetic relaxation [78]. A relaxation disturbs the coherence of the spin precession in the external magnetic field mixing S, T_0 and $T_{\pm}$ levels. This mechanism of MFE is of importance in the viscous medium for long-lived RP [79]. Such a mehanism, however, is most probably ineffective for the triplet carbene reactions in polymers and glasses as demonstrated by the large magnitude of MFE and its unmonotonic character. It seems plausible that paramagnetic relaxation in intermediate RP does not influence the effective rate constant of the carbene decay ($k_{ef} = 10^{-3} - 10^{-4}$ s^{-1}) by virtue of the fact that the

RP conversion rate is comparable with the spin evolution rate, whereas the rate-determining factor of the carbene decay is k_1 in (2.13) and (2.14).

The exchange energy distribution in RPs conforming to the MFE scale is not easily explained by the different distances between radicals. A formal appraisal of distances in RP from equation (2.16) shows that the carbene decay rate is changed by no more than 40–50% at $\Delta r = 0.01$–0.03 nm, whereas the equilibrium distance change of 5×10^{-3} nm can vary the process rate ten-fold for the hydrogen atom cage transfer [80]. Because of this, the orientation factor, connected with angles of rotation of the orbital axes of non-pair electrons about one another, seems to be responsible for the exchange energy spread. The calculations of the exchange integral J in the approach of MO LCAO were performed in reference [81] by varying the set of geometric parameters in the model RPs: $CH_3 \cdots H$ and $H_2NO \cdots H_2NO$.

Calculations indicate notably dramatic changes of J from the rotation angles at a constant distance between radicals.

It is suggested [66,67,77], according to Kaptein's model of spin dynamics, that parameters in equations (2.17) and (2.18) are fixed. It is believed in this connection that the reaction cages for carbenes, reacting with detectable rate at 77 K, are uniform for the RP distances but irregular in the radical angle orientations. A comparison of the k_{-1}/k_2 parameters, characterizing the RP recombination efficiency, implies also essential differences in the physical structure of the cage for different matrices in the carbene decay.

The effect of the external magnetic field (to 100 mT) on the kinetics of the fluorescence decay of carbenes in the low-temperature glasses [82] can also be explained seemingly in the context of the mechanism discussed above (2.12). The characteristic times of this process ($\sim 10^{-7}$ s) are roughly agreed with those of the spin evolutions in RPs.

By this means MFE can be used as a sensitive method to investigate the influence of the matrix physical structure on the kinetics of processes with RP participation. It follows from Fig. 2.7 that the recombination probability of RPs and hence the carbene decay rate are roughly the same in the resonance field at $J \gg a$. But rates can be distinguished as the J functions in zero magnetic field. In fact this deduction is borne out experimentally. The rate of TBCHC decay in ES is twice as much as the one in EA at zero field (Fig. 2.4). Thus the correlation rates and the exchange energy values predicted by the

kinetic model are observed. The carbene decay becomes more effective, for smaller J in the short-lived RPs. In this case a marked difference can be expected in the kinetic behaviour of carbenes from changes in the nearest surrounding molecular organization. The noticeable effect of the carbene precursor chemical structure on the composition of products of the diphenylcarbene reaction, with the secondary and tertiary C–H bonds of isopropanol [34] can be employed as indirect evidence of the agreement between the triplet carbene reactivity and the RP geometry. The carbene precursors of different molecular sizes give specific configurations of cages that are retained in RPs. In turn, these configurations can determine the spin dynamics of RPs and therefore the yield of their recombination products.

References

1. Cohen M.D. and Schmidt G.M.J. (1964) *J. Chem. Soc.*, **6**, 1996.
2. Schmidt G.M.J. (1964) *J. Chem. Soc.*, **6**, 2014.
3. Cohen M.D., Elgavi A., Green B.S., Ludmer Z. and Schmidt G.M.J. (1979) *J. Am. Chem. Soc.*, **101**, 6774.
4. Iguchi M., Nakanishi H. and Hasegava M. (1968) *J. Polym. Sci.*, p.A, **6**, 1055.
5. Suzuki F., Suzuki Y., Nakanishi H. and Hasegava M. (1969) *J. Polym. Sci.*, p.A, **7**, 2319.
6. Emanuel N.M. and Buchachenko A.L. (1987) *Chemical Physics of Polymer Degradation and Stabilization*. Utrecht, Science Press, p. 130.
7. Paul I.C. and Curtin D.V. (1973) *Acc. Chem. Res.*, **6**, 217.
8. Kurita Y. (1964) *J. Chem. Phys.*, **41**, 3926.
9. Lebedev Ya.S. (1966) *Doklady Akad. Nauk SSSR*, **171**, 378.
10. Gordy W. and Morehouse R.L. (1966) *Phys. Rev.*, **151**, 207.
11. Ershov B.G. and Pikajev A.K. (1969) *Rad. Research Rev.*, **2**, 1.
12. Vorotnikov A.P., Davydov E.Ya. and Toptygin D.Ya. (1983) *Izv. Akad. Nauk SSSR, ser. khimich.*, 1499.
13. Dobryakov S.N., Lazarev G.G., Lebedev Ya.S. and Serdobov M.V. (1976) *Izv. Adad. Nauk SSSR, ser. khimich.*, 2087.
14. Aleksandrov A.I., Buben N.N., Lazarev G.G., Lebedev Ya.S., Prokof'ev A.I., and Serdobov M.V. (1976) *Izv. Akad. Nauk SSSR, ser. khimich.*, 515.
15. Yakimchenko O.E. and Lebedev Ya.S. (1978) *Uspekhikhimii*, **47**, 1018.
16. Jaffe A.B., Malamant D.S., Slisz E.P. and McBride J.M. (1972) *J. Am. Chem. Soc.*, **94**, 8518.
17. Zhuravleva T.S., Lebedev Ya.S. and Shuvalov V.F. (1964) *Zhurn. Str. Khimii.*, **5**, 786.

18. Skinner R.J., Blaskiewicz R.J. and McBride J.M. (1972) *Israel J. Chem.*, **10**, 457.
19. Wiersma D., Lichtenbelt J.H. and Kommandeur J. (1969) *J. Chem. Phys.*, **50**, 2794.
20. Zubkov A.V., Koritskii A.T. and Lebedev Ya.S. (1968) *Doklady Akad. Nauk SSSR*, **180**, 138.
21. Koritskii A.T., Zubkov A.V. and Lebedev Ya.S. (1969) *Khimiya Vysok. Energii*, **3**, 387.
22. Lazarev G.G., Lebedev Ya.S. and Serdobov M.V. (1979) *Zhurn. Fiz. Khimii*, **73**, 375.
23. Lebedev Ya.S. and Burstein A.I. (1976) *Chem. Phys.*, **12**, 259.
24. Dubinskii A.A. Grinberg O.Ya., Tabachnik A.A. and Lebedev Ya.S. (1977) *Khimiya Vysok. Energii*, **11**, 156.
25. Fujimura T. and Tamura N. (1972) *J. Polymer Sci.*, **B10**, 469.
26. Grinberg O.Ya., Dubinskii A.A. and Lebedev Ya.S. (1972) *Kinetika i Kataliz*, **8**, 660.
27. Grinberg O.Ya., Dubinskii A.A. and Lebedev Ya.S. (1972) *Kinetika i Kataliz*, **8**, 850.
28. Lazarev G.G., Lebedev Ya.S. and Serdobov M.V. (1976) *Izv. Akad. Nauk SSSR, ser. Khimich.*, 2358.
29. Yakimchenko O.E. and Lebedev Ya.S. (1971) *Int. J. Rad. Phys. Chem.*, **3**, 17.
30. Yakimchenko O.E. and Lebedev Ya.S. (1971) *Khimiya Vysok. Energii*, **5**, 271.
31. Skell P.S. and Garner A.Y. (1956) *J. Am. Chem. Soc.*, **78**, 5430.
32. Skell P.S. and Garner A.Y. (1956) *J. Am. Chem. Soc.*, **78**, 3409.
33. Griller D., Nazran A.S. and Scaiano J.C. (1985) *Tetrahedron*, **41**, 1525.
34. Tomioka H., Griffin G.W. and Nishigama K. (1979) *J. Am. Chem. Soc.*, **101**, 6009.
35. Griffin G.W., Smith R.L. and Manmade A. (1976) *J. Org. Chem.*, **41**, 338.
36. Griffin G.W. and Manmade A. (1972) *J. Org. Chem.*, **37**, 2589.
37. Wasacz J.P., Joullier M.M., Mende U., Fuss I. and Griffin G.W. (1976) *J. Org. Chem.*, **41**, 572.
38. Wasserman E., Trozzolo A.M. and Yager W.A. (1964) *J. Chem. Phys.*, **40**, 2408.
39. Tomioka H., Nakanishi K. and Izawa Y. (1991) *J. Chem. Soc. Perkin I*, 465.
40. Tomioka H., Kimoto K., Murata H. and Izawa Y. (1991) *J. Chem. Soc. Perkin I*, 471.
41. Tomioka H., Ueda H., Kondo B. and Izawa Y. (1980) *J. Am. Chem. Soc.*, **102**, 7817.
42. Senthilnathan V.P. and Platz M.S. (1980) *J. Am. Chem. Soc.*, **102**, 7367.
43. Palik E.C. and Platz M.S. (1983) *J. Org. Chem.*, **48**, 963.

44. Mardaleishvili I.R., Kutyrkin V.A. and Anisimov V.M. (1984) *Vysokomolek. Soed.*, **A26**, 1513.
45. Savinov E.N., Anisimov V.M. and Karpukhin O.N. (1979) *Vysokomolek. Soed.*, **B21**, 834.
46. Boxer S.G., Chidsey C.E.D. and Roelofs M.G. (1982) *J. Am. Chem. Soc.*, **104**, 2674.
47. Platz M.S., Senthilnathan V.P., Wright B.B. and McCurdy C.W. (1982) *J. Am. Chem. Soc.*, **104**, 6494.
48. Zubkov A.V., Koritskii A.T. and Lebedev Ya.S. (1968) *Doklady. Akad. Nauk SSSR*, **180**, 1150.
49. Bartlet P.D. and McBride J.M. (1967) *Pure Appl. Chem.*, **15**, 89.
50. Iwasaki M. and Toriyama K. (1967) *J. Chem. Phys.*, **46**, 2852.
51. Iwasaki M. and Ichikawa T. (1967) *J. Chem. Phys.*, **46**, 2851.
52. Iwasaki M., Ichikawa T. and Ohmori T. (1969) *J. Chem. Phys.*, **50**, 1984.
53. Pudov V.S., Yasina L.L. and Buchachenko A.L. (1974) *Kinetika i Kataliz*, **15**, 1110.
54. Bauschlicher C.W., Bender C.F. and Schaefer H.F. (1976) *J. Am. Chem. Soc.*, **98**, 3072.
55. Benderskii V.A. and Filipov P.G. (1984) *Khimich. Fizika*, **3**, 147.
56. Misochko U.Ya., Filipov P.G., Benderskii V.A., Ovchinnikov A.A., Barkalov I.M. and Kiryukhin D.P. (1980) *Doklady. Akad. Nauk SSSR*, **253**, 163 (1980).
57. Vyazovkin V.L., Bolshakov B.N. and Tolkachev V.A. (1985) *Chem. Phys.*, **95**, 93.
58. Vyazovkin V.L., Tolkatchev V.A. and Burshtein A.I. (1985) *Khimich. Fizika*, **4**, 493.
59. Tolkatchev V.A. (1986) *Doklady. Akad. Nauk SSSR*, **287**, 165.
60. Berezhkovskii A.M. and Trakhtenberg L.I. (1989) *Doklady. Akad. Nauk SSSR*, **303**, 118.
61. Vorotnikov A.P., Davydov E.Ya. and Toptygin D.Ya. (1984) *Vysokomolek. Soed.*, **B26**, 664.
62. Korshak V.V., Vorotnikov A.P., Davydov E.Ya., Kozyreva N.M., Kirilin N.M., Skubina A.I. and Toptygin D.Ya. (1986) *Doklady. Akad. Nauk SSSR*, **291**, 376.
63. Sagdeev R.Z., Salikhov K.M. and Molin Yu.N. (1977) *Uspekhi Khimii*, **46**, 569.
64. Steiner U.E. and Ulhich T. (1989) *Chem. Rev.*, **89**, 51.
65. Ivanov V.B. (1991) *Vysokomolek. Soed.*, **A33**, 1811.
66. Vorotnikov A.P., Davydov E.Ya., Toptygin D.Ya. (1987) *Khimich. Fizika*, **6**, 639.
67. Davydov E.Ya., Vorotnikov A.P. and Toptygin D.Ya. (1990) *Int. J. Polym. Mat.*, **13**, 191.
68. Klochikhin V.L. and Trakhtenberg L.I. (1983) *Khimich. Fizika*, **2**, 810.

69. Dekanter F.J.J. and Kaptein R. (1982) *J. Am. Chem. Soc.*, **104**, 4759.
70. Closs G.L. and Doubleday C.E. (1973) *J. Am. Chem. Soc.*, **95**, 2735.
71. Zimmt M.B., Doubleday C. and Turro N.J. (1985) *J. Am. Chem. Soc.*, **107**, 6726.
72. Zimmt M.B., Doubleday C. and Turro N.J. (1986) *J. Am. Chem. Soc.*, **108**, 3618.
73. Aleksandrov Yu.A., Kurskii Yu.A., Lebedeva S.A. and Kuznetsova N.V. (1982) *Doklady. Akad. Nauk SSSR*, **265**, 1413.
74. Kaptein R. and Oosterhoff J.L. (1969) *Chem. Phys. Lett.*, **4**, 195.
75. Kaptein R. and Oosterhoff J.L. (1969) *Chem. Phys. Lett.*, **4**, 214.
76. Kaptein R. (1972) *J. Am. Chem. Soc.*, **94**, 6269.
77. Davydov E.Ya., Vorotnikov A.P. and Pustoshnyi V.P. (1996) *J. Phys. Chem.*, **100**, 12403.
78. Buchachenko A.L., Sagdeev R.Z. and Salikhov K.M. (1978) *Magnetic and Spin Effect in Chemical Reactions*, Novosibirsk, Nauka, 1978, p. 294.
79. Margulis L.A., Khudyakov L.V. and Kuzmin V.A. (1985) *Chem. Phys. Lett.*, **119**, 244.
80. Trakhtenberg L.I., Klochikhin V.L. and Pshezetsky S.Ya. (1982) *Chem. Phys.*, **59**, 191.
81. Musin R.N. and Schastnev P.V. (1976) *Zhurn. Strukt. Khimii*, **17**, 419.
82. Heired K.W., Platz M.S., Despres A., Leyeune V. and Migirdicyan E.J. (1990) *Phys. Chem.*, **94**, 142.

3 CONNECTION OF SOLID PHASE KINETICS WITH MOLECULAR DYNAMICS

Contents

There is now a wealth of evidence supporting a correlation between the kinetics of reactions in solids and local molecular movement. It is known, however, that the traditional spin probe technique [1] cannot be used to obtain information about molecular motions at the low-temperature range when the kinetics of different solid phase processes may be studied in some detail. Under these conditions the ESR method resolves only the high-frequency part of the paramagnetic probe movements. In most cases the solid phase reactions are defrosted even at low frequencies of the molecular motion when changes in the ESR spectrum of the spin probe are not yet observed. The use of elemetary reactions to explore the solid matrix opens up new avenues for first-hand examination of the molecular mobility influence on kinetics.

3.1 Role of the molecular mobility in the kinetics of reactions of radical pairs

Radical pair recombination does not require a great deal of movement and because of this, the RP decay is very sensitive to local movement. RPs are of great use in revealing phase and structure transitions in polymers. Two structural transitions have been noted by the availability of bends in the annealing curves of RPs in polyethylene at 160–260 K [2]. The frequency of translation may be measured by the ESR spectrum of RP. As this takes place, the radical exit from RP causes the corresponding signal to disappear and the signal for isolated radicals to emerge. Kinetic measurements of the diphenylnitrogen radical exit from cages which occurs on heating of the tetraphenylhydrazine frozen solution in toluene provides the possibility of determining the exit characteristic time $\tau \approx 10$ s and thus the translation movement frequency $\nu_{tr} \geqslant 10^{-1}$ s [3].

An examination of translation motions can be conducted by using stable RPs which arise from the accidental entry of nitroxyl radicals and biradicals into cages at high concentration ($\sim 10^{-1}$ M) [4]. To do this, the ESR spectra of forbidden and allowed transitions of RPs with $\Delta m_s = 2$ and $\Delta m_s = 1$, have been studied in vaseline as a function of temperature (200–300 K). The weak anisotropy of signals of forbidden transitions and the dependence of their width on the magnetic dipole–dipole interactions permitted the qualitative analysis of the rather complicated process of the molecular mobility of the systems investigated. It has been found [4] that the decrease in relative intensity of $\Delta m_s = 2$ transitions occurs on heating the nitroxyl biradical solution. Thus the $\Delta m_s = 2$ spectra do not show marked extensions under these conditions. These results cannot be explained in the framework of relaxation theory of the ESR spectrum form for $\Delta m_s = 1$ and $\Delta m_s = 2$ transitions [5]. They testify to the fact that there is a wide diversity in the set of translation frequencies τ_{tr}^{-1}. In this case the $\Delta m_s = 2$ signal represents a superposition of lines with distinct width. Only the narrowest of them, corresponding to a signal of cages with the jump minimum frequency, is registered. By this means it was shown [4] that stepwise kinetics is not unique to chemical reacitons but also to elementary movement in solids. The correlation time of motions averaging dipole–dipole interaction of RPs (τ_{tr}) has an estimated value of 10^{-9} s [4].

The narrowing of the $\Delta m_s = 2$ transition spectrum for the monoradical solution in vaseline [4] is also of interest. This narrowing arises from the average motion of the g-factor and the HFI remainder anisotropy of the forbidden transitions. These motions can be characterized by the time τ_r, which is the monoradical rotation, while the radical translations are required to average the dipole–dipole interactions. In solutions of nitroxyl biradicals τ_{tr} and τ_r coincide, and the line narrowing of the $\Delta m_s = 2$ spectrum is not exhibited, that is, the dipole–dipole interaction, g-factor and HFI anisotropy are averaged by the same kind of movement which is the biradical rotation.

In order to investigate the molecular dynamics in the solid phase, the method of the oriented spin probe [6] is very useful. One can separate the signals of particles with the dipole–dipole tensor axis oriented predominantly in a common direction in high magnetic fields (600–700 mT). Such procedure makes it possible to measure the rotational disorientation kinetics with a very extended correlation time ($10^7 - 10^8$ s). The measurements performed by this method shown that rotational motions have different frequencies in matrix sites.

3.2 Dynamics of biradical formation in cluster carbene reactions

The cage reaction of hydrogen atom transfer on triplet carbenes in the matirix-isolated state gives rise to RP formation [7,8]. As a rule the ESR spectra of such RP are different in various solids and for different carbenes. However, the appearance of radical particles with the identical ESR spectrum was discovered for diphenylcarbene (DPC) during the diphenyldiazomethane (DDM) photolysis in PMMA, polystyrene, deuterated PMMA-D_8 and polystyrene-D_8 and polycarbonate (PC) [9,10]. One can assert that they are not RP because they have the same parameters of the ESR spectra characterizing distances between radicals and the HFI of unpaired electrons. As molecules of low molecular substances are included in defects of polymer packing with decreased density [11,12], one can assure that carbenes are accumulated both in matrix-isolated states and in clusters of two or more DPC. Therefore products of the dimerous DPC reaction (1.17) can be as biradicals (BR). The reaction of the BR formation of carbenes localized in micropores is interesting for two reasons. The BR yield must reflect the apparent inhomogeneity of the

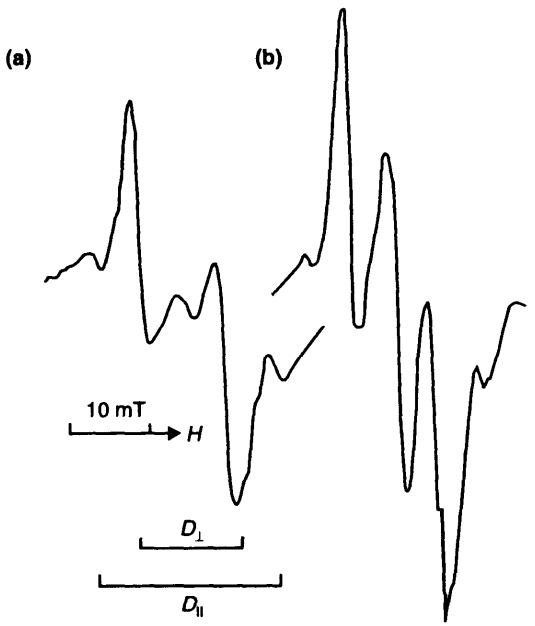

Figure 3.1 ESR spectra of biradicals arising by DDM photolysis in polymers at 77 K: [DDM] = 0.1 M (a); [DDM] = 0.2 M (b).

DDM distribution and can be used to estimate the concentration distribution of other low molecular additives in solid polymers. Also, the kinetics of this process must depend on the molecular organization of the micropore surroundings and the intensity of the small-scale molecular mobility. The same ESR spectrum of BRs in films of various polymers was registered at 77 K (Fig. 3.1(a)). This is an anisotropic signal with parameters of splitting in zero field $D_\perp$ = 11 mT and $D_\parallel$ = 22 mT. The average distance r between unpaired electrons, determined from $D_\perp$ (2.2) is 0.63 nm. The BR formation mechanism (1.17) is confirmed by increasing their yields as the DDM concentration increase (Fig. 3.2). The dependence of the BR yield on DDM concentration is described satisfactorily by equation [9]

$$\varphi = \frac{\varphi_\infty [\mathrm{DDM}]}{C + [\mathrm{DDM}]}, \tag{3.1}$$

where φ_∞ and C are constants. The deviation of φ[DDM] from linearity is connected, evidently, with the high filling of polymer

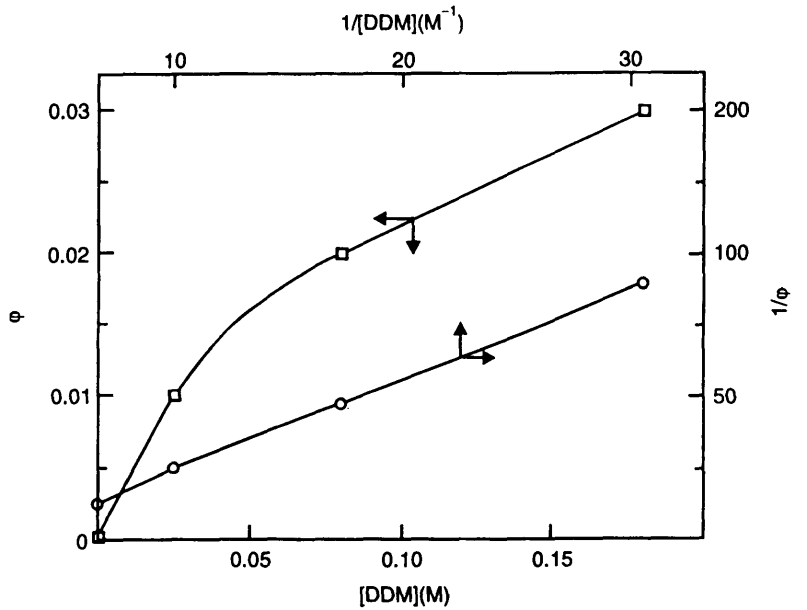

Figure 3.2 Dependencies of BR yield on DDM concentration.

micropores at [DDM] > C. The intense line belongs to BR with distances between spins of 0.9–1 nm or more has appeared in the central part of the ESR spectrum at higher concentrations of DDM (Fig. 3.1(b)). Such particles are formed if three or more DPC react in clusters:

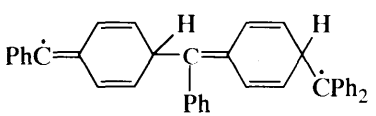

The ESR spectrum analysis shows that the portion of 'polymeric' BR in PC and PMMA does not exceed 20% relative to the total BR [10]. These results can be used to evaluate the distribution of the inhomogeneity of low molecular additives such as DDM by their chemical structure. For example, the distribution of bimolecular, three-molecular etc. clusters in glass polymers is analogous for some photostabilizers, antioxidants, photosensibilizers (salicylates, benzophenones and bisphenols).

The influence of the matrix molecular organization is displayed in the kinetics of the BR generation. The kinetic peculiarities of this

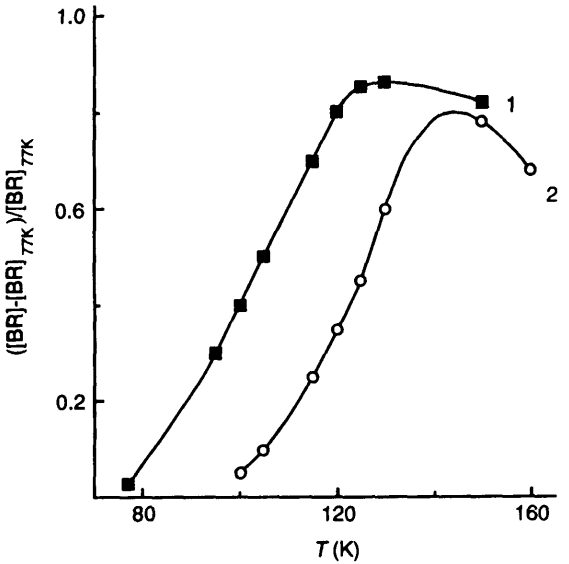

Figure 3.3 Annealing curves for BR formation in: PC (1) and PMMA (2).

process are expressed by annealing curves of samples irradiated by light at 77 K (Fig. 3.3). These curves were obtained by keeping samples in isothermal conditions. In PC, BRs are 100% of the initial quantity, in PMMA the number is lower (80%). The annealing curves are displaced relative to each other at 15–20 K showing that the reactivity of carbenes in micropores depends on the nature of the polymer matrix. It was established that annealing curves characterized the distribution function of particles in reactivity [14]. The BR formation curves which characterize the end of the kinetic process were obtained in the temperature range 95–125 K (Fig. 3.4). They appear as a straight line in the coordinates: 'concentration versus lg t'. This fact indicates that the distribution function given by the rate constants of this process takes the form of (1.8).

The inequivalence of reaction cages in micropores shows the distribution of reacting pairs of carbenes by kinetic ensembles. The gradual annealing of motions in these ensembles determines the character of the temperature dependencies of the BR formation. In PC the annealing of all ensembles of the reacting particles takes place at 130 K while the analogous effect in PMMA is seen at 150 K. The analysis of kinetics with the rate constant dispersion permits us to

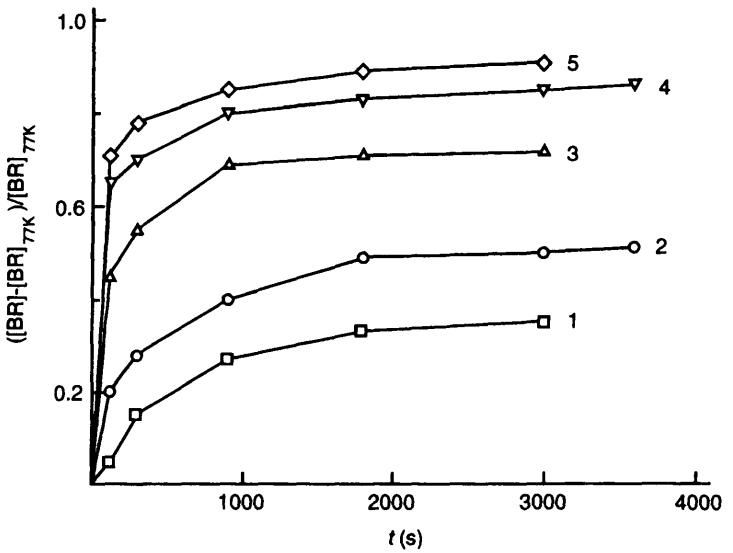

Figure 3.4 Kinetics of BR formation in PC at: (1) 94 K; (2) 100 K; (3) 107 K; (4) 115 K; (5) 120 K.

define the distribution by Arrhenius parameters which, in the general case, arise for distributions both by activation energies and by pre-exponential factors [14]. Referring to Fig. 1.2, the integral distribution functions of these parameters are practically linear. The extrapolation of linear dependencies of $\theta(E, k_0)$ by 1 and 0 gives values determining the distribution width of carbenes in reactivity. In PC these values are $E_{max} = 38\,kJ/mol$, $E_{min} = 26\,kJ/mol$, $\lg k_{0max} = 14.4$ and $\lg k_{0min} = 12.8$ [9]. The activation energy values obtained are typical of the relaxation processes in PC (40 kJ/mol) caused by the motions of monomer links and side groups of macrochains. These values are adjusted with the activation energy of the spin probe rotation [15]. In all probability, the BR formation (1.17) is controlled in PC by the rotative movements of carbenes in polymer micropores. In fact, the values $k_0 = 10^{13}$–$10^{14}\,s^{-1}$ can be compared with the frequencies of the orientational motions of the low-molecular particles in glass polymers. One can note the small dispersion of the Arrhenius parameters: $\Delta \lg k_0 = 1.5$, $\Delta E = 12\,kJ/mol$.

In PMMA the limiting effective values are $E_{max} = 50\,kJ/mol$, $E_{min} = 22\,kJ/mol$, $\lg k_{0max} = 16.0$ and $\lg k_{0min} = 10.5$. The average

Arrhenius parameters of the BR formation are $\lg k_{0av} = 13.25$ and $E_{av} = 36\,kJ/mol$. They correlate satisfactorily with activation energy and rotation time of spin probes in PMMA: $E = 38-42\,kJ/mol$, $\lg k_0 = 13.2$ [15]. But the high dispersion of Arrhenius parameters should be noted $\Delta\lg k_0 = 6.5$, $\Delta E = 28\,kJ/mol$. The result obtained can be explained by the existence of greater scattering of the impeded molecular motion in PMMA which anneals with increasing temperature [10]. The theoretical calculation [16] shows that the activation energy of the side ester group rotation combined with the rotative vibrations of the main chain near the equilibrium positions is 21.6 kJ/mol. This value coincides with the minimum activation energy of the BR formation. But the activation barrier of the ester group rotation increases with declination of the rotational angles from the equilibrium values. The calculation gives a maximum potential barrier of 68 kJ/mol for torsional oscillations around C–C bonds of the main chain. Therefore, the increase of the BR formation activation energy to 50 kJ/mol corresponds to a transition of the carbene orientational dynamics in the kinetic regime controlled mainly by mobility of the macrochain links. Thus, the differences observed in kinetic regularities of the BR formation in two polymers are caused by peculiarities of molecular organization of the micropore environments. In the temperature range studied (90–120 K) the distribution width of the rate constants determined by $\lg(K_{max}/K_{min})$ is 1.5–2 times more in PMMA than in PC.

At $T > 130$–$150\,K$ the BR thermal decay is greater than its formation (Fig. 3.3). The kinetics of the BR thermal decay expresses the molecular dynamics, defining a process for bigger particles than carbenes. Kinetic investigations into reacting in PMMA at 183–218 K show that BRs are unequal. The kinetic curves of this process are linear with coordinates $[BR]/[BR]_0 - \lg t$ (Fig. 3.5). One can see that the inclination angle of anamorphoses does not change with temperature, therefore the BR in equivalence observed in a given temperature interval appears to be unconnected with the activation energy distribution. The rate dependence of the BR thermal decay is subject to the Arrhenius law with the limiting constants: $K_{max} = 5 \times 10^{12} \exp(-46 \pm 4/RT)\ s^{-1}$, $K_{min} = 10^9 \exp(-46 \pm 4/RT)\ s^{-1}$.

From the limiting values obtained it follows that in PMMA the activation energy of the BR decay corresponds to the maximum activation energy of BR formation. The distributions of the frequency factors also overlap. It is believed that the limiting stages of the

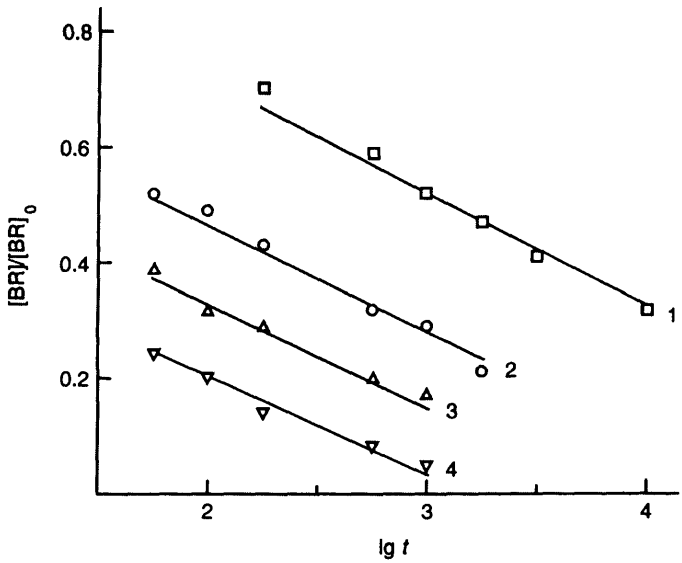

Figure 3.5 Kinetics of BR decay in PMMA at: (1) 183 K; (2) 193 K; (3) 203 K; (4) 218 K.

conversion of BRs and carbenes with the lowest reactivity are controlled in micropores by the same molecular dynamics: namely, the torsional movements of the main chains.

These results show the deterministic role of the rotational motion of carbenes concentrated in micropores of polymers in the generation of BR. This is therefore a good method to use to study molecular dynamics at low temperatures [9]. The method, based on kinetic measurements of BR formation with combination of the BR thermal decay kinetics can significantly extend the possibilities of investigating small-scale dynamics of macromolecules in a wide temperature range, including cryogenic temperatures when the use of other techniques is difficult.

3.3 Influence of relaxation processes on the mechanism of bis-carbene reactions in solid polymers

The analysis of molecular products is one way to investigate the mechanism of carbene reactions in the solid phase. However, the methods used for these purposes are limited by the low solubility of

the carbene precursors. A mechanism for product formation, apart from spectral techniques, can be established by measuring the insoluble gel quantity resulting during cross-linkage of macromolecules by biscarbenes. The kinetics and mechanism of the bis-cyclohexadienone carbenes (BCHC) in *polyvinlalcohol* (PVA) are given in references [8] and [17].

The BCHC precursor is bis-methylenequinonediazide (BQDA) which under photo- and thermal decomposition yields BCHC. The currently available evidence [18] suggests that cyclohexadienone carbenes are able to react with alcohols giving the carbene insertion products — hydroquinone esters $(OH)C_6H_4(OR)$. The PVA films with BQDA additives partly lose their water solubility during irradiation of the film by light or heating from 320 K to 363 K. Based on these results, the conclusion was reached that cross-linkage takes place owing to the BCHC insertion into PVA hydroxyl groups. For simplicity the cross-linkage process can be presented in the following manner

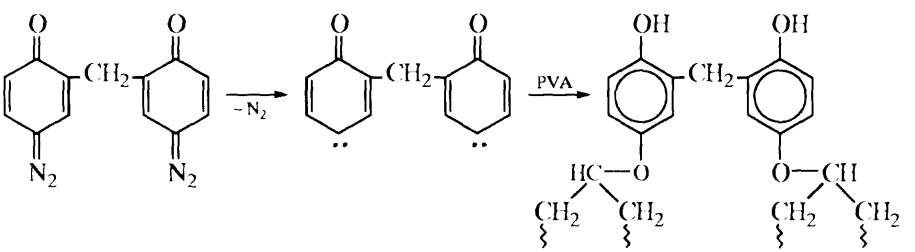

(3.2)

It was shown [17] that the cross-linkage of macromolecules is a result of the reaction of the singlet BCHC insertion into O–H bonds. The rate of the gel fraction formation decreases significantly with a decrease in temperature. It is evident from plots shown in Fig. 3.6 that the cross-linkage is linearly related to the degree of the BQDA conversion. On the other hand, carbenes are likely to be involved in the alternative specific reaction. They react in the triplet state with the formation of free radicals that are transformed into other products. The main carbene reactions in PVA initiated by BQDA photolysis can be represented by the following scheme

$$\mathrm{BQDA} \rightarrow {}^1\mathrm{BCHC} + \mathrm{RH} \xrightarrow{k_1} \mathrm{S} \tag{3.3}$$

$$k_{ST} \uparrow\downarrow k_{TS}$$

$$^3\mathrm{BCHC} + \mathrm{RH} \xrightarrow{k_2} \mathrm{R} \rightarrow \text{products} \tag{3.4}$$

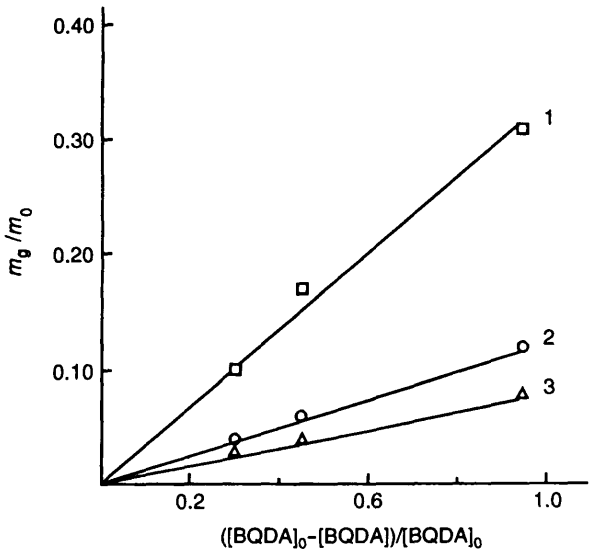

Figure 3.6 Dependencies of gel formation in PVA on BQDA photodecomposition degree at: (1) 295 K; (2) 243 K; (3) 183 K.

It was found that the optical density of the band with $\lambda_{max} = 290$ nm, associated with the cross-linkage groups, similarly increases as the insoluble fraction m_g. Therefore, $m_g/m_0 = \delta[S]$, where S is the cross-linkage and m_0 is the film weight. In the case when the carbene concentration is in the steady state at relatively high temperatures of 183–295 K, the gel fraction yield should be expressible as

$$\frac{M_g}{m_0} = \frac{[BQDA]_0 k_1 k_{TS}}{k_1 k_{TS} + k_2 k_{ST}} \left(1 - \frac{[BQDA]}{[BQDA]_0}\right) \tag{3.5}$$

It follows from plots in Fig. 3.6 that the efficiency of cross-linking, defined by $B = k_1 k_{TS}(k_1 k_{TS} + k_2 k_{TS})$, changes from 0.9 at 295 K to 0.08 at 183 K. The temperature dependence of the B parameter may be represented as

$$\ln\left(\frac{1}{B} - 1\right) = A + \frac{\Delta E_{TS} + E_1 - E_2}{RT}, \tag{3.6}$$

where A is constant.

The difference in the effective activation energies, including ΔE_{TS}, is 2.8 kJ/mol. By this is meant that $E_2 - E_1 < \Delta E_{TS}$. Therefore, the decrease in the efficiency of the cross-linkage caused by the lowering

of the photolysis temperature results from an increase in the relative population of the ground triplet state, similar to the temperature dependence of the product composition in the solid phase reaction of DPC with isobutylene [19].

Considerable differences in cross-linkage were observed at the BQDA thermal decomposition [10]. In this case an insoluble fraction is formed in the wake of the BQDA complete decay. The amount of gel fraction in PVA is proportional to the BQDA decomposed (Fig. 3.7). Hence the efficiency of cross-linkage is equal at different temperatures and about 0.3. As the yield of products increases late in the BQDA decay, an abrupt rise in the cross-linkage takes place. Assuming that the singlet–triplet equilibrium for carbenes is applicable to the BQDA photolysis one can allow their involvement in the two competitive reactions. One immediately produces cross-linkage as a result of the singlet BCHC insertion into O–H groups of macromolecules, and on other reaction of the triplet BCHC gives other products. Since the gel formation efficiency during the BQDA thermal decomposition does not depend on temperature and is three times smaller than during photolysis at 295 K, the mechanism of the reaction (3.4) is not applicable. The absence of the temperature

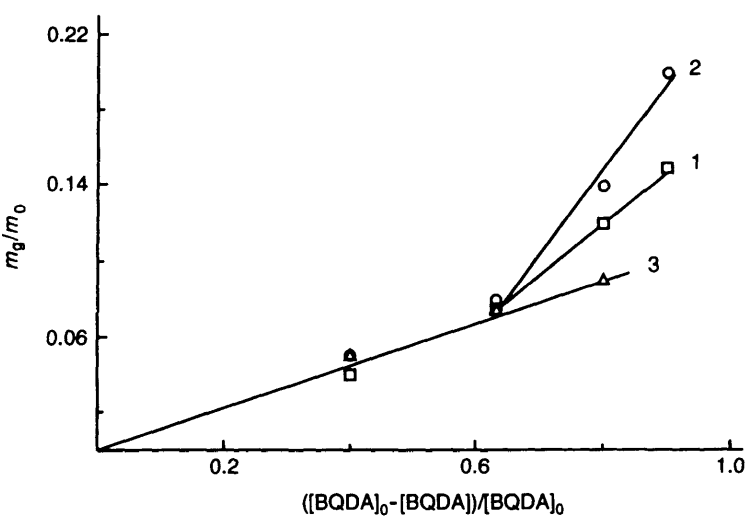

Figure 3.7 Dependencies of gel formation in PVA on BQDA thermal decomposition degree at: (1) 373 K; (2) 343 K; (3) 323 K.

dependence for the gel yield implies that $\Delta E_{TS} + E_1 = E_2$ in equation (3.6), and the triplet carbenes react effectively at high temperatures with larger activation energy than at low temperature conversions. Besides, the reaction product itself must undergo cross-linking during heating as evidenced by the drastic gain in the gel formation for high levels of diazocompound decay (Fig. 3.7).

To explain this effect one should take account of the possibility of intramolecular hydrogen atom transfer from the methylene group of triplet BQDA.

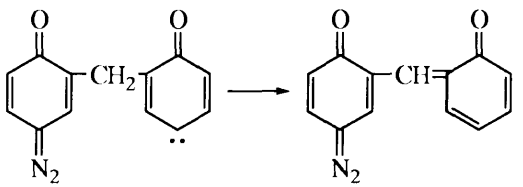

(3.7)

Such reactions in the intramolecular rearrangement with the participation of the hydrogen atom are characteristic of carbenes [20]. The monodiazocompound resulting by reaction (3.7) gives, on further transformation, the corresponding product of insertion in the O–H bond of PVA.

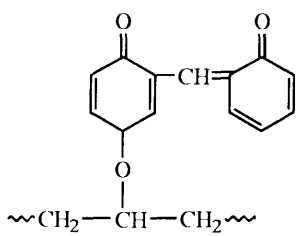

In turn, methylenequinone groups of these products are capable of reacting with hydroxyl groups of macromolecules:

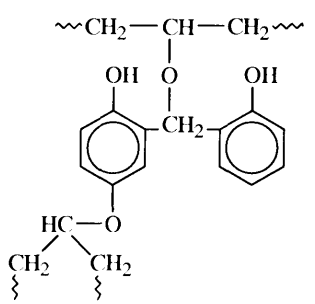

The data obtained show the mechanism of influence of the polymer

matrix physical state on the carbene reactivity. PVA has, at the glass transition temperature, a much higher intensity of molecular movement than at room and cryogenic temperatures. The different kinds of relaxation processes correspond to these temperature ranges. So the interval of 320–370 K is characteristic of the glass transition in randomly packed sites of PVA and the range of 180–279 K corresponds to the relaxation of hydrogen-non-bonded macrochains [21]. The distinctions observed for the PVA cross-linkage are analogous to the effect of a phase state of low-molecular alcohols on the products of the carbene reaction [22]. In going from the rigid matrix to $T > T_g$ the change of the triplet carbene conversion mechanism takes place. The bimolecular reaction of the hydrogen atom abstraction (3.4) is suppressed and the peculiar intramolecular reaction of BQDA (3.7) takes place. This suggests that the PVA matrix effect on the carbene reactions in polymers may be observed within the one phase state in the context of numerous relaxation processes.

3.4 Influence of molecular dynamics on the kinetics of bimolecular reactions: the compensation effect

One can distinguish the following stages for the A and B reaction centres [23]: (1) the macrodiffusion stage when A and B fill a sample, and their diffusion takes place through the average concentration gradient; (2) the microdiffusion stage when the concentration gradient is unavailable, and the rate is determined by the A and B approaching frequency (an A + B pair is formed in the cage as a result of this stage); (3) kinetic stage in which the process rate is determined by the reaction rate of A and B in pairs. Waite [24–26] has given a comprehensive kinetic analysis of bimolecular reactions in solids for microdiffusion and kinetic stages. The formal kinetic equation for the reaction rate follows from a model proposed in reference [27].

It is suggested that A and B can transfer in the solid sample with frequency k_t in response to thermal or certain other activation processes, and they react with the rate constant k_r in cages of the V^* volume. At a steady state

$$-\frac{d[A]}{dt} = -\frac{d[B]}{dt} = k_{ef}[A][B], \tag{3.8}$$

where

$$k_{\text{ef}} = \frac{k_t k_r V^*}{k_t + k_r}; \quad k_t = k_t^A + k_t^B \tag{3.9}$$

In such a manner the law of the addition of kinetic resistances for each stage holds for the effective rate constant of the combined process.

$$1/k_{\text{ef}}V^* = 1/k_t V^* + 1/k_r V^* \tag{3.10}$$

At $k_t \gg k_r$ the kinetics stage in a limiting one and $k_{\text{ef}} = k_r V^*$; at $k_t \ll k_r$ the macrodiffusion stage controls the process and $k_{\text{ef}} = k_t V^*$. In equations (3.8–3.10) k_t is a rate constant of physical or chemical diffusion of particles in solids, k_r is the monomolecular rate constant of the pair decay which, as noted above, can be governed by the rotation frequencies as well as orientations of particles in pairs. Since a wide diversity of particles can be involved in reactions, k_t and k_r have different physical meanings. Consequently, they can be related and any one of the two kinetic regimes can be realized [27].

According to Waite's model [25], the rate constant of the diffusion-controlled reaction is

$$k_D(t) = 4\pi RD\left(1 + \frac{R}{\sqrt{\pi Dt}}\right), \tag{3.11}$$

where R is the encounter sphere radius and D is the diffusion coefficient of the particles. Equation (3.11) has been derived from assumptions of the accidental and uniform distribution of particles along with the equal probability of motion in any directions. The second term of (3.11) dominates the first one in the early stages of the reaction, whence it follows that kinetics of the radical recombination, for example, is described in this stage by the following equation

$$(N/N_0) - 1 = 8R^2 N_0 \sqrt{\pi Dt} \tag{3.12}$$

The decay, non-steady stage of the particles, positioned closely to the encounter sphere, lasts only until $t \ll R^2\pi D$. This time interval is very short if the sphere radius is of molecular size. Only a few radicals which are spaced at intervals of one–two steps can decay in this period. What actually happens is that a major portion of radicals recombines at the non-steady stage [28]. An analysis of experimental kinetic curves gives therefore unrealistic magnitudes of R considerably exceeding molecular sizes: 4–8 nm. The radius of the encounter sphere becomes comparable to the average distance between radicals

before their recombination. However the conditions of Equation (3.11) in doing do not hold.

To overcome this contradiction it was assumed [29] that the radical initial distribution may be very inhomogeneous. Radicals are generated at a short distance from each other as compared with that of the diffusion transfer. Then a decay of radicals with the initial Gauss distribution of width l takes place according to the following equation:

$$N/N_0 = (2/\pi) \quad \text{arcctg} \quad [(2/l)\sqrt{Dt/\pi}] \tag{3.13}$$

The fundamental difference between (3.13) and (3.11) consists in the abandonment of the basic assumptions of Waite's theory, i.e., the homogeneity of the spatial diffusion and uniformity of the initial particle distribution. In this case the recombination process is described by 'root' kinetics. From the beginning to the end of any narrow distribution $\varphi(x)$:

$$N/N_0 = l/\sqrt{\pi Dt} \quad \text{at} \quad t \gg l^2/D \quad \text{and} \quad N \ll N_0, \tag{3.14}$$

where $l = \int x\varphi(x)\mathrm{d}x$.

The kinetic models of bimolecular reactions in solids [26,29] take account of the reactant diffusion specificity but do not provide a reason for the distinctive features of particles in the reaction cage. A number of works [30–32] are devoted to the elucidation of this question. The reaction of the 2,4,6-tri-t-butylphenoxyl with the hydroperoxide groups of polymers has been studied for this purpose.

$$\mathrm{PhO^{\bullet}} + \mathrm{ROOH} \rightarrow \mathrm{PhOH} + \mathrm{RO_2^{\bullet}} \tag{3.15}$$

$$\mathrm{PhO^{\bullet}} + \mathrm{RO_2} \rightarrow \text{products} \tag{3.16}$$

Reaction (3.15) is the limiting stage of this process. This reaction is slow and hence for the phenoxy radical uniform distribution is not limited by diffusion. The stable nitroxyl radical was introduced into a polymer as a spin probe along with $\mathrm{PhO^{\bullet}}$. As this takes place, the linear correlation between the reaction rate constant and the probe rotation frequency ν_r has been observed. The faster the radical rotation in the polymer matrix, the higher the rate constant. This correlation was interpreted in the following manner. The phenoxy radical and the hydroperoxide group, if they are located in the same cage, can react at a reasonable activation energy E and at required

configurations. The cage walls prevent the adoption of these configurations, and the higher the rigidity of the walls, the greater energy that would be required for the elementary act to occur. The activation energy of the nitroxyl radical rotation was found to be 28 kJ/mol in polyethylene and 32 kJ/mol in polypropylene at 290–370 K. The E_r value in chlorbenzene is 12 kJ/mol, that is, the difference in the activation energies for the radical rotation in polymers and chlorbenzene is almost the same as the activation energy of the PhO$^{\bullet}$+ROOH reaction in polymers and benzene. The results obtained allow representation of the rate constant of the bimolecular reaction in the condensed phase as [31]:

$$k = \frac{6\nu_r}{n} K_{AB} P_r P \exp\left[-(E_r + E)/RT\right], \tag{3.17}$$

where ν and n are the collision frequency and the number of neighbours in the cage, $P_r \exp(-E_r/RT)$ is the turning probability of reactants with the realization of the activated complex configuration, P is the steric factor of the reaction in the gas phase, K_{AB} is the equilibrium constant of the A+B pair formation in the condensed phase. The rotation frequency ν_r depends on the cage wall rigidity. The same reaction therefore goes slower and with higher activation energy in polymers as compared with liquids.

The mutual relation of the bimolecular reaction kinetics and molecular dynamics has not only a qualitative character but also a quantitative one. So the effective activation energy of the macroradical recombination in PMMA reaches 112 kJ/mol [33], whereas the activation energy of segmental movements measured by NMR is equal to 108 kJ/mol [34]. The radical decay in polypropylene at low temperatures (100–250 K) proceeds with the activation energy of 44 kJ/mol, while the activation energy of molecular mobility in this temperature range is equal to 52 kJ/mol. These activation energies are respectively equal to 192 and 232 kJ/mol at high temperatures (>250 K) [35].

These anomalous high values of the activation energies of the radical decay in a solid matrix are often explained by the co-operative nature of the particle diffusion to the reaction cage demanding concurrent realignment of structure and the packing of many segments and links. As a rule, pre-exponential factors of the rate constants in these cases are also anomalous and do not have any physical meaning. Examples are found in the bimolecular reaction of

the polyamide macroradical interaction with copper ions (II) [36].

$$R^{\bullet} + Cu^{2+} \rightarrow Cu^{+} + R^{+} \qquad (3.18)$$
$$R^{+} \rightarrow \text{products}$$

Macroradical decay (3.18) follows the kinetic regime in the temperature range 253–281 K, and the temperature dependence of the second-order rate constant is formally described by the Arrhenius law with $E \approx 68\,\text{kJ/mol}$ and $k_0 = 10^{13}$ (1/mol s). The kinetic parameter values obtained far exceed the corresponding values for the liquid phase oxidation of low-molecular radicals by Cu^{2+}. By way of example, $E = 13\,\text{kJ/mol}$ and $\lg k_0 = 10.1$ (1/mol s) for the *n*-butyl radical reaction [37] when the rate constant is close to the diffusion-controlled one. The rate of the bimolecular reaction in solid polymers with the involvement of macroradicals would be connected with the segmental mobility. According to available data [38,39], the activation energy of the relaxation process associated with motions of the hydrogen non-bonded amide groups in the range 60–68 kJ/mol. There is good reason to believe that the E value in (3.18) is conditioned largely by the activation energy of the amide group mobility. The k_0 value, however, is three orders of magnitude higher than the normal one. This qualitative explanation of the correlation between the reaction kinetics and the molecular mobility is inadequate.

A large body of data shows that there is a linear relationship between the pre-exponential logarithm and the activation energy for the solid phase reactions, the so called compensation effect (CEF) [40]. Several models have been proposed to explain CEF. It has been suggested in the context of the diffusion mechanism of the radical recombination that the activation energy declines with a rise in temperature because of the matrix structural changes [40]. Then the temperature dependencies of the effective activation energy and pre-exponent take the forms:

$$E_{ef} = E(T) - T\partial E/\partial T \qquad (3.19)$$

$$k^0_{ef} = k_0 \exp(-\partial E/R\partial T) \qquad (3.20)$$

From (3.19, 3.20) follows the compensation dependence

$$\lg k^0_{ef} = A + BE_{ef} \qquad (3.21)$$

The CEF interpretation was put forward within the limits of the chemical relay transfer of valence [41]. According to this mechanism

states in thermodynamic equilibrium precede the reaction [23]. The relay transfer of valence ($R^{\bullet} + RH$ or $RO_2^{\bullet} + RH$) necessitates some reorientation of reactants, and a number of states $i_1, i_2, \ldots, i_{p-1}$ must comply with distinct orientations of particles. Then the kinetic scheme of the free valence transfer can be represented as follows

$$R^{\bullet} + RH \overset{k_1}{\longleftrightarrow} i_1 \overset{k_2}{\longleftrightarrow} \cdots \overset{k_p}{\longleftrightarrow} i_p \overset{k_0}{\longrightarrow} RH + R^{\bullet}, \tag{3.22}$$

Where k_i is the equilibrium constant between different states, k_0 is the rate constant in the pre-starting state. Then the measured effective rate constant of recombination is $k_{ef} = k_0 \Pi k_p$. It is assumed for the sake of simplicity that all states are equal, that is, the equilibrium constant may be written as

$$k_p = \exp(\Delta S_p/R - \Delta H_p/RT) \tag{3.23}$$

Then the effective rate constant is

$$k_{ef} = k_0 \exp(p\Delta S_p/R) \exp[-(E + p\Delta H_p)/RT], \tag{3.24}$$

Where k_0 and E are the kinetic parameters of the reaction from the i_p state. Equation (3.24) is consistent with the compensation dependence (3.21). This equation also contains the relation between kinetics and molecular dynamics. In fact the scheme (3.22) is adaptable to molecular movement of different segments of macromolecules or some molecules. The analogous equation for the molecular mobility frequency is obtained when the pre-exponent ν_0 and the activation energy E_r of molecular movements appear in (3.23). In particular, if E and $E_r \ll p\Delta H_p$ then the effective activation energies of the reaction and the molecular mobility will be equal [33–36].

An effort was made to discuss CEF in the context of the free-volume theory [29]. In this case the temperature dependence of diffusion in solids has been associated with the probability of emptiness generation. This probability, by virtue of the free-volume model [42], is

$$P_0 = \exp[-\nu^*/(\nu - \nu_0)] \tag{3.25}$$

Where ν^* is an emptiness of molecular size, ν is the specific volume, ν_0 is the molecule's own volume. The emptiness generation results purely from the entropy fluctuations, which give rise to the free volume accumulation merely at the cost of a structural order without energy consumption. The accumulated volume involves many molecules in the form of the given magnitude cavity which occurs

with smaller probability, the larger the volume of the cavity ν^*. On the other hand, the larger the average free volume, for a molecule $(\nu - \nu_0)$, the more frequently will occur a cavity with sufficient volume for the spatial transfer of diffusing particles. Consequently, the temperature dependence of the free volume generation probability is uniquely related to the thermal expansion. The probability of the free volume change may be described in glassy matrices in the range of 50° near T_g by the equation

$$P_0 = \exp\left[-a/(T - T_0)\right] \text{ at } T_0 < T_g \tag{3.26}$$

From this dependence it is apparent that the effective activation energy rapidly increases as the temperature decreases only for CEF. Thus, the compensation dependence is associated with the free-volume model by the fact that elementary organization is made difficult in solid media [29].

One possible consideration of CEF is in terms of the macroscopic in-homogeneity of the solid phase reactions. Such an explanation of CEF was given by the example of kinetic regularities of poly-propylene photo-oxidation [43]. In this view, the polymer media consist of a large variety of chemical microreactors in which the chain propagation $RO_2^{\bullet} + RH$ proceeds with different rate constants. So there is a higher mobility in the friable disordered region, with the result that a reaction takes a more beneficial path for smaller E. The same result occurs at the temperature elevation when media realignment, with diminishing potential barriers of segmental motions, can take place. Because of this, a common reaction in various polymer regions can be seen as a number of one-type processes distinguished by the activation enthalpy and entropy. If the reaction in one region proceeds with ΔH_1 and ΔS_1, then the enthalpy and entropy of activation in any other region are

$$\begin{aligned} \Delta H &= \Delta H_1 + \Delta\Delta H \\ \Delta S &= \Delta S_1 + \Delta\Delta S, \end{aligned} \tag{3.27}$$

where $\Delta\Delta H$ and $\Delta\Delta S$ are the relevant build-ups connected by the linear relations

$$\Delta\Delta H = \beta\Delta\Delta S \tag{3.28}$$

Considering that $\ln k^0 = \Delta S/R$, the CEF equation follows from (3.27, 28):

$$\ln k^0 = \ln k_1^0 = E_1/\beta R + E/\beta R, \tag{3.29}$$

where k^0 is the pre-exponent for the reaction with E and k_1^0 and E_1 are values for the reaction relative to the build-ups counted.

From the foregoing attempts to explain CEF from different standpoints it is clear that the consideration of this widespread phenomenon can be ambiguous. The point is that the kinetic models advanced are difficult to test experimentally. However, they can provide the basis of the qualitative or half-quantitative analysis of complicated kinetic regularities in solids.

3.5 Kinetics of solid phase reactions under limited molecular mobility

The kinetics of reactions in solids, including polymers at $T < T_g$, characteristically show a rather wide distribution of reacting particles in a reactivity [13]. If the characteristic time of 'stirring' τ_s is far larger than the chemical reaction time τ_c, the distribution function during reaction is steadily depleted of more active particles. The liquid phase process is generally characterized by the one average rate constant, because $\tau_s \ll \tau_c$. A middle case is quite possible when τ_s is comparable to τ_c [44]. The steady-state distribution function, depleted slightly by active particles, is established in the τ_s time. Under these conditions, the reaction proceeds in the steady-state regime relative to the distribution function, and the kinetics will not differ superficially from the ordinary 'monochronal' kinetics. As a rule, the k_{ef} value under these conditions depends on processes leading to the distribution stirring. A similar situation is often encountered for radical reactions in solid polymers at temperatures comparable with T_g. Such 'monochronal' kinetics exhibit an increase in the effective activation energies, as compared with liquids, and CEF [40]. Also, the reactivity of the particles has only a weak dependence on the chemical structure. The efficiency of the interaction of chemically distinct inhibitors with peroxy radicals is reported in reference [45]. The rate constants of distinct inhibitors with RO_2 in polymers are found to be approximately the same, while in liquids they are different by two orders of magnitude. It was shown in this way that reactivity averaging does not limit the particle translational diffusion. A similar effect has been found in the reaction of singlet oxygen with aromatic hydrocarbons [46,47]. The difference in the rate constant magnitude can be of up to three orders in the liquid phase, whereas this value is no more than 30–40 in solids.

The reasons for these effects were analyzed in [48 and 49]. One consideration is based on the monomolecular reaction with the particle wide distribution in reactivity. Let us assume that $1/k_s$ is the average lifetime of particle R in the individual state without reaction, then k_s is the frequency of the R transition to another state, therefore the transition probability to the i-state correlates with its reactivity. This probability is equal $1/k_i \times \Sigma 1/k_i$, where k_i is the rate constant of R_i in the i-state. In a similar manner, the individual state population takes place when new particles R are generated at a rate w_0

$$d[R_i]/dt = -(k_i + k_s)[R_i] + \frac{w_0 + k_s/\Sigma[R_i]}{k_i/\Sigma k_i} \tag{3.30}$$

The portion of particles in the i-state after the attainment of a steady state is equal to $[(k_i + k_s)/k_i]/\Sigma\,(k_i + k_s)/k_i$ independently of w_0. Proceeding to the integration, the probability density of the distribution function is

$$\rho(k) = k_s/k(k + k_s)\left(\ln \frac{k_{\max}}{k_{\min}} - \ln \frac{k_{\max} + k_s}{k_{\min} + k_s}\right) \tag{3.31}$$

The averaged k_{ef} value in steady-state conditions is obtained as the integral

$$k_{ef} = \int_{k_{\min}}^{k_{\max}} \rho(x)dx \tag{3.32}$$

Thus, taking into consideration (3.31), it was found [49] that

$$k_{ef} = k_s\left(\ln \frac{k_{\max} + k_s}{k_{\min} + k_s}\right) \Big/ \left(\ln \frac{k_{\max}}{k_{\min}} - \ln \frac{k_{\max} + k_s}{k_{\min} + k_s}\right) \tag{3.33}$$

Likewise one can derive the expression for k_{ef} in the case of a bimolecular reaction $R + M \xrightarrow{k_m}$ with the understanding that it proceeds with a large excess of M, that is, $k_{ef} = k_m[M]$. The distribution in reactivity exists both for R and for M. The influence of the stirring intensity on the distribution function of R is more important, since only a small portion of M is consumed. The given model provides an explanation in principal for peculiarities of bimolecular reactions in solid matrices under limited molecular mobility. It is evident from (3.33) that the rate constant in the solid phase depends on the stirring intensity and decreases compared with the relative value in the liquid phase because k_s is decreasing. In effect, the reaction proceeds in the diffusion regime, but, here, by

diffusion is meant the particle transfer along the distribution function. The diffusion regime which proceeds in this manner can be survived, broadly speaking, when a process is no longer controlled by translation diffusion.

The main problem in using kinetic models under conditions of limited mobility is connected with the precise mechanism of distribution stirring. There are examples of different actions on the matrix, which affect the reactivity and which can restore the initial distribution function by rate constants. Along with the thermal action [44], the case of mechanical stirring has been described [50] for the propagation chain reaction $RO_2^{\bullet}+RH \rightarrow R^{\bullet}+ROOH$ in solid polystyrene at 210–290 K. It was observed that the rate decreases noticeably after 60 minutes of sample exposure at 240 K through the decay of the active peroxy radicals. A sample was then cooled to 77 K and mechanically treated during 10 minutes. The process rate increases sharply after this procedure, that is, the peroxy radical portion transfers to the more active form, and the distribution of a reactivity approaching the initial one, is restored. It is known that the mechanical degradation of polymers at low temperatures is accompanied by a plastic deformation which is a relative translation of the macromolecular segments. As a result, the structural state of the nearest surroundings of the radicals is changed.

We consider the chemical mechanism of the distribution stirring. This occurs because particles decay initially due to the reaction cycle and subsequently are newly reprodcued with new structural surroundings. Chemical stirring, in particular, may prevail for the free-radical processes in solid polymers. This conclusion has been obtained in studies of reactions of peroxy radicals with spatially hindered phenols in polypropylene [49]:

$$RO_2^{\bullet} + PhOH \xrightarrow{k_7} ROOH + PhO^{\bullet} \tag{3.34}$$

The rate constant of this reaction is smaller than k_7 in the liquid phase even though the temperature is 100° higher than T_g. The kinetic scheme, apart from (3.34), includes the following reactions:

$$\text{Initiation} \longrightarrow R^{\bullet} \tag{3.35}$$

$$R^{\bullet} + O_2 \longrightarrow RO_2^{\bullet} \tag{3.36}$$

$$RO_2^{\bullet} + RH \xrightarrow{k_2} ROOH + R^{\bullet} \tag{3.37}$$

$$RO_2^{\bullet} + PhO^{\bullet} \longrightarrow \text{products} \tag{3.38}$$

If the kinetic chain length ν is large ($\nu = k_2[\mathrm{RH}]/2k_7[\mathrm{PhOH}] \gg 1$) the distribution of $RO_2^{\cdot}$ in the reactivity appears to be important in the kinetics of the polymer oxidation. This feature implies that peroxy radicals change their 'position' within the distribution function with the frequency of $1/k_2[\mathrm{RH}]$ through ν cycles of the reactions (3.36, 3.37), and chemical stirring takes place with $k_s = k_2[\mathrm{RH}]$. Whence it follows that $\nu = k_s/2k_7[\mathrm{PhOH}]$. There is good reason to think that $k_{7\max} = k_{7\mathrm{liq}}$, $k_{\max} \gg k_{\min}$, $k_{\min} \ll k_s$. Then it can be shown [47] that

$$\ln (k_{\max}/k_{\min}) = (1 + \nu) \ln [(1 + k_{7\mathrm{liq}})/\nu k_{7\mathrm{sol}}] \tag{3.39}$$

This equation allows an estimation to be made of the distribution width from experimental values of k_7 in the liquid and solid phases.

A more common investigation of chemical stirring of rate constants involves the following cases using the example of the monomolecular reaction A→B [48]: (1) the spontaneous transfer between the two states of A with k_1 and k_2; (2) the equally probable jumping from any one of the A states with k_i to a certain other state with $k_1 \leqslant k_j \leqslant k_2$, i.e., strong stirring. The kinetic equations for the first (simplest) case take the forms:

$$\mathrm{d}p_1/\mathrm{d}t = -k_s(p_1 - p_2) - k_1 p_1 \tag{3.40}$$

$$\mathrm{d}p_2/\mathrm{d}t = -k_s(p_2 - p_1) - k_2 p_2, \tag{3.41}$$

where $p_{1,2}$ are populations of the corresponding states, $k_s = \tau^{-1}$, where τ is the lifetime in states of 1 or 2. It is assumed that $\tau_1 = \tau_2$. The measured value is $p(t) = p_1(t) + p_2(t)$. It is assumed that $p_1(0) = p_2(0) = 1/2$ at the initial instant, then

$$\begin{aligned} p(t) = {} & \tfrac{1}{2} r^2 (k_s^2 + r^2)^{-1/2} \{ [(k_s^2 + r^2)^{1/2} - k_s]^{-1} \\ & \exp \{ -[k + k_s - (k_s^2 + r^2)^{1/2}] t \} \\ & + [(k_s^2 + r^2)^{1/2} + k_s]^{-1} \\ & \exp \{ -[k + k_s + (k_s^2 + r^2)^{1/2}] t \} \}, \end{aligned} \tag{3.42}$$

where $r = \frac{1}{2}(k_2 - k_1)$, $k = \frac{1}{2}(k_1 + k_2)$. It is not difficult to see that when $k_s \gg r$ the reaction becomes 'monochronal' with the rate constant $k = \frac{1}{2}(k_1 + k_2)$.

The kinetic equation for a model with stirring of the distribution takes the following form:

$$dp(k,t)/dt = -kp - k_s p + (k_s/\Delta)\int_{k_1}^{k_2} p(k)dk, \tag{3.43}$$

where $\Delta = k_2 - k_1$, and $p(k,0) = 1/\Delta$. It was found [48] that

$$\begin{aligned} p(t) = {} & (\Delta/k_s)^2 \exp(\Delta k_s)[\exp(\Delta/k_s) - 1]^{-2} \\ & \exp\left[\left(\frac{\Delta}{\exp(\Delta/k_s) - 1} - k_1 - k_s\right)t\right] \\ & + \exp[-(k_1 + k_2)t]\int_0^1 \\ & \exp(z\Delta t)\left[\left(1 + \frac{k_s}{\Delta}\ln\frac{z}{1+z}\right)^2 + \frac{k_s^2}{\Delta^2}\right]^{-1} dz \end{aligned} \tag{3.44}$$

Equation (3.44) at $k_s \gg \Delta$ reduces to the simple exponential law:

$$p(t) = \exp\left[-\frac{(k_1 + k_2)t}{2}\right] \tag{3.45}$$

It should be mentioned that the rates of reaction and stirring are determined by different physical factors. For instance, monomolecular conversions depend on intramolecular movements in particles, while motions of a particle as an integer, govern the stirring process.

References

1. Buchachenko A.L. and Vasserman A.M. (1973) *Stable radicals*, Moscow Khimiya.
2. Bel'kova A.P. and Lebedev Ya.S. (1975) *Vysokomolek. Soed.*, **A17**, 324.
3. Grinberg O.Ya., Dubinskii A.A. and Lebedev Ya.S. (1972) *Kinetika i Kataliz*, **8**, 850.
4. Dubinskii A.A., Grinberg O.Ya., Tabachnik A.A. and Lebedev Ya.S. (1974) *Doklady Acad. Nauk SSSR*, **215**, 631.
5. Freed J.H., Bruno G.V. and Polnaszek C.F. (1971) *J. Chem. Phys.*, **55**, 5270.
6. Grinberg O.Ya., Dubinskii A.A., Oranskii, L.G., Shuvalov V.F., Kurochkin V.I. and Lebedev Ya.S. (1976) *Doklady Acad. Nauk SSSR*, **230**, 884.
7. Davydov E.Ya, Vorotnikov A.P. and Pustoshnyi V.P. (1996) *J. Phys. Chem.*, **100**, 12403.

8. Davydov E.Ya., Vorotnikov A.P. and Pustoshnyi V.P. (1997) *Int. J. Polymeric. Mater.*, **37**, 75.
9. Davydov E.Ya., Vorotnikov A.P. and Pustoshnyi V.P. (1995) *Oxidation Communications*, **18**, 230.
10. Vorotnikov A.P. and Davydov E.Ya. (1991) *Khimich. Fizika*, **10**, 1475.
11. Mar'in A.P. and Shlapnikov Yu.A. (1974) *Doklady Acad. Nauk SSSR*, **215** 1160.
12. Vasserman A.M., Barashkova I.I., Yashina L.L. and Pudov V.S. (1977) *Vysokomolek. Soed.*, **A19**, 2083.
13. Lebedev Ya.S. (1978) *Kinetika i Kataliz*, **19**, 1367.
14. Kuzina S.N. and Mikhailov A.I. (1974) *Doklady Acad. Nauk SSSR*, **231**, 1160.
15. Kovarskii A.L., Placek J. and Szocs F. (1978) *Polymer*, **19** 1137.
16. Grigor'eva F.P. and Gotlib Yu.Ya. (1968) *Vysokomolek. Soed.*, **A10**, 339.
17. Vorotnikov A.P., Davydov E.Ya. and Toptygin D.Ya. (1986) *Vysokomolek. Soed.*, **A28**, 510.
18. Nikiforov G.A. and Ershov V.V. (1979) *Mendeleev's JVHO*, **5**, 523.
19. Wright B.B. (1985) *Tetrahedron*, **42**, 1517.
20. Tomioka H., Ueda H., Kondo S. and Izawa Y. (1980) *J. Am. Chem. Soc.*, **102**, 7817.
21. Garrett P.D. and Gribb D. (1988) *J. Polymer Sci.*, **26**, 2507.
22. Tomioka H., Inagaki T., Nakamura S. and Izawa Y. (1979) *J. Chem. Soc. Perkin I*, **1**, 130.
23. Pudov V.S. and Buchachenko A.L. (1970) *Uspekhi Khimii*, **39**, 130.
24. Waite T.R. (1957) *Phys. Rev.*, **107**, 463.
25. Waite T.R. (1958) *J. Chem. Phys.*, **28**, 103.
26. Waite T.R. (1957) *Phys. Rev.*, **107**, 471.
27. Lebedev Ya.S. (1967) *Kinetika i Kataliz*, **8**, 245.
28. Butyagin P.Yu. (1974) *Vysokomolek. Soed.*, **A16**, 63.
29. Burshtein A.I. (1978) *Uspekhi Khimii*, **47**, 212.
30. Griva A.P. and Denisov E.T. (1976) *J. Polymer Sci., Polymer Chem. Ed.*, **14**, 1051.
31. Griva A.P. and Denisov E.T. (1974) *Doklady Acad. Nauk SSSR*, **219**, 640.
32. Griva A.P. and Denisov E.T. (1977) *Doklady Acad. Nauk SSSR*, **232**, 1343.
33. Ohnishi S. and Nitta I. (1959) *J. Polymer Sci.*, **38**, 451.
34. Powles J. (1956) *J. Polymer Sci.*, **22**, 79.
35. Nara S., Shimada S., Kashiwabara H. and Sohma J. (1968) *J. Polymer Sci.*, **A2**, 6, 1453.
36. Davydov E.Ya., Pariiskii G.B., and Toptygin D.Ya. (1977) *Vysokomolek. Soed.*, **B19**, 853.
37. Kochi J.K. and Subramanian R.V. (1965) *J. Am. Chem. Soc.*, **87**, 4855.
38. Frosini V. and Butta E. (1971) *J. Polymer Sci.*, **B9**, 253.

39. Kovarik J. and Janacek J. (1967) *J. Polymer Sci.*, **C16**, 411.
40. Lebedev Ya.S., Tsvetkov Yu.D. and Voevodskii V.V. (1960) *Kinetika i Kataliz*, **1**, 496.
41. Loy B.R. (1961) *J. Phys. Chem.*, **65**, 58.
42. Cohen M.H. and Turnbull D. (1959) *J. Chem. Phys.*, **31**, 1164.
43. Margolin A.L. (1995) *Khimich. Fizika*, **14**, 58.
44. Karpukhim O.N. (1978) *Uspekhi Khimii*, **47**, 1119.
45. Poholok T.V., Karpukhin O.N. and Shilapintokh V.Ya. (1975) *J. Polymer Sci., Polymer Chem. Ed.*, **13**, 525.
46. Bystritskaya E.V., Karpovitch T.S. and Karpukhin O.N. (1977) *Doklady Acad. Nauk SSSR*, **235**, 607.
47. Bystritskaya E.V. and Karpukhin O.N. (1976) *Vysokomolek. Soed.*, **A18**, 1963.
48. Goldanskii V.I. and Kojushner M.A. (1984) *Doklady Acad. Nauk SSSR*, **274**, 632.
49. Roginskii V.A. (1982) *Doklady Acad. Nauk SSSR*, **267**, 1407.
50. Radsig V.A. and Rainov M.M. (1976) *Vysokomolek. Soed.*, **A18**, 2022.

4 THE EFFECT OF THE STRUCTURAL-PHYSICAL MODIFICATION ON THE KINETICS OF RADICAL REACTIONS

Contents

The space-orientation and molecular-dynamic factors in kinetics, which were considered in earlier sections, demonstrate the structural effect at the levels of cages and nearest surroundings. The inhomogeneity of the cage structure leads to the wide distribution of reacting particles which becomes evident from the stepwise kinetics. The pronounced effect on the reactivity should be apparent in this connection from changes in the organization of the solid media molecules at the macroscopic level which is obtainable by means of direct structural modification.

A molecular organization change is achieved by surface forces. The extensive experimental evidence accumulated at the present time indicates that the influence of the filler on the structure extends non-uniformly over the polymer volume [1]. This influence is not exhibited at some distance from the filler surface. Because of this, the

concept of interfaces is introduced by which properties and the structure of layers adjacent to the filler particles differ from those in the volume of the polymer phase. The character of the equilibrium property dependence on the filler content serves as evidence for the appearance of interfaces. Experimental values of the specific volume in filled samples, for example, substantially exceed those expected [2]. The dependencies observed show the polymer transformation into the friable interface state. The increase of the filler volume fraction, regardless of the polymer filling procedure, entails a monotonic growing of interfaces up to the point where they overlap and the continuous phase formation point. The high-filled polymer coincides with this maximum degree of the polymer structural modification [3]. The filler effect on the polymer phase structure is attained through interfaces. The interface thickness determined experimentally, reflects the behaviour of the filled system with reference to the property being studied, that is, its value depends on the measurement technique applied [4]. Information on interfaces can be obtained, as a rule, not by direct study but on the basis of physical-chemistry characteristics which exhibit an essential dependence on the filling degree, for instance, heat capacity at the glassy transition [5,6]; density [2]; and viscosity [7,8]. In all likelihood, the peculiar changes of the kinetic parameters of reactions should be expected within the interface boundaries. The filling degree acts, in this case, as a factor governing the structural-physical state of the matrix and, consequently, the reactivity of particles.

4.1 The filler effect on the kinetics of the triplet carbene decay in polymers

The application of the low-temperature cage reactions has definite advantages for estimating the structural-physical modification influence on kinetics with polymer filling. The low-temperature conditions reveal the surface catalytic action on the mechanism of these processes [10]. The kinetic curves of di-t-butylcyclohexa-dienone carbene (TBCHC) decay (2.12) at 100 K in PMMA and acetylcellulose (AC) containing up to 65 mass percentage of aerosil are shown in Fig. 4.1(a),(b). Here, the filling reduces the rate of DTBCHC decay in both polymers. A similar effect was observed throughout the entire temperature range of 100–140 K. The view of kinetic curves clearly depicts the kinetic inequivalence of TBCHC. In this

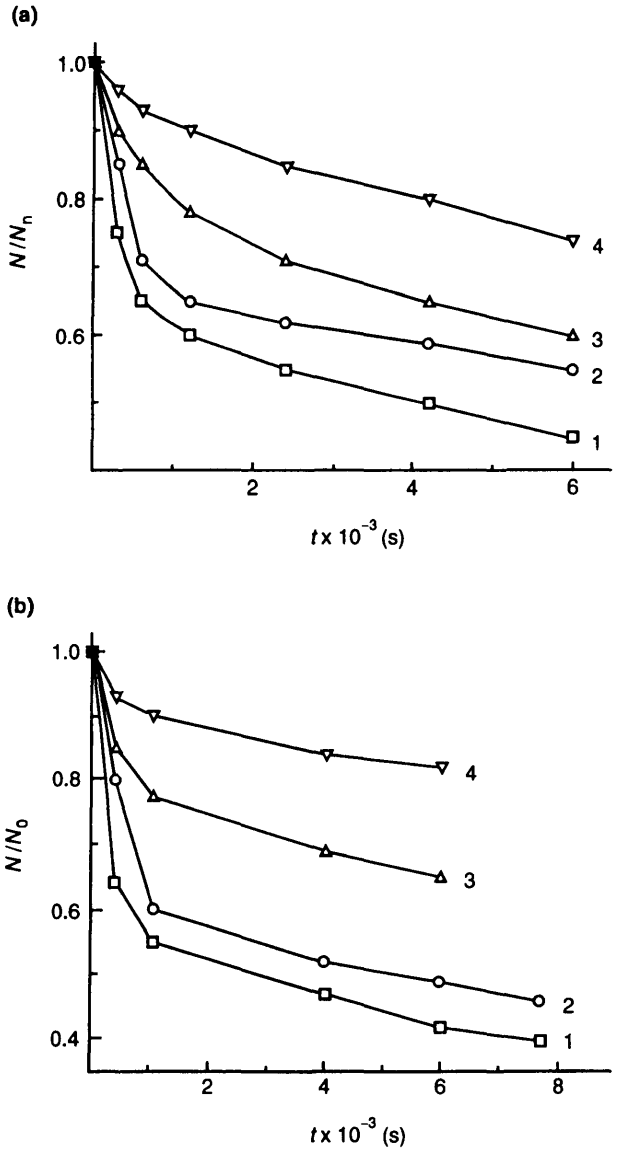

Figure 4.1 Kinetics of TBCHC decay at 100 K in PMMA (a) and AC (b) with: (1) 1; (2) 25; (3) 40; (4) 65% of aerosil.

temperature range, the kinetics is satisfactorily described by equation (1.13). As the aerosol content increases the limiting values of the rate constants in PMMA and AC decrease, but the parameter of the distribution width is kept constant. At 100 K $\lg(k_{max}/k_{min})$ are 6.8 and 5.5 respectively in PMMA and AC. The distribution becomes much narrower with increasing temperature. The constancy of the distribution width in samples with different fillings, including high-filled samples, is necessary in order to understand the nature of the structural modification effect on the carbene decay rate. Therefore, this conclusion has been confirmed by other methods of kinetic analysis involving approximation by equation (1.31) [10]. All curves are approximated in the same manner, regardless of the aerosil content and the parameter n, determining the distribution width, is constant at a given temperature. The values of the kinetic characteristics obtained are listed in Table 4.1.

The average rate constant k_{av} of the TBCHC decay diminishes as the aerosil content increases, but kinetic analysis performed by two methods gives the same result: the distribution width does not depend on the filler content.

Figure 4.2(a),(b) show relationships of k_{av} and distances between the filler particles. These distances were estimated by the equation:

$$l = d\left[\left(\frac{\eta_m}{1-\eta}\right)^{1/3} - 1\right], \tag{4.1}$$

where d is the diameter of the aerosil particles (≈ 20 nm), η is the aerosil volume fraction in polymers, $\eta_m \approx 0.8$ is the maximum aerosil volume fraction. As is seen from figure, the k_{av} values decrease moderately as the filler content increases in the range of l exceeding 20 nm. If $l < 20$ nm, k_{av} sharply decreases by more than tenfold. This critical distance may be considered as an effective thickness of interface layers in filled PMMA and AC.

As well as the physical structure modification of polymers, the filler effect on the kinetics of the TBCHC decay can be also caused by a change of mechanism on the surface. For instance, one can arrange that the fraction of carbenes on the filler surface decays with a smaller rate as compared with this reaction in the polymer volume. A special experiment was set up to demonstrate this fact in association with the filler effect [10]. The carbene decay rates were compared for two samples of filled polyvinylpyrrolidone containing the same quantity of

Table 4.1. Kinetic parameters of TBCHC decay in filled PMMA and AC

T(K)	PMMA Aerosil (%)	$k_{av} \times 10^4(s^{-1})$	n
100	1	28.0	6
	25	14.5	
	40	4.2	
	65	1.6	
113	1	35.0	4
	25	25.0	
	40	14.7	
	65	1.8	
125	1	38.0	2
	25	25.0	
	40	16.7	
	65	2.1	
	AC		
100	1	13.0	4
	25	11.8	
	40	2.5	
	65	0.7	
125	1	140.0	3
	25	–	
	40	87.0	
	65	6.9	
135	1	1000	2
	25	580	
	40	200	
	65	12	

aerosil (65%). The carbene precursor was tentatively coated on the aerosil surface for preparation of one filled sample (I). Another sample was prepared by a standard method when the carbene precursor is uniformly distributed through the volume of polymer (II). In these samples, irradiated at 77 K by light, the kinetics of the TBCHC decay were studied at 100–125 K. The k_{av} values in (I) were found to be considerably superior to those in (II). So, at 125 K, k_{av} =

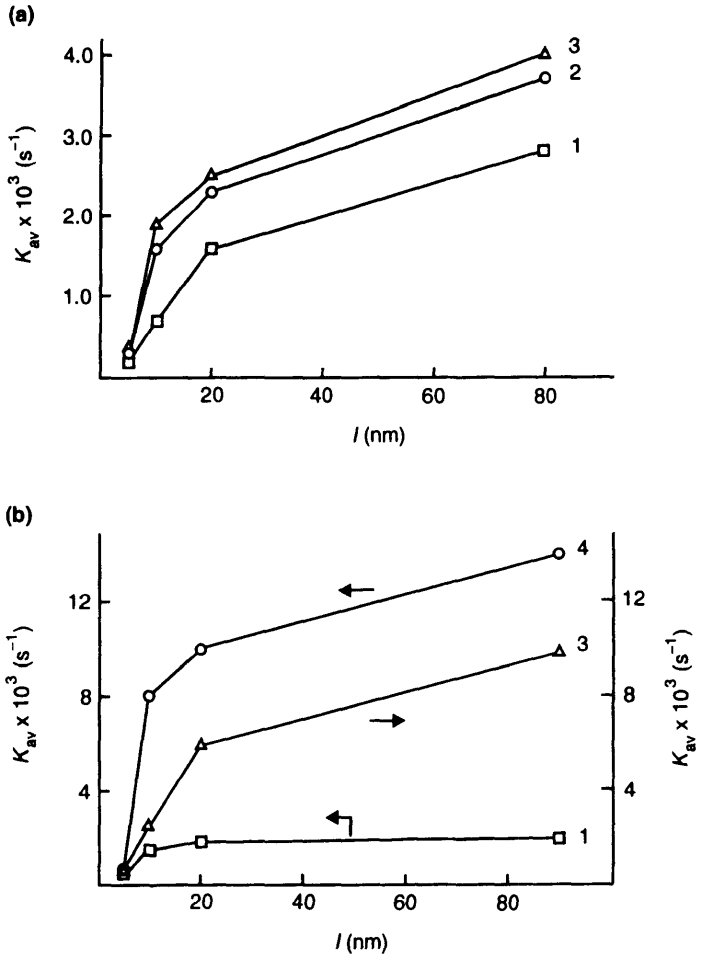

Figure 4.2 Relationships of average rate constants on distances between aerosil particles in PMMA at: (1)100 K; (2)113 K (3)125 K (a) and AC at: (1)100 K; (2)125 K; (3)145 K (b).

$1.58 \times 10^{-2}, s^{-1}$ in (I) and $k_{av} = 0.66 \times 10^{-2}, s^{-1}$ in (II); at 100 K $k_{av} = 9.6 \times 10^{-4}, s^{-1}$ in (I) and $k_{av} = 3.4 \times 10^{-4}, s^{-1}$ in (II). It follows from the results obtained that the TBCHC decay on the aerosil surface occurs more efficiently compared with polymeric phase. Notice that the increase in the decay rate for carbenes on the surface is not due to their mutual recombination, since the average distance between them is ~ 3 nm. By this means the carbene decay in filled

polymers takes place mainly during reaction with macromolecules. Thus, a decrease in the rate of this process with increase in the aerosil content must be associated with the physical structure changes in polymers on account of transformations in the interfaces. The interface thickness estimated by plots of Fig. 4.2 is 15–20 nm.

On the basis of kinetic data obtained, the following conclusions can be reached about the nature of the matrix structure changes caused by filling. As the width distribution in the carbene reactivity does not change with the conversion of the polymer, the structural-physical modification does not influence the distribution of the rate constant of the primary reaction of the hydrogen atom transfer from the C–H bond of macromolecules to carbenes (2.12). As it was shown in Chapter 2, this reaction is the limiting stage of the carbene decay and determines the kinetic inequivalence of carbenes by the dispersion of distances between the carbene centre and the C–H bonds of the matrix. In this connection one can conclude that structural changes affect the efficiency of the intermediate RP recombination, defined by the relations of the spin state populations and the rate constants of back hydrogen transfer and RP recombination (2.13): $(k_{-1}P_T/k_2P_S)$. It can be assumed that, as the filled polymer is prepared from solution, the formation of more friable packing of macromolecules is possible in interfaces because of difficulties with the relaxation processes during filled samples shaping. Such structural realignment can change the relation between the recombination rate of singlet RP and back hydrogen atom transfer, together with the relative population P_T/P_S as a result of the RP configuration change. The larger the declination of the non-pair electron axes from the right-angled orientations, the higher is the exchange energy value and the higher the population of the RP triplet level.

4.2 The filler effect on the kinetics of carbene reactions in clusters

As is shown in references [11] and [12], some fraction of carbenes (up to 20%) gives rise to clusters owing to the non-uniform distribution of the carbene precursors (diazocompounds) in polymers. These cluster carbenes are capable of giving biradicals (BR) by reaction (1.17). From the example of polycarbonate with different MM, the influence of the molecular organization on kinetics of this process has been demonstrated. Experiments with the polycarbonate filled samples

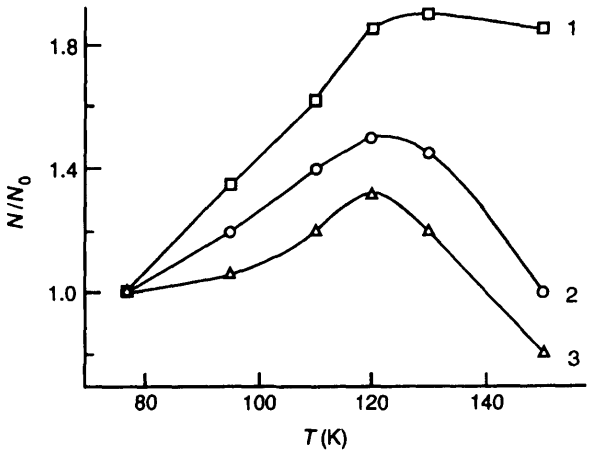

Figure 4.3 Annealing curves of the BR formation and decay in polycarbonate with: (1) 0; (2) 50; (3) 65% of aerosil.

exhibit more descriptively the structural-physical modification effect on the carbene reaction in micropores. Fig. 4.3 depicts the dependence of the annealing curves, reflecting the BR reactivity, on the aerosil content. The maximum quantity of BR is reached at 130–150 K in unfilled samples when molecular movements are enhanced for all ensembles of carbenes. In filled samples the maximum is shifted towards lower temperatures ($T \approx 120$ K) because of the BR thermal decay at $T > 120$ K. The relative increase of the BR quantity is much higher in unfilled samples (90%) as compared with filled ones (35%). It was established [12], that portions of decay are significantly offset at low temperatures in more filled samples. In this connection, one can assert that a different type of behaviour for annealing curves results from a substantial decrease in the BR thermostability with the degree of polymer filling. Kinetic studies of BR decay at the filler for varied content, enables the effective interface thickness to be estimated [12]. The introduction of the aerosil leads to the abrupt increase of the BR decay rate (Table 4.2)

The kinetics of this process are adequately described by the equation:

$$\frac{[\mathrm{BR}]}{[BR]_0} = \left(1 + \frac{w_0 t}{[\mathrm{BR}]}\right)^{-1}, \qquad (4.2)$$

Table 4.2. Dependence of the initial BR decay rates on the aerosil content at 146 K

Aerosil (%)	$W_0/[BR]_0 \times 10^4(s^{-1})$
0	0.25
40	3
50	9
65	15

which is similar to equation (1.31) at $n = 1$. This value of the n parameter, characterizing the distribution width, gives an indication of the dramatic distribution narrowing. The character of the W_0 relationship is out of proportion to the filler volume fraction. Its increase at 20% of aerosil content is conditioned by polymer transition into interfaces in which the BR decay efficiency is large. The interface thickness estimated by equation (4.1) (~ 12 nm) is fairly close to that determined from the filler effect on kinetics of the matrix insulated carbene conversion.

4.3 The filler effect on the kinetics of low-temperature reactions of macroradicals

The filler effect revealed by carbene reaction studies [10–12] assumes that the influence of the structural modification by filling on the kinetics of radical reactions, has a general nature. Experimental verification of this follows from results obtained in studies of macroradical reactions in filled PMMA and polyvinylpyrrolidone (PVP) [13]. Macroradicals were generated by the iron chloride photolysis at 77 K. The main component of macroradicals (80%) initiated by the $FeCl_3$ photoreduction in PMMA is $\sim C(CH_3)(COOCH_3)C^{\cdot}H(CH_3)(COOCH_3) \sim$ [14], and the aerosil presence has no effect on the composition of macroradicals generated. The kinetics of the radical decay at 170–200 K were found to be almost unchanged in samples containing up to 50% of filler, and yet the rate of decay increases noticeably with further increase in the aerosil quantity. An analysis of experimental dependencies points to the fact that macroradicals of PMMA in the thermal decay reaction may be characterized by the distribution in the rate constants. Parameters of

Table 4.3. Kinetic parameters of the macroradical decay in filled PMMA

Aerosil (%)	$k_{av} \times 10^3(s^{-1})$ $T = 170\,K$	n	$k_{av} \times 10^3(s^{-1})$ $T = 200\,K$	n
1	1.4	2	5	1.5
50	1.4	2	5	1.5
55	1.4	2	35	1.5
60	6.5	2	45	1.5
70	90	2	80	1.5

this distribution, namely the width n and the average rate constant k_{av} determined by equation (1.31), are listed in Table 4.3.

From the data in the table it will be obvious that the distribution width is not changed with the PMMA filling. A minor narrowing of this distribution was observed with an increase in temperature. It is remarkable that the rate decay sharply increases by a factor of 15–60 in samples containing upwards of 50% of aerosil. The regularity observed is not caused by a higher efficiency of the radical decay on the filler surface. Actually, the linear plot of k_{av} on the filler content should be observed in this case. The results obtained agree, however, with the interface concept [1,2]. The evaluation of the interface thickness by equation (4.1) substantiates the relative significance of this value, which is variable depending on the chosen investigation techniques and experimental conditions [5]. So this value changes in PMMA from ~ 5.5 nm at 170 K to ~ 8 nm at 200 K.

Unlike PMMA, in which the filler influences the kinetics of the radical decay at $T > 77$ K, the filler effect in PVP has come to light at the photoinitiation stage at 77 K. The composition of radicals generated by sample photolysis depends on the aerosil content. The ESR spectra obtained in PVP with different amounts of filler are shown in Fig. 4.4. As can be seen, the weakly-resolved ESR spectrum is observed in PVP containing no filler, but the fine structure components appear in the spectrum of PVP with 15% aerosil; and the five-component signal with $\Delta H \approx 1.8$ mT can be separated in samples with 50% of filler. This signal is for macroradicals $\sim CH_2C^{\cdot}(\underline{N(CH_2)_3CO})CH_2\sim$ (I) [15]. A transformation of the weak-resolved ESR spectrum into (I) is observed during heating of samples at $T = 100$–200 K (Fig. 4.4(d)). The appreciable thermal decay of radicals (I) takes place only at $T > 200$ K.

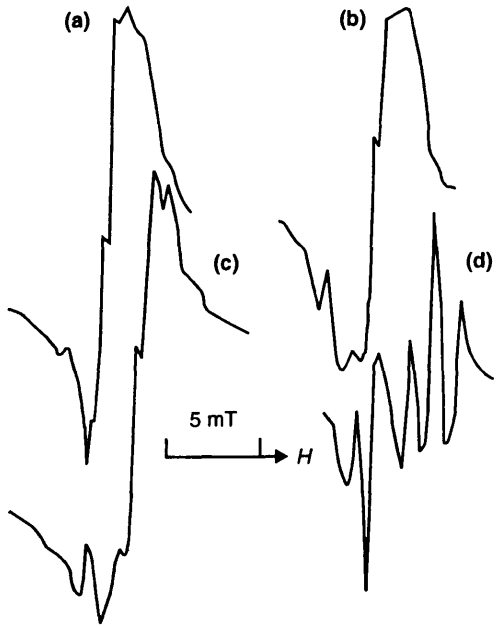

Figure 4.4 ESR spectra of PVP + $FeCl_3$ with: (a) 0%; (b) 15%; (c) 50% of aerosil, irradiated by light at 77 K, and after warming of (a) at 200 K (b).

The radical (I) formation can be outlined taking into account the photoinitiation mechanism caused by transition metal ions [16], as

$$FeCl_3 + PVP \xrightarrow{h\nu} FeCl_2 + Cl^- + \sim CH_2CH(^+\underline{N^\bullet(CH_2)_3CO})CH_2\sim \text{ (II)} \quad (4.3)$$

$$\text{(II)} \xrightarrow{kT} \text{(I)} + H^+ \quad (4.4)$$

$FeCl_3$ photolysis produces cation-radicals (II) [17] with the ESR spectrum shown in Fig. 4.4(a). The filler effect on the efficiency of the radical (I) formation by reactions (4.3 and 4.4) is represented by annealing curves (Fig. 4.5). These curves have a maximum at 180–200 K, which defines the fraction of cation-radicals (II) stabilized at 77 K during photolysis of the samples. It follows from the plots of Fig. 4.5 that as few as 10% of cation-radicals (II) are registered in high-filled ($\sim$ 50% aerosil) samples, whereas this fraction amounts to $\sim$ 70% in unfilled PVP [13]. A non-linear dependence of the radical composition on the aerosil content is evidence of the PVP structural

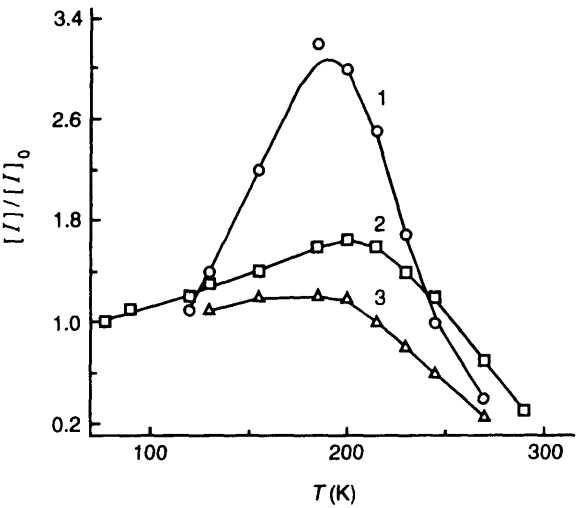

Figure 4.5 Temperature dependencies of the radical I yield during annealing of PVP + $FeCl_3$ with: (1) 0; (2) 15; (3) 50% of aerosil.

modification having the most pronounced influence on the conversion of (II) from reaction (4.4) as the filler particles approach each other for a distance of $\sim$ 25 nm. This distance estimated by equation (4.1) may be considered as the effective thickness of the filled PVP interface.

The studies performed show that the friable molecular packing in interfaces is the reason for the observed effect. The lowering of the packing density can be favourable to the decrease of the energy barrier of the carbon atom rehybridization in the radical (I). In this case the rate of the reaction (4.4) increases at 77 K. A lower density of molecular packing can assist in the realignment of local surroundings to assist the favourable mutual orientations of PMMA macroradicals at their cage recombination.

The low-temperature radical reactions considered, along with the carbene reactions, represent structural-sensitive processes. The influence of the structural modification on the kinetics of the matrix-insulated and cluster carbene reactions has fundamental differences. They are conditioned by peculiarities of the carbene reaction mechanism in these states. The structural modification of interface effects on the chemical and spin dynamics of intermediate RPs reduces the

probability of their recombination and, as a consequence of this, the rate of the carbene thermal decay in the matrix insulation state. By contrast, the carbene reactions in micropores with BR formation controlled by the rotational mobility of the particles does not undergo the essential filler effect on the kinetics. At the same time, the decay rate of BRs, which are more sizable particles compared with carbenes, increases in high-filled samples by more than ten-fold [13]. These results show that interface shaping causes a molecular-packing change. It seems likely that the micropore-free volume increases during this process. As this takes place, the BR recombination is formally described by the second-order kinetic equation (4.2) even at low temperatures (150–160 K). At first glance this fact seems to be surprising, since the BR decay at these temperatures is characterized by a kinetic stop with a 10–20% degree of conversion in unfilled samples.

Similar descriptions of the low-temperature reaction by a simple kinetic law have been cited for a recombination of peroxy radicals in polyamides [18]. Kinetics of the $RO_2^{\bullet}$ decay are governed in this case by the second-order equation with the rate constant: $k = 2.4 \times 10^{15} \exp(-64\,\text{kJ/RT})$ l/mol s. This value extrapolated to room temperature ($k = 3 \times 10^3$ l/mol s) is closely related to the rate constant of the peroxy radical decay in polymers at $T > T_g$ [19]. It should be pointed out that the apparent elimination of the BR kinetic inequivalence in filled PVP [12] cannot be connected with chemical stirring of the distribution function (Section 3.5). The attempt to analyze conditions in which a reaction with the rate constant distribution can simulate 'homogeneous' kinetics has been undertaken in references [20] and [21]. For this purpose, a model of the reaction increasing with distinct rates within different sites of the matrix, was proposed. The distribution of sites by the rate constants $V(k)$ is found. The function $S(k,t)$, which represents the concentration of particles in sites with rate constant k at the instant t, defines a spatial distribution of particles. Then the experimentally determined average concentration is

$$N = \int_0^\infty S(k,t)V(k)\mathrm{d}k \Big/ \int_0^\infty V(k)\mathrm{d}k \tag{4.5}$$

Equation (4.5) shows that a wide diversity of kinetic dependencies in isothermal conditions are possible by different forms of $S(k,t)$ and $V(k)$. In particular, the possibility exists of formal straightening of

kinetic curves in coordinates of the second-order equation even with a lack of particle stirring:

$$N_0/N = 1 + k_{ef}t, \tag{4.6}$$

Where k_{ef} is the effective rate constant. Assume that the first-order reaction is proceeding in sites, so that

$$S(k,t) = S(k,0)\exp(-kt) \tag{4.7}$$

If the distribution of sites is most probable then

$$V(k) = k\tau^2 \exp(-k\tau), \tag{4.8}$$

where $\tau > 0$. Furthermore, if the initial distribution of particles is

$$S(k,0) \sim (1/k)\exp(-k\alpha), \alpha \geqslant 0 \tag{4.9}$$

(where α and τ are parameters), then the substitution of (4.7–4.9) into equation (4.5) gives

$$N_0/N = 1 + t/(\alpha + \tau) \tag{4.10}$$

By this means kinetic curves will constitute straight lines in coordinates of the second-order law throughout the range of average concentrations.

The distribution hyperbolic function of (1.8) type is frequently used in the description of 'polychronal' kinetics:

$$V(k) = \begin{cases} 1/[k\ln(k_{max}/k_{min})] & \text{at} \quad k_{min} \leqslant k \leqslant k_{max} \\ 0 \quad \text{at} \quad k > k_{max}, & k < k_{min}. \end{cases} \tag{4.11}$$

Here, too, equation (4.6) follows from (4.5) with $k_{ef} = 1/\alpha$ if $S(k,0) \sim k\exp(-k\alpha)$; $k_{min} \leqslant 1/\alpha \leqslant k_{max}$. In this case equation (4.6) is true for the conversion degree $N/N_0 = 10\,\alpha k_{min} \ll 1$ [21]. A similar conclusion is arrived at for the case of bimolecular reactions in matrix sites, so that

$$S(k,t) = S(k,0)/[1 + S(k,0)kt] \tag{4.12}$$

Substituting (4.9, 4.11, 4.12) at $\alpha = 0$ into equation (4.5) gives equation (4.6) with $k_{ef} = N_0 k_{min}\ln(k_{max}/k_{min})$, which is true everywhere over the range of the average concentration change. The examples given in references [20] and [21] show that the inhomogeneous reaction can, in some instances, simulate, the formal kinetic regularities of the homogeneous reaction. The physical meaning of this simulation is that the range of sites with reacting

particles can be narrower than the whole range of matrix sites. The filled polymer composite is apparently a typical system simulating the conditions of the inhomogeneous solid phase reaction.

References

1. Lipatov Yu.S. (1977) *Fizicheskaya khimiya napolnennykh polimerov*, Moscow, Khimiya.
2. Silberberg A. (1975) *Faraday Disc. Chem. Soc.*, **59**, 203.
3. Privalko V.P., Besklubenko Yu.D., Lipatov Yu.S. and Demchenko S.S. (1977) *Vysolomolek. Soed.*, **A19**, 1744.
4. Lipatov Yu.S. and Privalko V.P. 1984 *Vysolomolek. Soed.*, **B26**, 257.
5. Malinskii Yu.M. (1970) *Uspekhi Khimii*, **39**, 1511.
6. Lipatov Yu.S. and Privalko V.P. (1972) *Vysolomolek. Soed.*, **A14**, 1643.
7. Lipatov Yu.S. and Privalko V. P. (1973) *Vysolomolek Soed.*, **B15**, 749.
8. Lipatov Yu.S., Privalko V.P. and Shumskii V.F. (1973) *Vysolomolek. Soed.*, **A15**, 2106.
9. Varoqui R. and Dejardin P.J. (1977) *Chem. Phys.*, **66**, 4395.
10. Davydov E.Ya, Vorotnikov A.P. and Toptygin D.Yu. (1989) *Izv. Akad. Nauk SSSR, ser. khimich.*, 2453.
11. Davydov E.Ya., Pustoshnyi V.P., Vorotnikov A.P. and Pariiskii G.B. (1992) *Int. J. Polymeric Mater.*, **16**, 295.
12. Vorotnikov A.P. and Davydov E.Ya. (1991) *Khimich. Fizika*, **11**, 1475.
13. Davydov E.Ya., Pustoshnyi V.P., Vorotnikov A.P. and Pariyskii G.B. (1991) *Vysolomolek. Soed.*, **B33**, 370.
14. Davydov E.Ya., Pariyskii G.B. and Toptygin D.Ya. (1975) *Vysolomolek. Soed.*, **A17**, 1504.
15. Monig H. and Ringsdorf H. (1974) *Makromolek. Chem.*, **B175**, 811.
16. Symons M.C.R., West D.X. and Wilkinson J.G. (1974) *J. Phys. Chem.*, **74**, 1335.
17. Eastland G.W., Ramakrishna D.N. and Symons M.C.R. (1986) *J. Chem. Soc. Faraday Trans. I*, **82**, 2833.
18. Davydov E.Ya., Margolin A.L., Pariyskii G.B., Postnikov L.M. and Toptygin D.Ya. (1978) *Doklady Akad. Nauk SSSR*, **243**, 1475.
19. Davis L.A., Pampillo C.A. and Chiang T.C. (1973) *J. Polymer Sci., Polym. Phys. Ed.*, **11**, 841.
20. Margolin A.L. (1995) *Khimich. Fizika*, **14**, 58.
21. Margolin A.L. and Makedonov Yu.V. (1985) *Vysolomolek. Soed.*, **A27**, 1377.

5 TUNNELLING IN SOLID PHASE REACTIONS

Contents

Much evidence points to a considerable deviation from the Arrhenius law in the temperature dependencies of kinetics in solids. The compensation effect in the radical recombination in polymers is a representative example of such deviation [1]. The apparent decrease in the activation energy with increase in temperature is connected, in this case, with structural features of the solid phase, in particular with the progressive ascent of the molecular mobility intensity. An alternative deviation from the Arrhenius law was noted, however, in the kinetics of various elementary reactions at cryogenic temperatures. One feature of the phenomena observed in these conditions is the low-temperature limit of the rate which decreases independently up to the point where the temperature approaches absolute zero. This was first discovered by the example of radiation-induced polymerization of formaldehyde [2–5]. It is easy to understand that this limit has a quantum origin when particles are capable of penetrating or tunnelling through a potential barrier of height in excess of the particle energy [6,7]. The availability of the low-temperature limit is taken to be the best indication of tunnelling.

This pattern conforms to the kinetic peculiarities of the hydrogen atom abstraction by free radicals in solids [8]. The curvatures of the

Arrhenius dependence were observed in reactions of methyl radicals with methanol and acetonitrile, where the effective activation energies and pre-exponents have anomalously small values. This reaction has an activation energy of as low as 5.6 kJ/mol at 77–87 K in γ-irradiated acetonitrile [9] and 3.6 kJ/mol at 67–77 K in the methanol glass [10]. The flow of reactions at these low temperatures which occurs at an appreciable rate is contradictory to the activation mechanism, because the activation energy of this reaction, measured in the liquid phase, is in the range 30–40 kJ/mol. The hydrogen atom abstraction by the activation mechanism occurs with a negligibly low rate at 77 K. These results have been interpreted in the context of H atom tunnelling at low temperatures [11].

There is some characteristic temperature T_q below which the rate constant at which the tunnel reaction begins, exceeds the Arrhenius rate constant as the temperature increases. It was shown [8,12,13] that experimental temperature dependencies may be linearized in using the equation

$$\ln k = \alpha + \beta T, \tag{5.1}$$

where α and β are constants. The nature of the dependence (5.1) is considered in a series of works. The models advanced provide a method for the quantitative evaluation of parameters determining the reactivity in the solid phase cage reactions.

5.1 Model of thermal populations of the highest vibration levels

This model, linking the potential barrier parameters, mass and temperature was originally proposed by Goldanskii [14,15]. It is interesting to note the date of the development of the model which was at a time when kinetic data for the low-temperature chemical reactions were unavailable. The tunnel reaction model, connected with thermal populations of the vibration levels has been further advanced in references [8], [13], [16] and [17]. In this model, the tunnelling role in the chemical reactions is determined by the relationship between three energies, namely, the activation energy E_0, the thermal motion energy kT and the characteristic energy of the system $\varepsilon = \hbar^2/Md^2$ (M is the effective mass, d is the activation barrier half-width) [14]. Two non-dimensional parameters, are inserted for this purpose: $\chi = E_0/kT$ and $\alpha = \pi\sqrt{2E/\varepsilon}$ ($a \gg 1$). The distribution

of inreacting particles will be considered to be of Maxwell's type. Then the reaction rate constant, taking into account the tunnelling effect, can be written as

$$k = \frac{2\sqrt{2\pi}R^2E_0^2}{\sqrt{M}(kT)^{3/2}}\int_0^\infty yW(y)e^{-xy}\,dy, \tag{5.2}$$

where $y = E/E_0, E$ is the energy of the relative motion of the particles, $R = r_1 + r_2$ is the radius sum of interacting particles in the bimolecular reaction and $W(y)$ is the probability of tunnelling ($y < 1$) or above-the-barrier transfer ($y > 1$).

Potential barriers of two kinds were considered:
Eckart's barrier

$$U(x) = \frac{E_0}{ch^2(x/d)} \tag{5.3}$$

and the parabolic barrier

$$U(x) = E_0\left(1 - \frac{x^2}{d^2}\right) \tag{5.4}$$

If $W(y > 1) \approx 1$ at both barriers, then the rate constant can be conceived as a sum of the Arrhenius constant

$$k_a = \frac{2\sqrt{2\pi}R^2\sqrt{kT}(1+\chi)e^{-\chi}}{\sqrt{M}} \tag{5.5}$$

and the tunnelling rate constant

$$k_t = \frac{2\sqrt{2\pi}E_0^2}{\sqrt{M}(kT)^{3/2}}\int_0^1 yW(y)e^{-zy}\,dy \tag{5.6}$$

The probability of tunnel penetration is written in the case of Eckart's barrier as

$$W(y) \approx \frac{e^{2a\sqrt{y}}}{e^{2a\sqrt{y}} + e^{2a}}, \quad \sqrt{y} \gg 1/a \tag{5.7}$$

By this means the integral function in equation (5.6) will be:

$$f(y) \approx \text{const}\quad e^{2a\sqrt{y}-xy} \tag{5.8}$$

and it has a maximum at

$$y = \frac{2\pi^2(kT)^2}{\varepsilon E_0} \tag{5.9}$$

A marked contribution to tunnelling in the reaction rate is observed if the $f(y)$ maximum occurs in the under-barrier energy range ($y_m < 1$), that is, if $x > a$.

The tunnelling transfer probability is $W_1(y) = e^{-a(1-y)}$ for a parabolic barrier, and the integral function in (5.6) then becomes:

$$f_1(y) = y e^{-a} e^{(a-x)y} \tag{5.10}$$

It is obvious that the following condition fits the integral function maximum in the limits of the activation barrier:

$$y_m = \frac{1}{\kappa - a} < 1, \tag{5.11}$$

that is, $k > a + 1$. Since $a \gg 1$, the condition for the tunnelling marked contribution may be written as $\kappa > a$ for the case of the parabolic barrier. Consequently, the characteristic temperature T_q is determined regardless of the barrier form by the equation:

$$T_q = \frac{E_0}{ak} = \frac{\hbar\sqrt{E_0}}{k\pi d\sqrt{2M}} \tag{5.12}$$

The rate constant of tunnelling in the temperature range $T < T_q$ for Eckart's barrier is expressed as

$$k_t \approx \frac{4\sqrt{2\pi}R^2\sqrt{kT_g}(T/T_g)^2 a^{3/2}}{\sqrt{M}} \exp\{-a[1 - (T/T_q - 1)]\} \tag{5.13}$$

In this case the dependence $\ln k_t = \alpha + \beta(T/T_g)$ arises instead of the Arrhenius law.

In the case of the parabolic barrier at $T < T_q$

$$k_t = \frac{2\sqrt{2\pi}R^2\sqrt{kT}\,e^{-a}}{\sqrt{M}(1 - T/T_g)^2}\{1 - \exp[-a(T/T_q - 1)][1 + a(T/T_q - 1)]\} \tag{5.14}$$

The rate constant ceases to depend on temperature with the accuracy of the pre-exponential factor at $\chi \gg a$, that is at $T/T_q \ll 1$.

The rate constant expressions are essentially coincident at $T > T_q$ for the two forms of potential barriers considered. A changeover in the energies of tunnelling particles from a continuous distribution to a quantized distribution does not alter the criteria (5.12) for T_q in the case of a symmetric barrier [11]. Energetic states for each potential well are characterized by a set of discrete levels, and the tunnelling is

feasible solely for the resonance condition when energetic levels coincide in both wells. If two identical 'traps' for the tunnelling particle are brought close together, we have the system of two equal potential wells. As this takes place, a particle appears to be delocalized and uninterruptedly transfers from one well to another. The lower and narrower the barrier, the shorter the characteristic time (τ_0) of this under-the-barrier transfer. Neither of the wave functions ψ_l (particle in left well) nor the function ψ_r (right well) represent the stationary functions of the system themselves but their combinations are:

$$\text{symmetric } \psi_s = \frac{1}{\sqrt{2}}(\psi_l + \psi_r)$$

and antisymmetric:

$$\psi_\alpha = \frac{1}{\sqrt{2}}(\psi_l - \psi_r).$$

This means that a system is to be found in two energetic states distinguished by energies $\Delta E_{as} + \hbar/\tau_0$. Functions ψ_s and ψ_a are in line with ψ_l and ψ_r only if $\tau \to \infty$, when two wells are separated by an infinite distance.

The absolute equality of two wells is very rare. They are generally very different from one another. The levels of the wells become non-stationary, and tunnelling of the particle m between wells A and B ($A + B_m \to A_m + B$) is made possible by a coincidence of the levels with an accuracy of $\Delta E + \hbar/\tau$, where $\tau \gg \tau_0$ (τ_0 is the tunnelling time in the case of a symmetric barrier). Let all molecules B_m be at the zero vibration level. If the closest to the zero level is separated by $\Delta E \gg \Delta E_0$ ($\Delta E_0 = \hbar/\tau_0$) then a tunnel transfer is impossible in adiabatic conditions with no interactions between m, A, B and the surroundings. The transfer energy ΔE cannot be transmitted anywhere in these conditions. For a transfer to be feasible either 'runoff' of this energy must occur or the shape of the potential well must be changed so as to equalize the energetic levels in the wells A and B if $\Delta E < \Delta E_0$. The transmission of energy ΔE to the ambient molecules can serve as a 'runoff'. The interaction, with the resulting dissipation of the particle excitation energy, permits non-adiabatic tunnel transfer. Interaction with the lattice widens the energetic levels and in doing so promotes tunnelling by a ΔE decrease due to the approach and overlap of levels. Another way of tunnelling at the cost of the energetic levelling in two potential wells is linked with time variant

fluctuations of the polarization forces in the interaction with the surroundings [11]. These fluctuations correspond to the change in time of depth and shape of both potential wells. The energetic levels in the wells move up and down and can coincide for a short time with the advent of the resonance condition required for tunnel transfer.

The tunnelling model associated with the population of higher vibration levels has been experimentally tested [8]. Two unknown parameters of the potential barrier (height and width) were determined by fitting the model to experimental data. Five low-temperature reactions proceeding via hydrogen atom tunnelling were considered. It was shown that heights of the potential barrier determined by fitting were from 44 to 60 kJ/mol and widths from 0.17 to 0.38 nm. Nevertheless, in reality these parameters are not independent. According to a model of the reaction $AH + B \rightarrow A + HB$, the potential function $U(x, R)$ of the hydrogen atom depends on one parameter, that is, distance R between A and B [18]. Both the height and width of the potential barrier may be calculated from the potential function $U(x, R)$ with fixed parameter R. The widths of the barriers obtained (0.17–0.32 nm) correspond to relatively large distances between A and B (0.39–0.45 nm). The heights of the barriers in this case must be substantially greater (3–5 times) than 44–60 kJ/mol [19].

5.2 Model of the oscillating potential barrier

The recombination of free radicals in solids provided the basis for this model. It was first proposed in references [20] and [21], that the free valence migration occurs due to tunnelling of the hydrogen atom from molecules to radicals at low temperatures. The temperature conditions of the tunnelling predominance over the activation transfer ($T < T_q$) were dealt with under the parabolic potential barrier. Substituting $d \approx 0,1$ nm and $E \approx 1$ eV in equation (5.12) shows that $T < 330$ K. It follows from this condition that the hydrogen atom tunnel transfer can prevail at quite high temperatures. If we assume that the temperature influence on the tunnelling probability is related to a thermal excitation of higher vibration levels of C–H bonds, then the quasiclassic probability of the H atom transfer from the n-level for a parabolic barrier takes the form:

$$W_n = \exp\left[-\frac{\pi}{n}\sqrt{\frac{M}{2E_0}}\, d(E_0 - n\Delta E)\right], \qquad (5.15)$$

where ΔE is the difference between the energy levels of the C–H bond in the harmonic approximation and E_0 is the barrier height. The ratio of the populations is $P_n/P_0 = \exp(-n\Delta E/kT)$ (where P_n and P_0 are the respective n and zero level populations). It is evident that populations of higher levels must be taken into account when $P_nW_n > P_0W_0$. From equation (5.15) we can obtain that this non-equality holds under the following condition:

$$T > \frac{\hbar}{\pi kd}\sqrt{\frac{2E_0}{M}} \tag{5.16}$$

Thus, the higher level population leads to an essential acceleration of tunnelling only at those temperatures when the above-barrier transfer cannot be ignored. Correlation of the inequalities $T < T_q$ and (5.16) shows that the excitation of higher vibration levels is not of importance at those temperatures where tunnelling becomes dominant.

It was assumed [20,21] that the tunnel transfer probability of the H atom depends on the temperature caused by the oscillation of the distance between the molecule and the radical due to lattice thermal vibrations. The higher the temperature, the greater the amplitude of the thermal vibrations, the closer together are the radical and molecular, and the greater the probability of tunnelling. It is thought that a hydrogen-type bond is formed between molecules and radicals $\diagdown\!\!\diagup\!\!\text{C—H}\cdots\dot{\text{C}}\!\!\diagdown\!\!\diagup$ along which transfer takes place. The interaction in this complex is said to be stronger than with other molecules. The complex 'radical + molecule' is in equilibrium with the surroundings, and therefore, the probability that the distance between molecule and radical is equal to R can be represented by a diagonal element of the density matrix for oscillator

$$\rho(R,T) = \sqrt{\frac{M\omega}{2\pi\hbar cth\frac{\pi\Omega}{2kT}}}\exp\left[-\frac{(R-R_0)^2}{\frac{\hbar^2}{M\omega}cth\frac{\hbar\Omega}{2kT}}\right] \tag{5.17}$$

where M, Ω are the effective mass and own frequency of relative oscillations in complex 'molecule + radical', R_0 is the equilibrium distance.

The expansion of the exponent index of the tunnelling probability in terms of displacements from the equilibrium position (first two

terms) gives

$$W(R) = \exp\left[-I(R_0) - \frac{\partial I}{\partial R}(R - R_0)\right], \tag{5.18}$$

where

$$I(R_0) = 2/\hbar \int_{x_1(R_0)}^{x_2(R_0)} \sqrt{2m[U(x, R_0) - E}\,\mathrm{d}x \tag{5.19}$$

In (5.19) $U(x, R_0)$ is the potential energy, E is the hydrogen atom energy, $x_1(R_0)$ and $x_2(R_0)$ are boundaries of the potential barrier. In response to the intermolecular vibrations in lattice the potential barrier width oscillates with frequency $x = x_0(1 + \frac{R}{R_0}\sin\Omega t)$. The temperature dependence of the tunnelling probability was obtained by averaging of the equation (5.18) through the use of the matrix density (5.17) in following form

$$\bar{W}(T) = \exp\left\{-I(R_0) + \frac{\hbar[I'(R_0)]^2}{4M\Omega\, th\,(\hbar\Omega/2kT)}\right\} \tag{5.20}$$

Expression (5.20) for the classic oscillator ($\hbar\Omega \ll 2kT$) transforms to

$$\bar{W}(T) = \exp\left\{-I(R_0) + \frac{[I'(R_0)]^2 kT}{2\xi}\right\}, \tag{5.21}$$

where ξ is the rigidity of the $\rangle\!\!-\!\mathrm{C}\!-\!\mathrm{H}\cdots\dot{\mathrm{C}}\!-\!\langle$ bond in the complex; $\xi = M\Omega^2$.

The rate constant of recombination is readily obtainable from (5.21) if the hydrogen atom tunnelling is the controlling stage of the reaction:

$$k(R_0, \xi, T) = \omega_{\mathrm{C-H}}\, W_0 \exp(\beta T), \tag{5.22}$$

where $\omega_{\mathrm{C-H}}$ is the frequency of the hydrogen atom vibrations in the potential well, W_0 is the probability of the H atom tunnelling obtained by extrapolation of k at $T \to 0$. Equation (5.22) is see to be coincident with the experimentally observed dependence (5.1).

A related approach derived from the oscillating barrier model has been drawn on to provide an explanation of the tunnelling patterns in references [22]–[27]. The subsequent development of this theory was reflected in a number of works [28–33]. In addition to the classic oscillator described by equation (5.20), a quantum consideration of

the tunnelling process based on intermolecular oscillation of the surroundings has been accomplished. It was conceived [30] that the oscillation frequency of tunnelling particles in potential wells is well above the intermolecular oscillations. In this connection two systems are prominent in the nucleous motion of the tunnelling process considered: fast and slow. This approach, referred to as the double adiabatic approximation, permits a description of the wave function in the following form

$$\Phi_{ln\nu}(\rho, r, R) = \psi_l(\rho, r, R)\varphi_{ln}(r, R)\chi_{ln\nu}(R), \tag{5.23}$$

where $\psi_l, \varphi_{ln}, \chi_{ln\nu}$ are wave functions and l, n, ν are quantum numbers, ρ, r, R are the respective coordinates of electronic, fast and slow systems. The matrix element of transfer from the initial state i to the end state f may be represented as

$$M_{fi} = \langle l_f n_f \nu_f / V(\rho, r, R) / l_i n_i \nu_i \rangle = \langle \nu_f / V_{ln} / \nu_i \rangle, \tag{5.24}$$

where $V(\rho, r, R)$ is the perturbation operator and $V_{ln} = \langle l_f n_f / V / l_i n_i \rangle$ is the matrix element of the perturbation operator in states of electronic and fast systems. Because n_i and n_f correspond to the fast system localized in the different potential wells, there is a strong dependence of V_{ln} on R. It is assumed that

$$V_{\ln}(R) \approx V'_{\ln} \exp\left(-\frac{1}{\hbar} \int |P(r, R)| \mathrm{d}r \right), \tag{5.25}$$

where $V'_{\ln}$ is a value independent of R and $P(r, R)$ is the fast system pulse. Integration is effected over the transfer coordinate r. Since $V_{\ln}$ depends strongly on R the expansion of $\ln V_{\ln}$ in terms of displacement from the equilibrium position may be carried out. Then the matrix element (5.24) is described as

$$M_\xi = V_{\ln}(R_0) \left\langle \nu_f \left| \exp\left[-\frac{I'}{2}(R - R_0) \right] \right| \nu_i \right\rangle, \tag{5.26}$$

where R_0 are equilibrium coordinates of the slow system,

$$I' = 2 \frac{\partial}{\partial R} [\ln V_{\ln}(R_0)].$$

The tunnelling probability in a unit time is expressed by (5.24):

$$\bar{W} = \frac{2\pi}{\hbar}|V_{\ln}(R_0)|^2 \exp\left[\frac{\Delta E}{2kT} + \frac{\hbar(I')^2}{4M\Omega}\operatorname{cth}\frac{\hbar\Omega}{2kT}\right] \cdot \sum_m I_m\left[\frac{\hbar(I')^2}{4M\Omega sh(\hbar\Omega)/2kT}\right]\delta(\Delta E - m\hbar\Omega) \qquad (5.27)$$

where ΔE is the energy transmitted to the slow system ($\Delta E > 0$) or taken from it ($\Delta E < 0$), the δ-function conforms to the energy conservation law, I_m is the Bessel function of the imaginary argument. Equation (5.27) entails the exponential temperature dependence (5.1) at relatively high temperatures ($\hbar\Omega \ll 2kT$).

The foregoing equations for hydrogen atom tunnelling were derived from a complex condition. It is assumed that an interaction between the molecule and the radical in this complex is stronger than the interactions between the matrix molecules, or the mass of the radicals is much less than that of the molecules. Only local intermolecular oscillations are taken into account, while the lattice acts as a thermostat. An alternative situation results when this complex is not formed, or the masses of the molecules and radicals are comparable. In these conditions, consideration must be given to the overall spectrum of the lattice oscillations. With this approximation, atom tunnelling may be described in the ordered media, say, in the case of the diffusion of hydrogen atoms in crystals. The potential barrier, by virtue of the crystal lattice oscillations, is changed, and thus the temperature acts on the tunnelling probability as in the case of the 'molecule + radical' complex. These two cases were analyzed in reference [31]. Probabilities of the atom tunnelling were shown to be essentially coincident at $\hbar\Omega \ll 2kT$. Variations in rates are in evidence, however, at $T \to 0$. The temperature dependence of the tunnelling rate constant has the form of a plateau if only local oscillations in the complex are accounted for, but for the ideal crystal lattice [7]:

$$\ln k \approx \frac{\pi^6(I')^2(kT)^4}{60\hbar^3\omega_D^5 M}, \qquad (5.28)$$

where ω_D is the Debye frequency of molecular crystals and M is the mass of the matrix molecules.

5.3 Experimental estimation of hydrogen atom tunnelling parameters

The experimental verification of existing models of the tunnelling transfer is complicated in many instances by the fact that the kinetics of reacting particles are inequivalent at low temperature. Kinetic investigations of the triplet carbene decay (Chapter 2) show the decisive role of the space-orientation factors in this process. The low-temperature decay of carbenes both in low-molecular glasses and polymers is characterized by anomalous values of the effective Arrhenius parameters. So the activation energy of the diphenylcarbene decay is 1.8–8 kJ/mol in mixtures of methanol, ethanol and propanol with tetrahydrofurane [34]. About the same values were determined from the kinetics of other arylcarbenes in matrices of toluene, ether, and methylcyclohexane [35]. The temperature dependencies of the rate constants during carbene decay in polymers show appreciable deviations from the Arrhenius law (Fig. 5.1). The effective activation energy drops from 12–16 to 5 kJ/mol with a temperature decrease from 180 to 77 K [36–40]. As observed, the kinetic peculiarities are

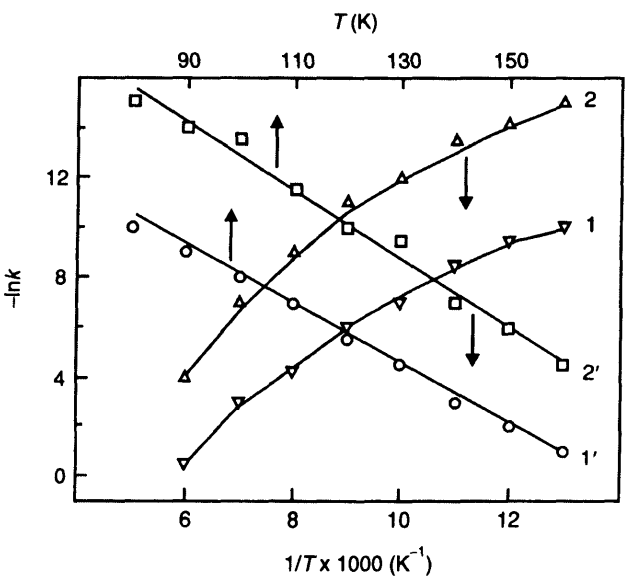

Figure 5.1 Temperature dependencies of $k_{max}(1, 1')$ and $k_{min}(2, 2')$ of CHC decay in PMMA.

coordinated with those of the hydrogen atom abstraction by free radicals in the course of tunnelling [8]. Equation (5.1) represents the temperature dependence in polymers very well, as exhibited in Fig. 5.1. It is important to note that $k(T)$ is in agreement with the tunnelling of the H atom by reaction (2.12) for all numbers of triplet carbenes due to the similarity of the temperature plots for k_{max} and k_{min}. This result is essential in order to understand the cause of non-exponential kinetics. It is likely that this same scattering of the parameters of the hydrogen atom tunnelling causes the rate constant distribution.

It is suggested that some complex incorporating a C–H bond of the matrix and carbene can be formed by analogy with radicals [20,21]:

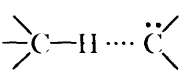

The H atom tunnelling proceeds along the bond in the complex 'molecule + carbene'. Using the model considered and the experimental values of the rate constants, the estimation of height U and width x of the potential barrier of hydrogen atom transfer to diphenylcarbene (DPC) and cyclohexadienone carbene (CHC), have been carried out in the polypiperpylene matrix [39]. In addition, the equilibrium distance R_0 between C–H bonds and carbenes has been determined. The potential barrier was represented for simplicity by the superposition of two potential curves [41] for the C–H bond of macromolecules and radicals resulting from the atom transfer to carbenes (Fig. 5.2):

$$U(r, R_0) = -D\left\{\exp\left[-\frac{\gamma(r - r_0)^2}{2r}\right] + \exp\left[-\frac{\gamma(R_0 - r - r_0)^2}{2(R_0 - r)}\right]\right\} \tag{5.29}$$

In (5.29) r_0 is the C–H bond length, D is the dissociation energy of C–H bonds. This energy is assumed to be the same in molecules and radicals. The parameter γ is determined as follows

$$\gamma = \frac{m\omega_{C-H}^2 r_0}{D} \tag{5.30}$$

The experimental values of α and β in equation (5.1) were used to estimate the limiting parameters of tunnelling. The W_0 value in (5.22) was found from α. The tunnelling probability was calculated from equations (5.18, 5.19, 5.29, and 5.30) at given R_0 and was related to

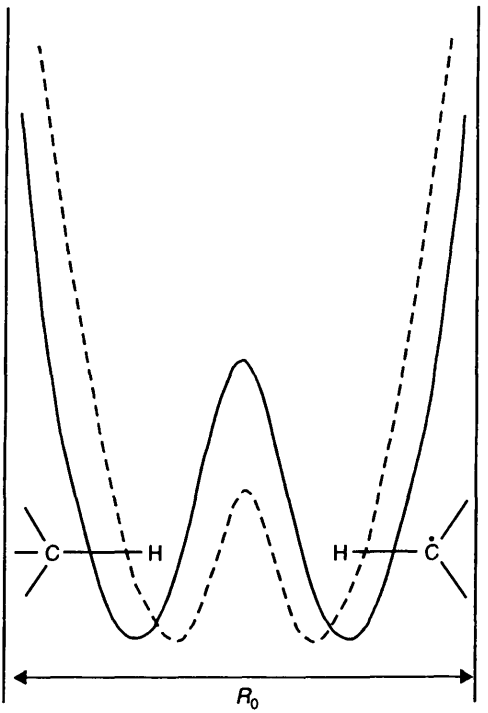

Figure 5.2 Potential energy diagram of hydrogen atom tunnelling through oscillating barrier to triplet carbene.

the experimental W_0. In this manner R_0 values were determined. Table 5.1 lists the results obtained.

From these data it will be noticed that the decrease in the width and height of the potential barrier occurs with increase in temperature.

Table 5.1. Parameters of hydrogen atom tunnelling to CHC and DPC in polypiperylene

Carbene	T(K)	U_{min} (kJ/mol)	U_{max} (kJ/mol)	X_{min} (nm)	X_{max} (nm)	R_{0min} (nm)	R_{0max} (nm)
CHC	$\rightarrow 0$	150	208	0.115	0.140	0.375	0.400
	77	125	150	0.100	0.115	0.375	0.400
	133	108	121	0.094	0.100	0.375	0.400
DPC	$\rightarrow 0$	167	188	0.120	0.130	0.360	0.370
	77	138	159	0.110	0.118	0.360	0.370
	133	121	138	0.103	0.110	0.360	0.370

Increasing the intermolecular oscillation amplitude, as a result of which carbene and C–H bonds of macromolecules approach each other, causes this effect. The hydrogen atom transfer for CHC take place over larger distances than for DPC, while the height and width are somewhat smaller. These data are indicative of more activity of CHC relative to DPC in the H atom abstraction from the matrix. Mention may be made of the proximity of the barrier heights for hydrogen atom tunnelling in reactions of triplet carbenes with macromolecules and also the macroradical recombination by chemical relay transfer of the valence [21].

A correlation of this theory with experimental data was made for reactions of methyl radicals with methanol and ethanol [8]. The correlation procedure includes choosing two fitted parameters R_0, Ω and searching for the values which give the best agreement between the calculated rate constants and experimental ones [33]. Reasonable values were obtained for equilibrium distances between potential wells and oscillation frequencies: $R_0 = 0.366\,\text{nm}$, $\Omega = 3.56 \times 10^{13}\,\text{s}^{-1}$ (methanol) and $R_0 = 0.364\,\text{nm}$, $\Omega = 3.5 \times 10^{13}\,\text{s}^{-1}$ (ethanol). The defined values of Ω coincide in order of magnitude with the Debye frequencies for molecular crystals with rigid bonds $[\omega_D \approx (1.3\text{–}3.5) \times 10^{13}\,\text{s}^{-1}]$. Experimental data concerning hydrogen atom transfer in dimethylglyoxime [42] and in the fluorene-acridine complex [43] have been considered [33]. The decay of radical pairs in dimethylglyoxime crystals, which includes H atom tunnelling, takes place at $R_0 = 0.317\,\text{nm}$ and a Debye frequency $\omega_D = 2.92 \times 10^{13}\,\text{s}^{-1}$. The hydrogen atom transfer from fluorene to the acridine excited molecule occurs at $R_0 = 0.342\,\text{nm}$, $\omega_D = 2 \times 14 \times 10^{13}\,\text{s}^{-1}$ and on the basis of intermolecular oscillations allows the kinetic pattern of solid phase reactions to be described over a wide range of temperatures. This description relates the potential barrier parameters to the structural physical properties of the medium from low to comparatively high temperatures when tunnelling becomes the activation process.

References

1. Lebedev Ya.S., Tsvetkov Yu.D. and Voevodskii V.V. (1960) *Kinetika i kataliz*, **1**, 496.
2. Kiryukhin D.P., Kaplan A.M., Barkalov I.M. and Goldanskii V.I. (1970) *Vysokomolek. Soed.*, **B12**, 491.

3. Kiryukhin D.P., Kaplan A.M., Barkalov I.M. and Goldanskii V.I. (1971) *Doklady Akad. Nauk SSSR*, **199**, 857.
4. Kiryukhin D.P., Kaplan A.M., Barkalov I.M. and Goldanskii V.I. (1992) *Vysokomolek. Soed.*, **A14**, 2115.
5. Goldanskii V.I., Frank-Kamenetskii M.D. and Barkalov I.M. (1973) *Doklady Akad. Nauk SSSR*, **211**, 133.
6. Bell R.P. (1980) *The Tunnel Effect in Chemistry*. London: Chapman and Hall.
7. Goldanskii V.I., Trakhtenberg L.I. and Flerov V.N. (1989) *Tunnelling Phenomena in Chemical Physics*. N.Y.-L.: Gordon and Breach, Science Publ.
8. Le Roy R.J., Murai H. and Williams F. (1980) *J. Am. Chem. Soc.*, **102**, 2325.
9. Sprague E.D. and Williams F. (1971) *J. Am. Chem. Soc.*, **93**, 787.
10. Campion A. and Williams F. (1972) *J. Am. Chem. Soc.*, **94**, 7633.
11. Goldanskii V.I. (1975) *Uspekhi Khimii*, **44**, 2122.
12. McKinnon W.R. and Hurd C.M. (1983) *J. Phys. Chem.*, **87**, 1283.
13. Le Roy R.J. (1980) *J. Phys. Chem.*, **84**, 3508.
14. Goldanskii V.I. (1959) *Doklady Akad. Nauk SSSR*, **124**, 1261.
15. Goldanskii V.I. (1959) *Doklady Akad. Nauk SSSR*, **127**, 1037.
16. Christov St.G. (1961) *Doklady Akad. Nauk SSSR*, **136**, 663.
17. Jortner J. and Ulstrup J. (1979) *Chem. Phys. Lett.*, **63**, 236.
18. Ovchinnikova M.Ya. (1979) *Chem. Phys.*, **36**, 85.
19. Kuntz P.J., Nemeth E.M., Polanyi J.C., Rosner S.D. and Yang C.E. (1966) *J. Chem. Phys.*, **44**, 1168.
20. Klochikhin V.L. and Trakhtenberg L.I. (1978) *Doklady Akad. Nauk SSSR*, **239**, 879.
21. Klochikhin V.L., Pshezhetsky S.Ya. and Trakhtenberg L.I. (1979) *Vysokomolek. Soed.*, **A21**, 2792.
22. Siebrand W., Wildman T.A. and Zgierski M.Z. (1984) *Chem. Phys. Lett.*, **98**, 108.
23. Siebrand W., Wildman T.A. and Zgierski M.Z. (1984) *J. Am. Chem. Soc.*, **106**, 4083.
24. Siebrand W., Wildman T.A. and Zgierski M.Z. (1984) *J. Am. Chem. Soc.*, **106**, 4089.
25. Benderskii V.A., Philipov P.G., Dakhnovskii Yu.I. and Ovchinnikov A.A. (1982) *Chem. Phys.*, **67**, 301.
26. Benderskii V.A., Goldanskii V.I. and Ovchinnikov A.A. (1980) *Chem. Phys. Lett.*, **73**, 492.
27. Misochko E.Ya., Philipov P.G. Benderskii V.A., Ovchinnikov A.A., Barkalov I.M. and Kiryukhin D.P. (1980) *Doklady Akad. Nauk SSSR*, **253**, 163.
28. Klochikhin V.L. and Trakhtenberg L.I. (1983) *Khimich. Fizika*, **2**, 810.

29. Klochikhin V.L. and Trakhtenberg L.I. (1981) *Doklady Akad. Nauk SSSR*, **259**, 399.
30. Klochikhin V.L., Pshezhetsky S.Ya. and Trakhtenberg L.I. (1980) *Zhurn. Fiz. Khimii*, **54**, 1324.
31. Trakhtenberg L.I., Klochikhin V.L. and Pshezhetsky S.Ya. (1981) *Chem. Phys.*, **59**, 191.
32. Trakhtenberg L.I. (1982) *Khimich. Fizika*, **1**, 53.
33. Trakhtenberg L.I. (1995) *Khimich. Fizika*, **14**, 96.
34. Senthilnathan V.P. and Platz M.S. (1980) *J. Am. Chem. Soc.*, **102**, 7637.
35. Senthilnathan V.P. and Platz M.S. (1981) *J. Am. Chem. Soc.*, **103**, 5503.
36. Vorotnikov A.P., Davydov E.Ya. and Toptygin D.Ya. (1984) *Vysokomolek. Soed.*, **B26**, 664.
37. Vorotnikov, A.P., Davydov, E.Ya., Pariyskii G.B. and Toptygin D.Ya (1983) *Khimich. Fizika*, **2**, 818.
38. Korshak V.V., Vorotnikov A.P., Davydov E.Ya., Kozyreva N.M., Kirillin A.I., Skubina S.B. and Toptygin D.Ya. (1986) *Doklady Akad. Nauk SSSR*, **291**, 376.
39. Vorotnikov A.P., Davydov E.Ya. and Toptygin D.Ya. (1985) *Izv. Akad. Nauk SSSR, ser. Khimich.*, 1275.
40. Vorotinikov A.P., Davydov E.Ya and Toptygin D.Ya. (1983) *Izv. Akad. Nauk SSSR, ser. Khimich.*, 1499.
41. Lippincott E.R. and Schroeder R. (1955) *J. Chem. Phys.*, **23**, 1131.
42. Toriyama K., Nunome K. and Iwasaki M. (1977) *J. Am. Chem. Soc.*, **99**, 5823.
43. Prass B., Colpa J.P. and Stehlik D. (1989) *Chem. Phys.*, **136**, 187.

6 THE KINETIC ISOTOPE EFFECT IN SOLID PHASE REACTIONS

Contents

Isotope substitution is important for an explanation of the kinetics of the hydrogen atom abstraction by radicals in the solid phase. This procedure does not change the geometry of the nearest surroundings of the cage. The excess of the kinetic isotope effect (KIE) was to be expected in the low-temperature reactions involving hydrogen atom tunnelling as compared with classic effect resulting from the difference of zero vibration energies of C–H and C–D bonds [1–4]. For example, the 'normal' KIE in the absence of tunnelling is 1.5×10^3 at 77 K for the reaction: $^{\bullet}CH_3 + CH_3CN \rightarrow CH_4 + {}^{\bullet}CH_2CN$. The experimental effect is, however, 20 times greater than that. Measurements of the 2,4,6-t-tretbutyl phenyl radical isomerization rate constant as a result of the intramolecular rearrangement

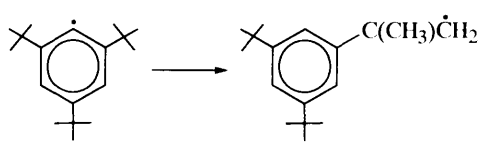

(6.1)

were performed over a wide temperature range from 293 to 123 K [5]. The maximum values of k_H/k_D at 243 K, 173 K and 123 K are

correspondingly 17, 53 and 260 without the tunnelling process for C–H (C–D) bond scissions in accordance with the maximum difference of the H and D atom transfer activation energy: $\Delta E_0 \approx 5.4$ kJ/mol. The experimentally determined relations of k_H/k_D, however, increase from 80 at 243 K to 1.4×10^3 at 173 K and 1.3×10^4 at 123 K.

Nevertheless, the high KIE is not necessarily intrinsic to reactions in the tunnelling mechanism. The low-temperature reaction (77–100 K) of the hydrogen atom with organic substances ($H + RH \rightarrow H_2 + R^{\bullet}$) is one process of this type. KIE for the hydrogen (deuterium) atom abstraction from ethane in xenon is equal to 1 at 4.2 K, 2 at 35 K and 60 at 50 K [6]. This is also the case for hydrogen atom reactions in sulfuric acid glasses [7]. It is conceivable that an unrealistically small KIE in this case is explained by hydrogen atom diffusion, which controls the reaction. Because of this, KIE studies at various temperatures and the matrix isotope composition are carried out using the example of the H atom transfer reactions under the kinetic regime:

$$r^{\bullet} + RH \rightarrow rH + R^{\bullet},$$

where $r^{\bullet}$ is the free radical generated photochemically or by γ-irradiation from the matrix or molecules introduced beforehand.

6.1 The influence of the spatial factor on the kinetic isotope effect in hydrogen atom transfer

The strong dependence of the hydrogen atom transfer probability on the equilibrium distance (R_0) between radicals and matrix C–H bonds is one of the consequences of tunnelling. Equation (5.18) may be written as

$$W(R) = W_0 \exp[-I'(R - R_0)] \tag{6.2}$$

The transfer of a heavy particle (atom) during tunnelling takes place only with nearest neighbours, and the spatial positions of the reacting particles are moderately deflected from the average distance. The quantitative estimation of the tunnelling rate dependence on the distance dispersion has been given in references [8] and [9] by the following example:

$$^{\bullet}CH_3 + CH_3OD \rightarrow CH_4 + {}^{\bullet}CH_2OD \tag{6.3}$$

The kinetics of this reaction are well described by the 'root' law (1.18). This kinetic law was interpreted as a 'polychronal' tunnel process at a particular scale of the intermolecular distance spread. It is assumed for simplicity that the distribution in the variations of the average distances is uniform in the range of ΔR_0

$$\varphi(R) = \begin{cases} 1/\Delta R, & R_0 - (\Delta R_0/2) \leqslant R \leqslant R_0 + (R_0/2) \\ 0, & R < R_0 - (\Delta R_0/2), \quad R > R_0 + (\Delta R_0/2) \end{cases} \tag{6.4}$$

The kinetic equation in terms of (4.4) can be written as follows:

$$N/N_0 = (1/\Delta R) \int_{R_1}^{R_2} \exp\{-W_0 t[\exp - I'(R - R_0)]\} \mathrm{d}R, \tag{6.5}$$

where $R_1 = R_0 + \Delta R_0/2$; $R_2 = R_0 - \Delta R_0/2$.

Equation (6.5) can be represented in another form:

$$N/N_0 = (1/I'\Delta R_0) \int_{x_1}^{x_2} \exp[-\exp(-x)]\mathrm{d}x, \tag{6.6}$$

where $x_1 = -\ln W_0 t - I'\Delta R_0/2$; $x_2 = -\ln W_0 t + I'\Delta R_0/2$.

The principal distinction between above-the-barrier and tunnel reactions is determined by the integration limits in (6.6). They depend, in this case, on the spatial inhmogeneity scale ΔR_0 and the particle mass through I'. The plot calculated from equation (6.6) is a straight line in coordinates of (1.18): $\ln(N/N_0), (W_0 t)^{1/2}$. The optimum value of $I'\Delta R_0$, when the 'root' law shows the best correlation with the linear plot, is equal to 5.5 [8]. Then the distribution width ΔR_0 can be obtained readily with $I' = 7 \times 10^9\,\mathrm{cm}^{-1}$ for the alcohol hydrogenated molecules [9]. Consequently, ΔR_0 is 7×10^{-3}–8×10^{-3} nm.

The situation is different in mixed proton–deuterium matrices. Special experiments were set up to establish the influence of the cage distance dispersion on KIE in the hydrogen atom transfer reactions [10–12]. A model was used to analyze experimental data in which all matrix particles occupy positions at sites in the crystal lattice with equal probability. The probability of the H-containing molecule locating in the given site, is equal to the fraction C. It is suggested that the radical concentration in the matrix varies exponentially (pseudo-first order). The kinetics for the matrix of the mixed isotope

composition will appear as:

$$N(C,t)/N(C,0)=\prod_{i=1}^{n} C\exp(-W_i^{H}t)+(1-C)\exp(-W_i^{D}t)], \quad (6.7)$$

where W_i^{H} and W_i^{D} are probabilities of the H, D atom abstraction (from the molecule occupying the i position in the lattice), n is the number of accessible molecules, and $N(C,t)$ is the radical concentration at the instant of time t in matrix of the composition C. Equation (6.7) is obtained under the assumption that the probability of a reaction with the given molecule does not depend on the filling of other sites. When H-containing sites burn away at a high degree of conversion, the radical decay is described as follows:

$$N(C,t)/N(C,0) = (1-C)^{n}\exp\left(-\sum_{i=1}^{n} W_i^{D}t\right) \quad (6.8)$$

The number of molecules n available for the abstraction reaction can be estimated from (6.8). It is as well to bear in mind that equation (6.7) is appropriate only in the case of equal probability of the $\dot{C}H_3$ radical formation in sites of the distinct isotope composition. Experiments were performed in zinc acetate crystals and acetic acid at 135–160 K to test equation (6.7) and to determine the probability of reactions with molecules sited in different positions with respect to radicals [10,11]. It was found that $n \approx 3$ in these matrices. The values obtained for the transfer probability for C, in the limits 0–0.75 were correlated with the crystallographic data of zinc acetate. The four molecules closest to $\dot{C}H_3$ were found to be inequivalent both in relative orientation and distance. The variation in distance ranges from 0.05 nm to 0.1 nm. The activation energy of the hydrogen atom transfer has an estimated value of 20 kJ/mol, whereas KIE amounts to 600 (160 K) [10]. The small value of the activation energy and the rather high KIE correspond to the tunnelling mechanism. The increase in the distance by 0.05–0.1 nm must be brought close to the decrease in the hydrogen atom transfer probability by 9–17 orders [9]. The experimental probabilities of transfer are changed only by the order ($W_1 = 8.5 \times 10^{-2}\,\text{min}^{-1}$, W_2, $W_3 = 2 \times 10^{-3}\,\text{min}^{-1}$ at 135 K).

A qualitative explanation of the explicit contradiction between the tunnelling character of the reaction and the weak dependence of the transfer probability on distances has been given in [12]. It is believed that the potential energy has a multitude of minimum values for

interaction within the molecule [13]. Each minimum is consistent with the distinct mutual configuration of molecules, and the equilibrium configuration corresponds to the deepest energetic minimum. Fluctuations in the surroundings of the radicals are required in order for a reaction to occur. By this is meant that the system involving a radical and its environment goes through a series of energy minima in its own configuration space. It is assumed that the reaction behaviour does not reduce to a complex vibration process only in the closest environment. It is necessary to consider the lifetime of the reacting system in the potential minimum. If this lifetime is more extended than the D-atom transfer time, it can limit the reaction rate, with the disappearance of some regularities of tunnelling, in particular, the dependence of the tunnelling transfer probability on distance.

The data obtained in studies of KIE for heavy radicals point to the existence of states which precede the transfer act, when it is unlikely that there is a diffusion of radicals. The isotope effect is missing for the decay of $^{\cdot}CH_2CO_2^-$ radicals in partially substituted glycine $ND_3^+CH_2CO_2^-/ND_3^+CD_2CO_2^-$ from reaction [14]:

$$^{\cdot}CH_2CO_2^- + ND_3^+CH_2CO_2^- \rightarrow CH_3CO_2^- + ND_3^+ \, ^{\cdot}CHCO_2^- \quad (6.9)$$

The lack of KIE is observed at 273 K independently of the $ND_3^+CH_2CO_2^-$ mole fraction in the limit 0.33–1. If it is suggested that the realization of intermediate states precedes H atom transfer, the KIE absence can be stipulated by the comparable or longer lifetime of this state in comparison with the time of D transfer. An anomalously low KIE (1.4) was registered during low-temperature hydrobromination of ethylene: $HBr + C_2H_4Br \rightarrow Br + C_2H_5Br$ [15]. Two stages of the reaction were considered to provide the explanation for this fact. The particles approach each other in the first stage, and the H(D) tunnelling to the C_2H_4Br radical takes place in the second stage. If the transfer of particles for a distance d is the limiting stage, the chain propagation rate will be determined by the overlapping factor (F_v) of the HBr, C_2H_4Br nuclear oscillatory wave functions in the initial (i) and final (f) states:

$$F_v \approx \exp\left[-d^2 M \omega_i \omega_f / \hbar(\omega_i + \omega_f)\right], \quad (6.10)$$

where ω is the oscillation characteristic frequency and M is the effective mass of reacting particles. The value of M increases no more than 2.2% in fully deuterated reactants, resulting in a reaction retardation of $\sim 35\%$ according to (6.10). Thus, the dramatic

distinction of KIE is observed in the given case, relative to transfer reactions in which the limiting stage is the atom tunnelling.

6.2 The Kinetic isotope effect and structural relaxation

The kinetics of stepwise reactions in solids can be described in the general case by equation (1.1). Similarly, one can describe the H(D) atom abstraction in mixed matrices involving hydrogenated and deuterated molecules [12]:

$$N(C,t)/N(C,0) \approx \int \varphi(k) \exp(-kCt)\mathrm{d}k, \qquad (6.11)$$

where $k = \Sigma W_i^H$ (see (6.7)), C is the mole fraction of the hydrogenated molecules, $\varphi(k)$ is the 'weight' of sites with the given rate constant. The D atom transfer reaction is not taken into account in (6.11) assuming that KIE is reasonably large. It is seen from (6.11) that the conversion degree is unequivocally connected with the product of Ct. This fact offers a criterion for the distribution by rate constants. In this case, the conversion degree is, exceptionally, the function of Ct irrespective of $\varphi(k)$. The kinetic analysis of methyl radical decay at low temperatures in the mixed crystal matrix of sodium acetate gives a possibile description of this process using (6.11) [16].

However, the kinetic behaviour of radicals was found to be more complicated for similar processes in low-molecular glasses. The distinctive feature of the hydrogen atom abstraction is the kinetic law in the form of

$$N/N_0 = \exp(-kt^{\alpha}), \qquad 0 < \alpha \leqslant 1, \qquad (6.12)$$

where k and α are parameters depending on temperature, matrix and structure of radicals [17, 18]. The α value changes from 0.26 at 20 K to 0.8 at 105 K for the reaction:

$$^{\bullet}CH_3 + CH_3OH \rightarrow CH_4 + {}^{\bullet}CH_2OH \text{ [17]}.$$

It has not always been possible to relate the kinetics of the hydrogen atom abstraction to the rate constant distribution at the matrix dilution by deuterated analogs. Because of this, the coordinates $\ln(N/N_0)$, $(Ct)^{\alpha}$ are not universal for the estimation of the degree of conversion. For example, kinetic plots in alcohol glasses have been considered on the assumption that the rate constant changes with time [19]. By analogy with equation (2.10), the kinetics for the mixed matrix may

be described as

$$N(C,t)/N(C,0) = \exp\left[-C\int_0^t k(t)\mathrm{d}t\right]. \tag{6.13}$$

If the time dependence of the rate constants is approximated by

$$k(t) \sim t^{\alpha-1}, \qquad 0 < \alpha \leqslant 1, \tag{6.14}$$

then equation (6.12) follows from (6.13). The kinetics of the reaction described by (6.13) is different from that determined by the rate constant distribution (6.11). One distinction lies in the other rate dependence on the protonated molecule fraction in the matrix. The experimental criteria for the time dependent rate constant is the straightening of kinetic curves in coordinates $\ln(N/N_0)$, $C\int_0^t k(t)\mathrm{d}t$ or Ct^{α} for $k(t)$ in the form of (6.14).

Conceivable reasons for the decrease in the rate constant with time have been considered [20,21] in the framework of the fractal model [22] having regard to energetic and temporal disorders. According to this model the rate constant may be represented as

$$k = b\mathrm{d}S(t)/\mathrm{d}t, \tag{6.15}$$

where $S(t)$ denotes a number of different reaction cells visited by a random walker on a lattice after time t, and b is the cell volume. For a regular, three-dimensional lattice

$$S(t) \sim t, \tag{6.16}$$

Then the classic time-independent rate constant results from equation (6.15). The random walk model determines the kinetics of reactions in structurally disordered matrices. Temporal disorder is accounted for by a continuous-time random walk which incorporates the distribution function of waiting times into the motion

$$\psi(t) \sim t^{-\alpha-1}, \qquad 0 < \alpha \leqslant 1 \tag{6.17}$$

For three-dimensional lattices

$$S(t) \sim t^{\alpha} \tag{6.18}$$

Fractals are taken to be a measure of the spatial disorder of the solid media and the parameter $S(t)$ for a walker on fractal structures is

$$\begin{aligned} S(t) &\sim t^{\bar{d}/2}, \qquad \bar{d} < 2 \\ S(t) &\sim t, \qquad \bar{d} > 2, \end{aligned} \tag{6.19}$$

where $\bar{d}$ is the dimension of the fractal structure. For a random walk on spaces which exemplify the energetic disorder of the system

$$\begin{aligned} S(t) &\sim t^{\delta}, \qquad \delta < 1 \\ S(t) &\sim t, \qquad \delta > 1, \end{aligned} \tag{6.20}$$

where $\delta = kT \ln b/\Delta$ for consecutive energy levels differing by Δ and for branching ratio b. The same expression for the time dependent rate constant (6.14) reflects kinetic inequivalence in the context of fractal theory in terms of activation energy distribution for thermally activated processes or distributions of barrier height and/or width for tunnelling. A wide diversity of relaxation processes in solids can be described by the Kohlrausch exponential equation [23]

$$\Phi(t) = \exp\left[-(t/\tau_0)^{\beta}\right], \qquad 0 < \beta \leqslant 1 \tag{6.21}$$

If one regards relaxation as a first-order process then the rate coefficient is exactly of the same form as the rate constant (6.14):

$$\varphi(t) = -\frac{\mathrm{d}\Phi(t)}{\mathrm{d}t}\frac{1}{\Phi(t)} = \frac{\beta}{\tau_0}\left(\frac{t}{\tau_0}\right)^{\beta-1} \tag{6.22}$$

The non-equilibrium structure is formed at the radical location site. Such structures can arise, for instance, from the radiation damage of the matrix during the formation and stabilization of radicals under γ-irradiation. It is possible that a chemical reaction follows the relaxation course of the radical surroundings, resulting in the rate constant dependent of time [24].

6.3 The influence of intermolecular oscillations on the kinetic isotope effect

A peculiar characteristic of KIE in the atom transfer reactions has been observed in polymers. A wide distribution of particles in reactivity is a distinctive feature of radical reactions in solid polymers. This feature allows us to determine the dependence of KIE on the reactivity in a wide temperature range as well as giving reasons for the anomalously low isotope effect observed in a series of solid phase reactions. The complicated dependence of KIE on the temperature has come to light in the examination of the decay of diphenylcarbene (DPC) and di-t-butylcyclohexadienone carbene (TBCHC) in PMMA and PS with protonated and fully deuterated macromolecules [25]. Kinetic curves of TBCHC decay are shown in Fig. 6.1. The TBCHC

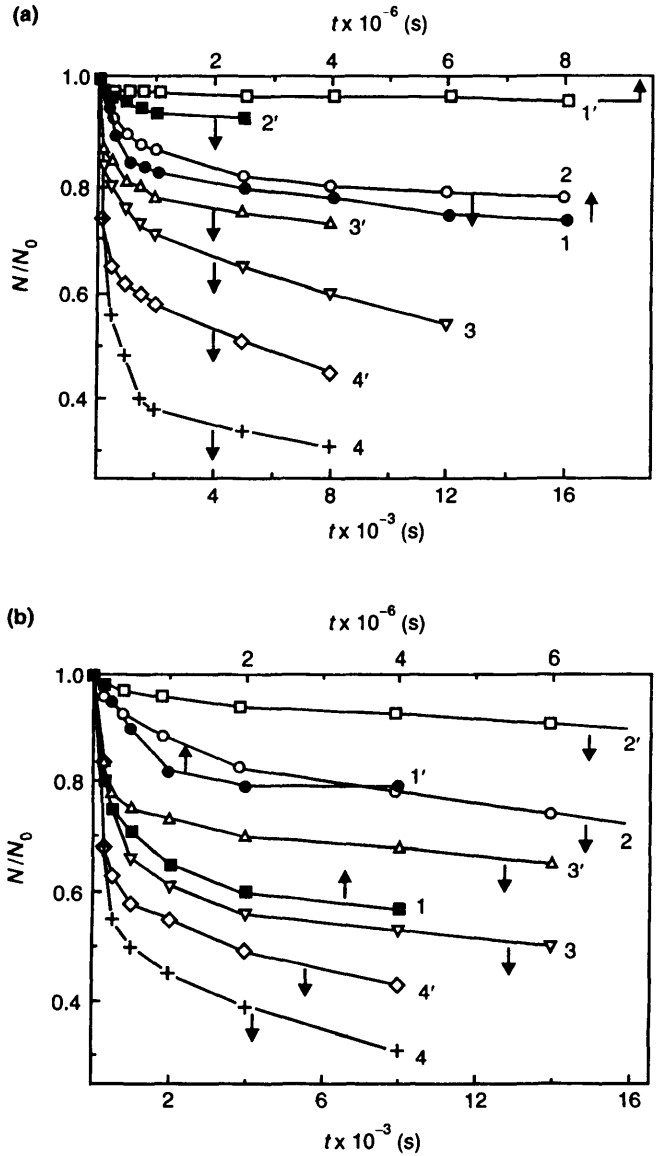

Figure 6.1 Kinetics of TBCHC decay in PS, PS-D_g (a) and PMMA, PMMA-D_g (b) at: (1)(1′) 77 K; (2)(2′) 100 K (3)(3′)115 K; (4)(4′)135 K.

decay at 77 K in deuterated polymers occurs only by up to 20% with a subsequent stop (PMMA-D_g) or not at all (PS-D_g). Carbenes decay in the same time by up to 50% in protonated PMMA and PS. It is notable that initial rates of the carbene decay are coincident in H and D-containing polymers, but later in the process kinetic curves become widely separated. Thus, the clearly defined dependence of the isotope effect on the carbene reactivity is evident. Carbene ensembles with higher rate constants of decay have lower KIE; the isotope effect for the maximum rate constants is virtually nil.

The complicated temperature dependencies of KIE can be explained on the basis of the modified model of tunnelling under the influence of intermolecular oscillations [26]. As a model of the solid phase reaction, the atom transfer is considered from the C–H(D) bond situated in the lattice site 1 to the radical (carbene) in adjacent site 2. The reaction is regarded as a non-adiabatic transfer from the ground state of a parabolic term rigidly bound with C–H(D) bond to the ground state of the same parabolic term bound with the second reactant. This model involves the disturbance of the resonance in energies of the initial and final states (ΔE) which is compensated for by intermolecular vibrations. The pseudo-elementary process of the atom tunnelling from the molecule of the matrix to a radical (carbene) constitutes a two-stage process. At $T < \hbar M\Omega^2/m\omega_{C-H}k$ (M is the effective mass of reactants participating in tunnelling, Ω is the intermolecular oscillation frequency and m is the hydrogen atom mass), the process proceeds as follows: the medium attains the classical transition state with consumption of energy E_r (reorganization energy) following which the tunnelling takes place. Three factors influence the transfer probability: the approach of reactants under intermolecular vibrations, the reorganization of the medium and the energy ΔE transferred by intermolecular vibrations. The respective probability of the hydrogen atom transfer takes the form [26]:

$$W \sim \left[-\frac{(\Delta E - E_r)^2}{4E_r} - \frac{m\omega_{C-H}R_0^2}{2\hbar} + \frac{m^2\omega_{C-H}^2 R_0^2 kT}{2\hbar^2 M\Omega^2} \right], \qquad (6.23)$$

where R_0 is the equilibrium distance between potential wells. The energy of the environmental reorganization is defined by the equation

$$E_r = \frac{1}{2}\sum_{\lambda}(\Delta q_\lambda)^2 \hbar\Omega_\lambda, \qquad (6.24)$$

where λ is the vibration mode of the environment and q_λ is a non-dimensional coordinate. The terms of the initial and final states of the intermolecular vibrations represent, in this case, the identical multi-dimensional parabolas displaced relative to each other in the space of coordinates Δq_λ and by energy ΔE.

At high temperatures $T > \hbar M\Omega^2 m\omega_{C-H}k$; the barrier between potential wells disappears owing to thermal fluctuations, and both the environmental reorganization and atom transfer proceed classically. The isotope effect on the carbene decay was studied by equation (6.23) [27]. In the temperature range

$$\frac{\hbar\Omega}{4k} < T < \frac{\hbar M\Omega^2}{m\omega_{C-H}k}$$

KIE was shown to fall off linearly in accordance with the equation:

$$\ln\frac{k_H}{k_D} = \frac{\theta^{0.5}R_0^2}{2\hbar}(m_D^{0.5} - m_H^{0.5}) - \frac{\theta R_0^2}{2\hbar}(m_D - m_H)\frac{kT}{\hbar M\Omega^2} \qquad (6.25)$$

where $\theta = m_H\omega_{C-H}^2 = m_D\omega_{C-D}^2$ is the parameter characterizing the rigidity of C–H and C–D bonds. At higher temperature $T > \hbar M\Omega^2/km\omega_{C-H}$ KIE varies as T^{-2}:

$$\ln\frac{k_H}{k_D} \approx \frac{\hbar}{2\theta^{0.5}}\left(\frac{1}{m_H^{0.5}} - \frac{1}{m_D^{0.5}}\right)\left(\frac{M\Omega^2R_0}{kT}\right)^2 \qquad (6.26)$$

The relative oscillations of reactants in the complex of the 'C–H(D)-acceptor' are substantially hindered at low temperatures $T \ll \hbar\Omega/4k$, and KIE has only a weak dependence on temperature. The weak dependence of the transfer probability on the mass of the particles is due to fluctuations of the potential barrier [28].

The temperature dependencies of $\ln(k_H/k_D)$ were constructed for various ensembles of carbenes characterized by a conversion degree N/N_0 including KIE for maximum rate constants. These later were determined by the extrapolation of plots $N/N_0 - \ln t$ at $N/N_0 \to 1$. Corresponding plots are shown in Figs. 6.2–6.4. All systems studied differ in the behaviour of KIE with temperature. It has not been possible to measure KIE at $T < 100$ K in PS because of the complete stopping of TBCHC decay in a deuterated matrix. The temperature dependence is adequately described by equation (6.26) at $T > 100$ K (Fig. 6.2). Two portions can be separated in the temperature plot for the same carbene decay in PMMA: linear from 77 K up to 100 K and straight in coordinates of equation (6.26) at $T > 100$ K (Fig. 6.3).

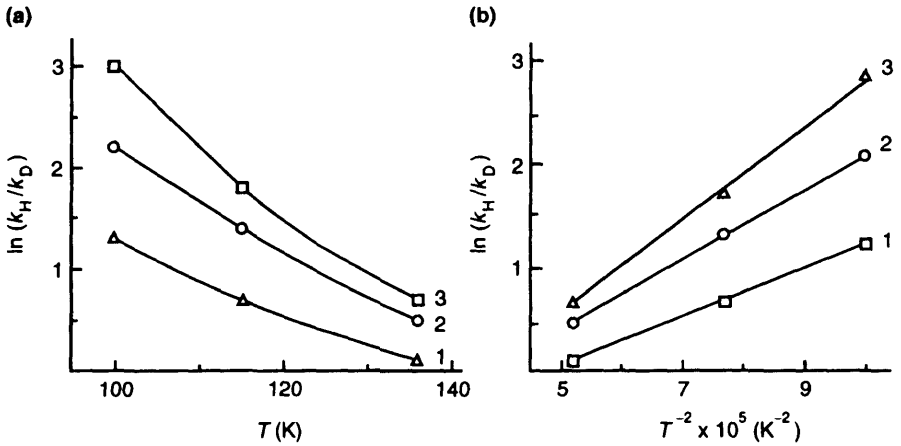

Figure 6.2 Temperature dependencies of KIE on TBCHC decay in PS according to equations (6.25) (a) and (6.26) (b): N/N_0 = (1) 1; (2) 0.8; (3) 0.7.

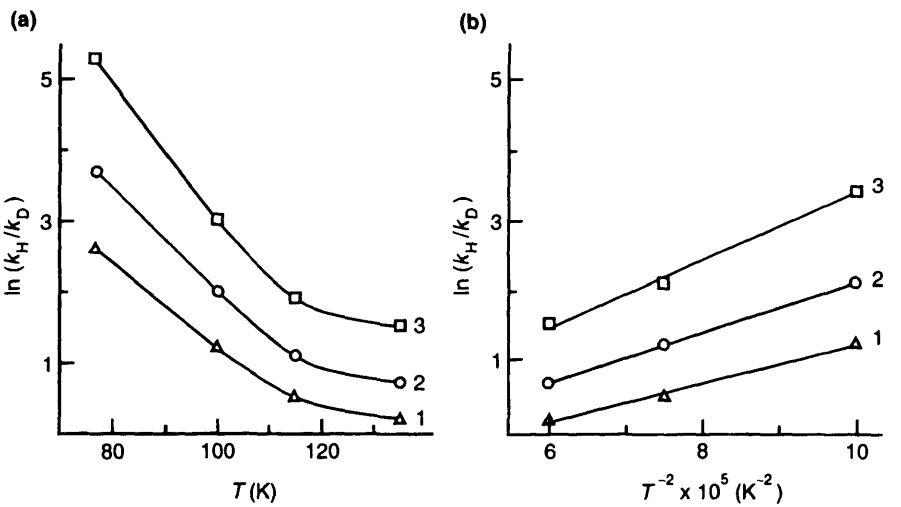

Figure 6.3 Temperature dependencies of KIE on TBCHC decay in PMMA according to equations (6.25) (a) and (6.26) (b): N/N_0 = (1) 1; (2) 0.8; (3) 0.6.

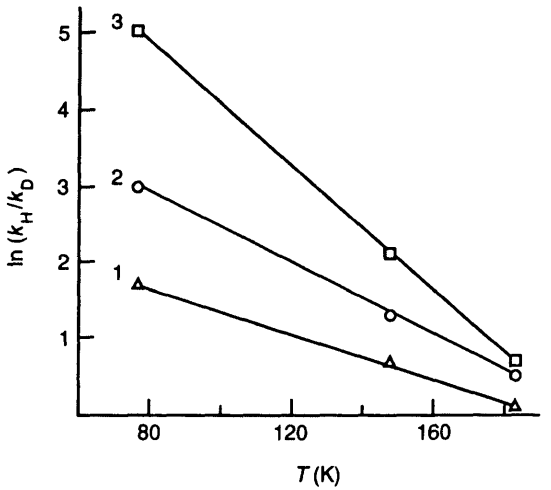

Figure 6.4 Temperature dependencies of KIE on DPC decay in PMMA according to equation (6.25): N/N_0 = (1) 1; (2) 0.8; (3) 0.5.

Such a run of KIE temperature dependence makes it possible to estimate the frequencies of intermolecular oscillations, which activate the hydrogen atom transfer to a triplet carbene in PMMA. Going from the linear portion to that described by the T^{-2} law

$$T \approx \frac{\hbar M \Omega^2}{m\omega_{C-H}k},$$

we obtain $\Omega \approx 52\,\text{cm}^{-1} \approx 10^{13}\,\text{s}^{-1}$ taking into consideration the effective mass of the reaction complex incorporating the PMMA monomer link. The value obtained is in agreement with Debye frequencies of a molecular crystal [29].

The isotope effect on the thermal decay of DPC in PMMA is linearly changed with temperature increase from 77 K, that is, the high-temperature limit of the transformation of (6.25) into (6.26) is not observed throughout the studied temperature range (Fig. 6.4). This fact may be explained by the higher frequency of intermolecular oscillations and, consequently, greater rigidity of the bond in the DPC-PMMA complex in comparison with TBCHC-PMMA. The value of the lower limit of frequency was determined by equation (6.25). Since $\ln(k_H/k_D) \approx 0$ for maximum rate constant at 183 K, $\Omega \geqslant 2 \times 10^{13}\,\text{s}^{-1}$. Thus, the intermolecular oscillation frequency in the DPC-PMMA complex is at least twice that in TBCHC-PMMA. It

must be emphasized that equations (6.25) and (6.26) were deduced from the model in which a reaction is considered as the non-radiating transfer from the ground state of C–H bond to the ground state of the hydrogen atom acceptor [26]. It is apparent that this approximation is fairly rough, because the exchange interaction can be quite significant in chemical reactions, and thus terms of the initial and final states can be considerably distorted.

The difference in distances between potential wells for the transfer reaction of the carbene ensembles with distinct reactivity ΔR_0 was determined by the experimental temperature dependencies of KIE [27]. It is interesting to compare these values and the rate constants of

Table 6.1. The dependence of the rate constants of TBCHC and DPC decay in PMMA and PMMA-D_g on the change of equilibrium distances in complex 'C–H-carbene'

Carbene	T(K)	$\psi = N/N_0$	$\Delta R_0 = R_0^{\psi} - R_0^{\psi=1}$(nm)	$-\lg k_H$	$-\lg k_D$
TBCHC	77	1.0	0	4.0	5.0
	100			2.7	3.3
	115			1.7	1.8
	131			0.6	0.6
	77	0.8	6×10^{-3}	5.0	6.4
	100			3.6	4.4
	115			2.6	2.9
	131			1.4	1.6
DPC	77	0.6	1.3×10^{-2}	6.2	7.9
	100			4.6	5.6
	115			3.4	3.9
	131			2.3	2.6
	77	1.0	0	4.0	4.9
	148			0.9	1.3
	183			−0.9	−0.9
	77	0.8	1.2×10^{-2}	5.0	6.3
	148			1.7	2.3
	183			0.4	0.5
	77	0.5	2.7×10^{-2}	6.7	8.6
	148			2.9	3.9
	183			1.3	1.6

the carbene decay of the same kinetic ensembles. The estimation of ΔR_0 for TBCHC and DPC in PMMA was found by the extrapolation of linear portion plots $\ln(k_H/k_D)_T$ shown in Figs. 6.3 and 6.4 at $T \rightarrow 0$. The results obtained are listed in Table 6.1.

As can be seen the decrease of the rate constant of TBCHC decay by orders of magnitude is consistent with the increase in the distance between potential wells of 0.006 nm. This value for DPC is about two-fold. The sharp dependence of the reaction rate on distances is in good agreement with hydrogen atom tunnelling from the C–H bond of macromolecules to carbenes. The ΔR_0 values obtained for carbene decay correspond to those of the typical tunnel reaction of the H atom abstraction by methyl radicals in frozen alcohol and acetonitrile having regard to a dispersion of the distances between the reactants [8, 30]. Thus, the temperature dependence of KIE in the reaction of triplet carbenes appears explicable on the basis of the tunnelling model of the oscillating potential barrier. The results of KIE investigations discussed above support the kinetic features of the low-temperature elementary process of atom transfer.

References

1. Sprague E.D. (1977) *J. Phys. Chem.*, **81**, 516.
2. Sprague E.D. and Williams F. (1971) *J. Am. Chem. Soc.*, **93**, 787.
3. Takeda K., Wang J.T. and Williams F. (1974) *Can. J. Chem.*, **52**, 2840.
4. Wang J.T. and Williams F. (1972) *J. Am. Chem. Soc.*, **94**, 7633.
5. Brunton G., Griller D., Barclay L.R.C. and Ingold K.U. (1976) *J. Am. Chem. Soc.*, **98**, 6803.
6. Toriyama K., Nunome K. and Iwasaki M. (1980) *J. Phys. Chem.*, **84**, 2374.
7. Dainton F.S., Holf B.J., Philipson N.A. and Pilling M.J. (1976) *J. Chem. Soc. Farad. Trans. I*, **72**, 257.
8. Burshtein A.I., Klochikhin V.L. and Trakhtenberg L.I. (1984) *Khimich. Fizika*, **3**, 155.
9. Trakhtenberg L.I., Klochikhin V.L. and Pshezhetsky S.Ya. (1982) *Chem. Phys.*, **69**, 121.
10. Syutkin V.M. and Tolkatchev V.A. (1985) *Chem. Phys.*, **95**, 115.
11. Syutkin V.M. and Tolkatchev V.A. (1989) *Khimich. Fizika*, **8**, 93.
12. Tolkatchev V.A. (1991) *Khimich. Fizika*, **10**, 1207.
13. Ovchinnikov A.A. and Onistchuk V.A. (1984) *Khimich. Fizika*, **3**, 511.
14. Syutkin V.M. and Tolkatchev V.A. (1985) *Chem. Phys. Lett.*, **122**, 201.

15. Zanin A.M., Kiryukhin D.P., Barkalov I.M. and Goldanskii V.I. (1980) *Doklady Akad. Nauk SSSR*, **253**, 142.
16. Syutkin V.M. and Tolkatchev V.A. (1985) *React. Kinet. Catal. Lett.*, **29**, 417.
17. Vyazovkin V.L., Bolshakov B.V. and Tolkatchev V.A. (1983) *Chem. Phys.*, **75**, 11.
18. Plonka A. (1986) *Lecture notes in chemistry*, Heidelberg, N.Y., L., Paris, Toronto: Springer-Verlag, p. 151.
19. Zaskulnikov V.M., Vyazovkin V.L., Bolshakov B.V. and Tolkatchev V.A. (1981) *Int. J. Chem. Kinet.*, **13**, 707.
20. Plonka A. and Paszkiewicz A. (1992) *J. Chem. Phys.*, **96**, 1128.
21. Plonka A. (1991) *Rad. Phys. Chem.*, **37**, 411.
22. Blumen A., Klafter J. and Zumofen G. (1986) in *Fractals in Physics*, Ed. Pietronero L. and Tosatti E., Amsterdam, Elsevier.
23. Williams G. and Watts D.C. (1970) *Trans. Faraday Soc.*, **66**, 80.
24. Tolkatchev V.A. (1987) *Chem. Phys.*, **116**, 283.
25. Korshak V.V., Vorotnikov A.P., Davydov E.Ya., Kozyreva N.M., Kirillin A.I. and Skubina S.B. (1986) *Doklady Akad. Nauk SSSR*, **291**, 376.
26. Klochikhin V.L. and Trakhtenberg L.I. (1983) *Khimich. Fizika*, **2**, 810.
27. Davydov E.Ya., Vorotnikov A.P., Pustoshnyi V.P. and Zaikov G.E. (1997) *Int. J. Polym. Mater.*, **37**, 75.
28. Benderskii V.A., Goldanskii V.I. and Makarov D.E. (1990) *Doklady Akad. Nauk SSSR*, **311**, 626.
29. Doba T., Ingold K.U., Siebrand W. and Wildman T.A. (1985) *Chem. Phys. Lett.*, **115**, 51.
30. Trakhtenberg L.I., Klochikhin V.L. and Pshezhetsky S.Ya. (1981) *Chem. Phys.*, **59**, 191.

7 KINETICS OF PHOTOINITIATED REACTIONS IN SOLIDS

Contents

A photoinitiated chemical process involves a succession of physical and chemical stages resulting from light absorption. Any drastic impedance in the molecular motion has a profound impact on the efficiency of the photochemical processes by virtue of the kinetic inequivalence of the reacting particles in the solid phase. The kinetics of the chemical reactions is controlled in these conditions on one hand by the distribution particles in reactivity and on the other by relaxation processes in the matrix. As mentioned in Chapter 6, the nature of non-exponential kinetics cannot often be determined even for elementary thermal reactions. The investigation of photochemical reactions allows us, in specific cases, to consider the influence individually, of these two factors on kinetics.

7.1 Application of the free volume model to estimations of the photochemical process efficiency

The cage effect plays an important role in photochemical processes proceeding in the solid phase [1]. By virtue of the fact that absorbed

quantum energy usually exceeds the energy of the chemical bond dissociation, the radical pair formed has an excess of energy which provides the radical yield from the cages. Rigid surroundings impede the exit from the cages and increase the probability of the radical back recombination. The theoretical consideration of the cage effect, depending upon the media viscosity, absorbed light energy and sizes of radicals in the course of photolysis has been carried out only for the liquid phase [2,3]. The problem of the estimation of the cage effect in solid phase reactions reduces to the determination of macroscopic parameters, which are characteristics of the matrix properties. To estimate the cage effect, the quantum yield of stabilized radicals Φ_R was been proposed [4]. This parameter can be determined experimentally, relatively simply, by the ESR technique. The calculation of the cage effect during the photodecomposition of molecules is based on the following assumptions. The probability of the radical yield from cages is equal to that of the free volume ν_f, located adjacent to the original molecule with $\nu_f \gg \nu_R$, where ν_R is the volume of the radical, coming out of the cage. The probability of the radical yield from the cage is related quantitatively to Φ_R. In [4] the expression for the quantum yield of stabilized radicals was derived from the free volume theory [5]:

$$\Phi_R = \exp(-\nu_R/\bar{\nu}_f), \tag{7.1}$$

where $\bar{\nu}_f$ is the equilibrium free volume per matrix molecule. The $\bar{\nu}_f$ value may be calculated using the equation:

$$\bar{\nu}_f = Mf/\rho N_A, \tag{7.2}$$

where M is the molecular weight, ρ is the matrix density, N_A is the Avogadro number and f is the free volume fraction. The f value was calculated in terms of the Doolittle empirical equation [6] linking the media viscosity, the Van der Waals volume of the molecules and the free volume. The following expression was obtained [4]:

$$f = (2.3 \ln \eta + 12.4)^{-1}, \tag{7.3}$$

where η is the viscosity. It was shown that equations (7.1–7.3) are valid for glassy matrices of diethylcarbinol, isopropanol, 4-methylheptane and 3-methylpentane.

The feasibility of equation (7.1) to estimate a quantum yield in the low-temperature photochemical processes has been shown by the example of the photodissociation of acyl radicals (HCO, CH_3CO,

C_2H_5CO, i-C_4H_9CO) at 77 K [7]. If the acyl radical dissociation is limited by mutual separation of the alkyl radical and CO, the dependence (7.1) in the form of $\ln \Phi_R = \nu_R/\bar{\nu}_f$ would appear as a curve, since starting from $\nu_R > \nu_{CO}$ the reaction effectiveness would be determined solely by CO diffusion. It was shown that the experimental values of Φ_R in photodissociation processes are satisfactorily described in terms of the free volume model.

Formula (7.1) ignores the photon energy influence on the Φ value, while the Φ growth was observed with as increasing in the absorbed quantum energy, in all cases where such influence has been studied [4]. The simple empirical relationship taking into account the dependence of quantum yield on the photon energy was proposed in reference [8]. The photon energy calculation was conducted on the following assumptions. The exit of particles from cages involves some energy to overcome the potential barrier. The free volume, residing close to the dissociated molecule, uniquely defines the value of the potential barrier, and this value is a monotonically decreasing function of the photon energy. The exit from cages takes place on condition that a difference in the photon and dissociation energies exceeds the potential barrier. It was shown [8] that the following relation is valid for the same photodissociation process on irradiation by different light:

$$\frac{\ln \Phi_1}{\ln \Phi_2} = \left(\frac{h\nu_1 - D}{h\nu_2 - D}\right)^{1/2}, \tag{7.4}$$

where D is the bond dissociation energy. The difference in the calculated magnitude of Φ and its experimental value does not exceed four times. For example, Φ_{exp} and Φ_{calc} amount respectively to 6.5×10^{-2} and 8.9×10^{-2} for the H_2O_2 photodecomposition in isopropanol. For the $(CH_3)_2N_2$ photodecomposition $\Phi_{exp} = 4 \times 10^{-5}$, $\Phi_{calc} = 1.8 \times 10^{-4}$ [8].

7.2 Kinetic inequivalence in photochemical reactions

The use of the free volume model to estimate the effectiveness of the photochemical reaction assumes that the quantum yield is constant for the duration of the process. The optical density D of photodecomposing molecules is linearly proportional to the absorbed light dose Δ:

$$D/D_0 = 1 - \Phi\Delta/D_0 \tag{7.5}$$

The dose is calculated using the light intensity I_0:

$$\Delta(t) = I_0 \int_0^t (1 - 10^{-D})dt \tag{7.6}$$

For the most part, the non-linear plot of D on Δ is observed for the solid phase photochemical reactions, especially at low temperatures. The general reason for the non-linear appearance may be the distribution of molecules by the Φ value, due to the structural inhomogeneity of the local surroundings. The influence of the kinetic inequivalence of particles on the photochemical process kinetics was first discovered during the photo-oxidation of the aromatic hydrocarbons with condensed rings in solid polymers [9,10]. The photo-oxidation proceeds with the participation of singlet oxygen and represents a multi-stage process:

$$\begin{aligned}
&A + h\nu \longrightarrow A^* + {}^TA \\
&{}^TA + {}^3O_2 \xrightarrow{k_0} A + {}^1O_2 \\
&{}^TA + {}^3O_2 \xrightarrow{k_{r0}} AO_2 \\
&A + {}^1O_2 \xrightarrow{k_r} AO_2 \\
&Q + {}^1O_2 \xrightarrow{k_q} {}^3O_2 \\
&{}^1O_2 \xrightarrow{k_d} {}^3O_2,
\end{aligned} \tag{7.7}$$

where A, A^* and ${}^TA$ are aromatic molecules in the ground, excited and triplet states; ${}^3O_2$ and ${}^1O_2$ are oxygen molecules in the ground triplet and singlet states. A detailed kinetic analysis of aromatic hydrocarbon photo-oxidation has been carried out in reference [11]. The kinetic relation obtained in accordance with the acting mass law takes the form

$$\frac{d[A]}{dt} = \alpha\left\{1 - \gamma\left[1 - \frac{(k_r/k_d)[A]}{1 + (k_r/k_d)[A] + (k_q/k_d)[Q]}\right]\right\}[A], \tag{7.8}$$

where α is the light intensity-dependent constant, $\gamma = k_0/(k_0 + k_{r_0})$ is the probability of the singlet oxygen yield to volume. Equation (7.8) represents the kinetics only in conditions of sufficiently mobile media. The initial stage of a process only may be approximated by this equation in solid polymers at $T < T_g$; the photo-oxidation is retarded

appreciably faster and this follows from (7.8). The assumption of the inequivalence of the surroundings of molecule A has been put forward to explain the kinetics observed. This inequivalence is concerned with the different penetration of surrounding cells with respect to singlet oxygen. A penetration is characterized by the parameter U. This value is distinct for different molecules and remains constant throughout the process. In the context of these assumptions, the kinetic dependence is determined by the distribution $\rho(U)$ of molecules A in cells with a different penetration. Then the kinetic equation is written as

$$\frac{\mathrm{d}[\mathrm{A}]}{\mathrm{d}t} = -(\alpha I_1 + k_1 I_2[{}^1\mathrm{O}_2])k_3[\mathrm{A}], \tag{7.9}$$

where

$$I_1 = \int \frac{\rho(U)\mathrm{d}U}{k_2 U + k_3}, \; I_2 = \int \frac{U\rho(U)\mathrm{d}U}{k_2 U + k_3},$$

k_1 and k_2 are rate constants of elementary acts, respectively, of the formation and decomposition of the pair $[{}^1\mathrm{O}_2 \cdots \mathrm{A}]$ and k_3 is the rate constant of oxidation in these pairs. The equation describing the photo-oxidation kinetics to deep conversions at steady state relative to the ${}^1\mathrm{O}_2$ concentration has the following form:

$$\frac{\mathrm{d}[\mathrm{A}]/[\mathrm{A}]_0}{\mathrm{d}t} = -\alpha k_3 I_1 - \frac{\alpha k_1 k_2 k_3 I_2^2 [\mathrm{A}]_0}{k_1 k_3 I_2 [\mathrm{A}]_0 + k_d} \tag{7.10}$$

The kinetic inequivalence was detected for inevitable photochemical processes involving particles in the triplet state [13]. These processes cannot be completely suppressed using the triplet state quenchers. So the benzophenone photoreduction in PMMA by the reaction

$${}^{\mathrm{T}}\mathrm{A} + \mathrm{RH} \rightarrow {}^{\cdot}\mathrm{AH} + {}^{\cdot}\mathrm{R} \tag{7.11}$$

is retarded by oxygen less effectively than the phosphorescence quenching. The usual relationship

$$\Phi = \frac{k_r RH}{k_r RH + k_f + k_d}, \tag{7.12}$$

where k_r, k_f and k_d are rate constants of the chemical interaction, phosphorescence and other methods of de-activation, does not determine the quantum yield in this case. The integral over all

possible states, rather than (7.12), should be written as:

$$\Phi = \int \frac{k_r(U)\rho(U)\mathrm{d}URH}{k_r(U)RH + k_s(U) + k_d(U)}, \tag{7.13}$$

where U is the kinetic parameter determining the inequivalence of benzophenone molecules, $\rho(U)$ is the distribution density of the probability of finding the molecule with U. Instead of the straight line in coordinates of the Stern–Volmer equation [14], Φ_0/Φ, P_{O_2} the following equation $\Phi_0/\Phi = 1 + \tau k_q O_2$, can be written:

$$\Phi_0/\Phi = \int \frac{k_r(U)\rho(U)\mathrm{d}URH}{k_r(U)RH + k_f(U) + k_d(U)} \Bigg/ \int \frac{k_r(U)\rho(U)\mathrm{d}URH}{k_r(U)RH + k_q(U)O_2 + k_d(U)} \tag{7.14}$$

As experiment shows [13], oxygen quenches the phosphorescence twice as effectively as the benzophenone photoreduction by reaction (7.11). Thus, the non-Stern–Volmer behaviour of the quantum yield arises from the benzophenone kinetic inequivalence.

The examples of photochemical processes with the active molecule distribution in reactivity, discussed above, represent reasonably complicated systems of consecutive and parallel reactions. A correlation of the distribution parameters with specific stages of these processes, presents difficulties. The introduction of $\rho(U)$ [11,13] into the kinetic dependencies seems to be a rather formal approach. In this connection, the investigations of the kinetic features of pseudo-elementary photochemical reactions are of interest to elucidate the peculiarities of molecular organization at the cage level. A series of works concerned with the kinetics of iron chloride photoreduction in solid polymers has been carried out along these lines [15–18]. The iron chloride in polymers is in the form of chloride complexes $FeCl_2^+$ and $FeCl_4^-$, which have different bands of UV absorption with different extinction coefficient, ε. The intensity of the $FeCl_2^+$ band ($\lambda_{max} = 340$ nm) is several times lower than that of $FeCl_4^-$ ($\lambda_{max} = 313, 365$ nm) [19]. The iron chloride photoreduction in the solid phase may be represented as follows [16]

$$Fe^{3+}Cl_n^{n-} \underset{\overleftarrow{k_1}}{\overset{h\nu(\varphi_0)}{\longrightarrow}} [Fe^{2+}Cl_{n-1}{}^{(n-1)-} \cdots Cl] \xrightarrow{k_2} Fe^{2+}Cl_{n-1}{}^{(n-1)-} + Cl, \tag{7.15}$$

where φ_0 is the quantum yield of the intermediate state formation, k_1 is the rate constant of the back conversion of the intermediate state into the original chloride complex and k_2 is the rate constant of the chlorine atom migration from cages. In view of the fact that the photoactive form is $FeCl_4^-$; the rate of iron chloride photoreduction will look like:

$$-\frac{d[FeCl_4^-]}{dt} = \frac{\Phi}{l} I_0 (1 - 10^{-\varepsilon [FeCl_4^-] l}), \tag{7.16}$$

where $\Phi = \varphi_0 k_2/(k_1 + k_2)$ is the quantum yield of photoreduction determined experimentally, I_0 is the UV light intensity and l is the sample (film) thickness. The integration of (7.16) gives a kinetic equation in the form of (7.5).

The kinetics of the $FeCl_4^-$ photolysis in PMMA at 77 K is shown in Fig. 7.1. As can be seen from the figure, the kinetics are not described by equation (7.5) at low temperatures. This fact has been explained in [16] by the Φ spread. The form of this distribution is given by the following expression:

$$\Phi = \frac{\varphi_0 k_2}{k_1 + k_2} = e^s, \tag{7.17}$$

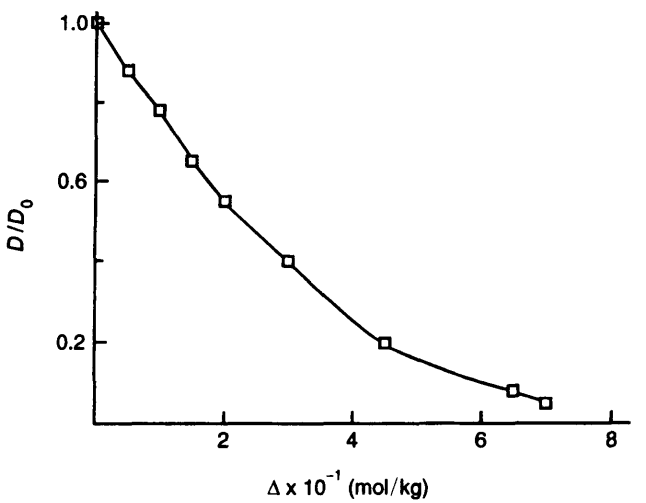

Figure 7.1 Kinetics of the optical density change in PMMA with iron chloride at 77 K under action of light with $\lambda = 365$ nm in coordinates of equation (7.5).

where S is the parameter distributed uniformly in the range from S_1 to S_2 which corresponds to Φ_{min} and Φ_{max}. The availability of the distribution (7.17) is associated with the two thermal stages of the unified process: the cage recombination into $FeCl_4^-(k_1)$ and the Cl atom exit from the cage (k_2). The physical structure of the cage surroundings apparently has a strong action on these stages. The polymer sample constitutes a number of sites in which the reaction rates differ over a wide range. The kinetics in each site are governed by equation (7.5). Then the optical density change in the early stages of the process, when $FeCl_4^-$ is present over all sites ($\Phi_{max}\Delta < [FeCl_4^-]_0$), will be linear in the irradiation dose:

$$\frac{D}{D_0} = \frac{1}{S_2 - S_1}\int_{S_1}^{S_2}(1 - e^S\Delta/[FeCl_4^-]_0)dS$$
$$= 1 - \frac{(e^{S_2} - e^{S_1})\Delta}{(S_2 - S_1)[FeCl_4^-]_0} = 1 - \frac{\bar{\Phi}\Delta}{[FeCl_4^-]_0}, \tag{7.18}$$

where $\bar{\Phi}$ is the average quantum yield. Later in the process, when ($\Phi_{max}\Delta > [FeCl_4^-]_0$), the kinetics is expressed by the equation:

$$\frac{D}{D_0} = \frac{1}{S_2 - S_1}\int_{S_1}^{\ln([FeCl_4^-]_0/\Delta)}(1 - e^S\Delta/[FeCl_4^-]_0)dS$$
$$= \frac{1}{S_2 - S_1}\left(\ln\frac{\Delta}{[FeCl_4^-]_0} + S_1 + \frac{e^{S_1}\Delta}{[FeCl_4^-]_0} + 1\right) \tag{7.19}$$

Expression (7.19) becomes a straight line in coordinates D/D_0, $\ln(\Delta/[FeCl_4^-]_0)$ at small term $e^{S_1}\Delta/[FeCl_4^-]_0$.

$$\frac{D}{D_0} = -\frac{(S_1 + 1)}{S_2 - S_1} - \frac{\ln(\Delta/[FeCl_4^-]_0)}{S_2 - S_1} \tag{7.20}$$

The experimental kinetics at 77 K and 293 K plotted in coordinates of (7.19) is given in Fig. 7.2. The values of Φ_{max}, Φ_{min}, $\ln(\Phi_{max}/\Phi_{min})$ defined from these dependencies are listed in Table 7.1.

Iron chloride photoreduction can reveal the kinetic features of photochemical reactions in solids because the chlorine atoms generated by reaction (7.15) are converted into macroradicals: $Cl + RH \rightarrow HCl + R^{\cdot}$. This provides the possibility of correlating distributions of photoactive particles in the reactivity obtained by two independent techniques. The kinetics of the accumulation of

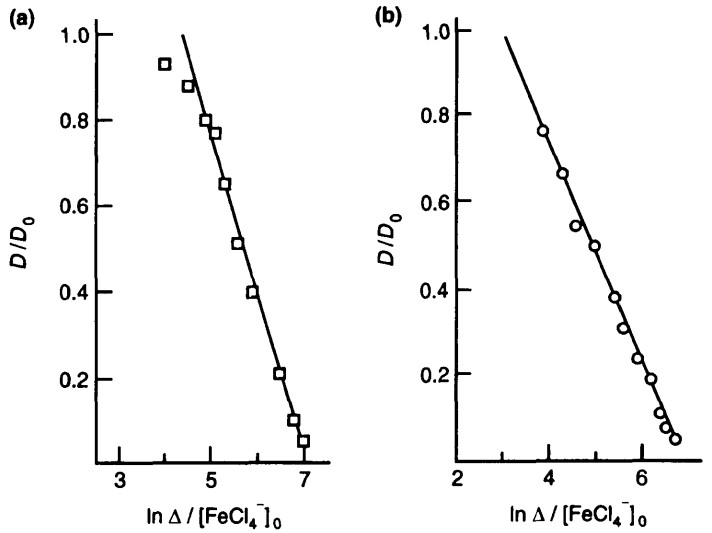

Figure 7.2 Kinetics of the optical density change in PMMA with iron chloride during photolysis at 77 K (a) and 293 K (b) in coordinates of equation (7.21).

Table 7.1. Quantum yields of the iron chloride photolysis in PMMA, $[FeCl_3]_0 = 0.137$ mol/kg

T(K)	λ(nm)	$\bar{\Phi} \times 10^3$	$\Phi_{min} \times 10^4$	$\Phi_{max} \times 10^3$	$\ln(\Phi_{max}/\Phi_{min})$
77	365	1.6	2.5	4.7	3
293	365	2.0	1.2	8.5	4
77	313	3.8	5.6	11	3
293	313	4.8	3.3	19	4
77	405	1.1	1.8	3.1	3

radicals during the low-temperature photolysis of initiators can be described as

$$[R] = \Phi^* \Delta, \tag{7.21}$$

where Φ^* is the quantum yield of radical formation. The parameters S_1^* and S_2^* of the Φ^* distribution were estimated from the relation $\Phi^* = e^s$ [16,18]. With this condition, the linear law of the radical

accumulation can be obtained in the initial stage.

$$[\mathrm{R}] = \frac{1}{S_2 - S_1}\int_{S_1}^{S_2} \Phi^* \Delta \mathrm{d}S \approx \frac{\Phi^*_{\max}\Delta}{S_2 - S_1} = \bar{\Phi}^*\Delta \qquad (7.22)$$

Later in the process, the kinetics of the radical formation are linearly connected with the logarithm of the absorbed light dose on the condition that $e^{S_1}\Delta$ is small:

$$\frac{[\mathrm{R}]}{[\mathrm{R}]_{St}} = \frac{1 + S_2}{S_2 - S_1} + \frac{\ln(\Delta/[\mathrm{R}]_{St})}{S_2 - S_1}, \qquad (7.23)$$

where $[\mathrm{R}]_{St}$ is the limiting concentration of radicals. Experimental kinetic plots of macroradical formation in PMMA during iron chloride photoreduction are shown in Fig. 7.3. Equation (7.23) governs the kinetics aside from the initial stage (~15%). The distribution width $(S_2 - S_1)$ from quantum yields of chlorine atoms, amounts to 2.9. This value is equal to the distribution width of Φ for

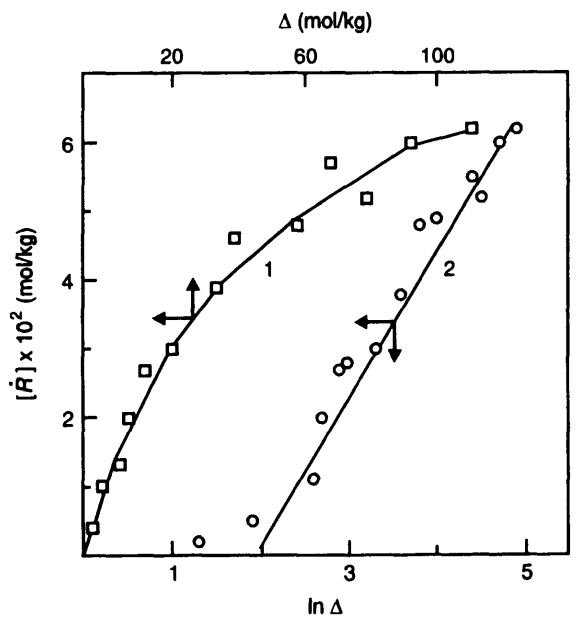

Figure 7.3 Kinetics of macroradical formation in PMMA at 77 K during iron chloride photoreduction in coordinates of equations (7.22) (1) and (7.23) (2).

the $FeCl_4^-$ photoreduction; $\Phi^*_{max} = 3.8 \times 10^{-3}$. Thus, experimental results may be quantitatively described in the context of the exit of chlorine atoms from cages.

The nature of the iron chloride kinetic inequivalence was supported by photolysis of the specifically prepared initiator $FeCl_4N(C_2H_5)_4$ (I), which contains one type of chloride complex: $FeCl_4^-$ [18]. The possibility of mutual transformations of $FeCl_2^+$, $FeCl_4^-$ and Fe_2Cl_6, resulting from dissolving iron chloride in PMMA, was therefore excluded. It turns out that the kinetics of (I) photolysis is controlled by the same equations (7.18) and (7.20). However, the $\bar{\Phi}$ value for (I) is two to three times as large as that for iron chloride, which seems to imply that both additives have a dissimilar influence on the plasticity of the polymer matrix.

The distribution by quantum yields of $FeCl_3$ photolysis in PMMA at 77 K and 293 K is due to the matrix rigidity ($T_g = 370$ K). To examine the role of molecular motion in photoreduction kinetics, similar experiments were performed in polypropylene ($T_g = 256$ K) at 77 K and room temperature [17]. As illustrated in Fig. 7.4, the $FeCl_4^-$ consumption occurs almost completely with a constant quantum yield at 293 K. The value of $\Phi = 1.7 \times 10^2$ is nearly tenfold

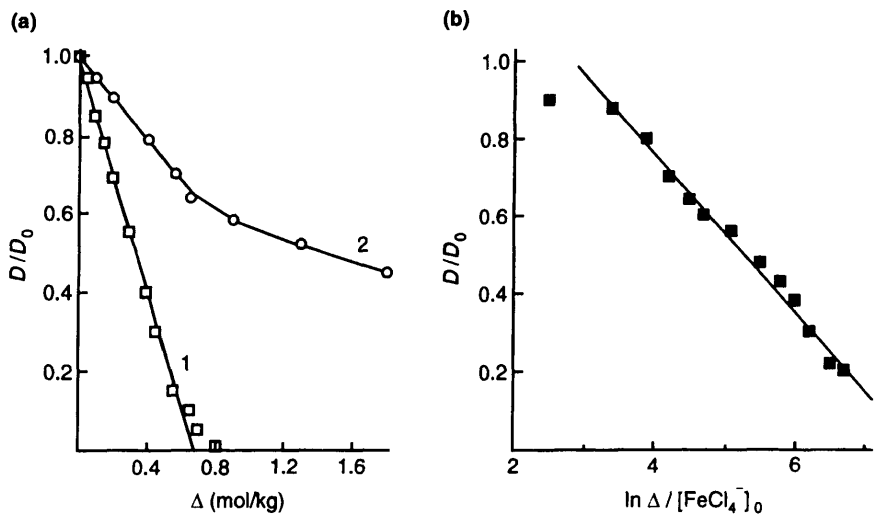

Figure 7.4 Kinetics of optical density change in polypropylene during iron chloride photoreduction: (a) in coordinates of equation (7.5): (1) 293 K; (2)77 K and (b) in coordinates of equation (7.20), 77 K.

in excess of that for the $FeCl_4^-$ photolysis in PMMA in similar conditions (Table 7.1). The process rate is noticeably retarded in polypropylene at 77 K. The Φ value becomes variable, and the kinetic curve takes on the appearance of the typical stepwise process. Limiting values of Φ_{max} and Φ_{min} were found to be 2×10^{-2} and 1.3×10^{-4}, $S_2 - S_1 = 5$ from approximation by equation (7.20) (Fig. 7.4b).

7.3. The effect of light energy on reactivity

The reactivity change under exposure to light has been displayed in studies of the photochemical exchange in chromium complexes [20, 21]:

$$[Cr(NH_3)_6]^{3+} \xrightarrow{h\nu, OH} [Cr(NH_3)_5OH]^{2+} + NH_3 \qquad (7.24)$$

The dependence of the conversion degree on the light dose was studied in an alkali solution at 88–168 K. The effective quantum yield appears to increase with a increasing temperature. This effect is caused by the partial restoration of the initial distribution in reactivity as the molecular mobility increases. The restoration of the distribution can be accounted for by both thermal and photochemical processes in the matrix. It was shown that the thermal change of a distribution took place only at $T > 170$ K. The reactivity change observed at $T < 170$ K is conditioned by a structural reorganization of the media under exposure to light. The light energy is scattered into the matrix when absorbed photons are photochemically inactive. This causes the molecular motions to increase in the vicinity of the particles.

The assumption that the surroundings become warmer as a result of light absorption has been made for sometime [22,23]. The additional mobility due to a part of the absorbed photon energy being dissipated into the matrix was detected during the trans–cis and cis–trans photoizomerization of azoethane in hydrocarbon glasses at 77 K [24]. These reactions proceed with quantum yields Φ_1 (trans–cis) and Φ_2 (cis–trans). The quantum yield of cis–trans isomerization depends on how the sample was prepared. If the solution containing cis-isomer was frozen, Φ_2 exceeded Φ_1 only slightly ($\Phi_1 = 0.28$, $\Phi_2 = 0.31$). If the cis-isomer was obtained by photolysis of the trans-isomer at 77 K and the quantum yield of cis–trans isomerization was determined, Φ_2^* turned out to be considerably larger than $\Phi_1 (\Phi_2^* = 0.7)$. Thus, the matrix 'remembered' the method of preparing the sample. To explain

this effect it should be assumed that the matrix molecules around the molecules which absorbed the photon, increase their mobility and facilitate stereoisomerization. The photon energy dissipation into the matrix may be described by the diffusion equation [25]:

$$\partial U/\partial t = (K/\rho S)^{1/2}\partial^2 U/\partial x^2, \tag{7.25}$$

where U is the photon energy, K is thermal conductivity, ρ is the specific gravity and S is the specific heat. The solution (7.25) is given as

$$U(r,t) = (\rho S)^{3/2}(4\pi Kt)^{-3/2}\exp(-\rho Sr^2/4Kt) \tag{7.26}$$

The unit volume at radius r and time t contains a fraction of energy $h\nu U(r,t)$. If this energy is distributed among the molecules within a volume element, one may consider the temperature T in that volume by the relation

$$h\nu U = kT/\nu, \tag{7.27}$$

where k is the Boltzmann constant and ν is the molecular volume.

The experimental evidence for energy transfer into the matrix in photochemical processes was given in [26] by the example of anthracene photo-oxidation in the polymer matrix. The non-photochemical action of light upon the anthracene molecules can be distinguished in this case if the oxygen is evacuated. Samples with O_2 were irradiated by UV light at room temperature. In this way the retardation of photo-oxidation was observed because of the disturbance of the reactivity distribution at the cost of consumption of the most active molecules. The samples were then evacuated and exposed to UV light. As a result of light irradiation during 50 minutes, the initial rate of further photo-oxidation is increased three-fold. The reactivity change takes place, apparently due to the relaxation ambient macromolecules in the electronic excitation transferring into the polymer matrix.

The availability of photorelaxation processes in polymers has been show in studies of the radical formation photoinitiated by dyes in PMMA at 77 K [27]. The kinetic curves of radical formation in films with dye additives during photolysis are shown in Fig. 7.5. As can be seen from the figure, the rate of radical formation decreases during exposure, therefore the faster, the 'softer' the light acting on samples. It was shown that the retardation in the kinetics of radical formation is

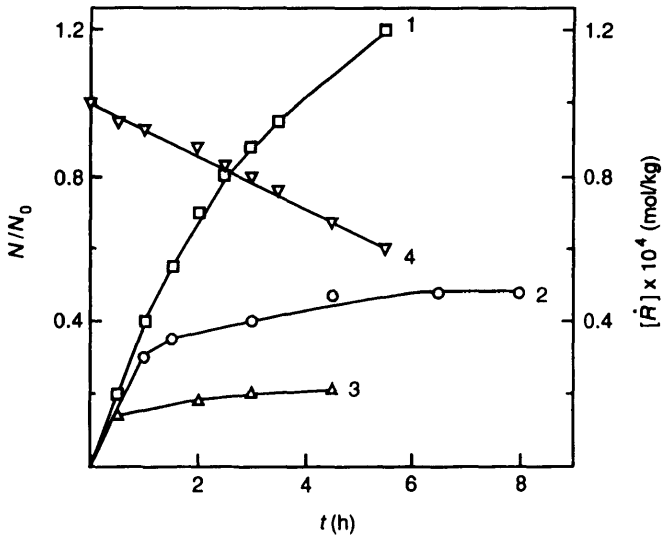

Figure 7.5 Kinetics of radical formation (1)–(3) and rodamine consumption (4) in PMMA at 77 K under exposure to light with $\lambda \geqslant 280$ (1) and (4); 340 (2); and 350 nm (3).

not connected with radical decay under the action of light and may be explained by inequivalence of the dye molecules in relation to their radical photoinitiation. However, the dye concentration decreases in the course of photodecomposition with a constant rate in the same time (Fig. 7.5 (4)). Consequently, to describe the decrease in rate of the radical photoinitiation, the concept of a dynamic model of the kinetic inequivalence needs to be used. This model presumes a reactivity change under the action of light in the course of the photoprocess.

7.4 The kinetics of photoradical chains

One feature of photochemical reactions in solids is the possibility of their proceeding by a chain mechanism. This phenomenon was first revealed by studies of the H_2O_2 low-temperature photolysis in ethanol [28]. The total quantity of gaseous products (CO, CH_4, H_2) which comprise photolysis account for 2.9×10^{18} molecules, while the stationary quantity of radicals in the matrix comes to only 4.5×10^{16}.

The phenomenon of photoradical chains is due to the fact that the reactions

$$R_1 \xrightarrow{h\nu} M_1 + R_2 \tag{7.28}$$

$$R_2 + M_0 \rightarrow M_2 + R_1 \tag{7.29}$$

are repeated when the light acts only upon radicals generated in the solid phase, for instance, by γ-irradiation. These reactions lead to the decomposition of molecules M_0 of the original substance in amounts much greater than the initial concentration of radicals R_1. The photoradical chains play an important role on the photo-ageing of polymers giving rise to macromolecular destruction, cross-linking and the formation of low-molecular products. To date extensive studies of the mechanism and kinetics of photoradical degradation have been performed in a wide range of carbo- and hetero-chain polymers: polytetrafluorethylene [29], polyvinyl alcohol [30], polyethylene [31], polyacrylic acid and polyacrylamide [32]. Free radicals are stable as a rule at 77 K in the absence of light. Hence, their decay under irradiation by light and the chain termination is intimately associated with reactions of the chain propagation. In response to one cycle (7.28,7.29) the transfer of a free valence occurs over an intermolecular distance, if R_1 and R_2 are comparably sized. The valence transfer at low temperatures over large distances is realized evidently then R_2 represents a light radical or atom [31].

The kinetic analysis of the radical decay owing to the transfer initiated by external action has been carried out by the method of statistical tests (Monte-Carlo) [33,34]. The initial distribution of radicals is assumed to be in the form of radical pairs with an average distance R_0 between radicals. The recombination radius and distance of the elementary transfer of radicals are consequently defined as r and l. The arbitrary values of R_0 and r are chosen so that in the probable range their reasonable values would overlap: $1 \leqslant R_0 \leqslant 5$, $0.4 \leqslant r \leqslant 2.5$, $l = 1.0$. The initial number of pairs N_0 is 500, the total number tests of $n > 2000$. The initial rate of decay is dependent on R_0 and r. With the proviso that $r + l > R_0$, the probability of pair decay is given by the equation

$$P = [r^2 - (R_0 - e)^2]/4R_0 l \tag{7.30}$$

The kinetics of the radical decay depend significantly on the distribution of pairs at that moment; the time here is the number

of tests. The most probable average distance in pairs can be represented as

$$\bar{R} = (R_0^2 + l^2 n/N_0)^{1/2} \tag{7.31}$$

The estimation of the recombination radius and the distance of the free valence transfer gives, for isopropanol radicals $r = 0.65$ nm, $l = 0.3$–0.4 nm [33]. The higher values of r and l were obtained for photoradical processes in polyacrylic acid (2.2 nm and 1.5 nm) and polyacrylamide (1.7 nm and 1 nm). This fact may be explained by the involvement of light radicals (OH, NH_2) in the free valence transfer [32].

The kinetics of photoradical processes depend on the radical phototransformation mechanism defining the propagation chain stage. This process in polyethylene occurs because of the breaking of the C–H bond photosensitized by macroradicals [31]:

$$\begin{aligned} &\sim CH_2C^{\cdot}HCH_2 \sim \xrightarrow{k\nu} \sim CH_2CH = CHCH_2 \sim + H \\ &\sim CH_2CH_2CH_2 \sim + H \longrightarrow \sim CH_2C^{\cdot}HCH_2 \sim + H_2 \qquad (7.32) \\ &\sim CH_2C^{\cdot}HCH_2 \sim + \sim CH_2CH_2CH_2 \end{aligned}$$

$$\sim \xrightarrow{h\nu} \begin{matrix} \sim CH_2\dot{C}HCH_2 \sim \\ \sim CH_2\dot{C}HCH_2 \sim \end{matrix} + H \tag{7.33}$$

The kinetics of the photorecombination of macroradicals in polyethylene obeys the second-order equation:

$$-d[R]/dt = [R]^2 \frac{2}{3}\pi l^3(\varphi_1 + \varphi_2) \int_{\lambda_{min}}^{\lambda_{max}} \varepsilon(\lambda) I(\lambda) d\lambda, \tag{7.34}$$

where $\varepsilon(\lambda)$ is the extinction coefficient of radicals, $I(\lambda)$ is the light intensity, φ_1 and φ_2 are the quantum yields of the hydrogen atom generation in reactions (7.32) and (7.33). The chain length of photoradical reactions ν is equal to the ratio of the rates of the propagation and termination stages. The rate of the photoradical chain propagation is determined by the rate of molecular hydrogen formation:

$$d[H_2]/dt = [R](\varphi_1 + \varphi_2) \int_{\lambda_{min}}^{\lambda_{max}} \varepsilon(\lambda) I(\lambda) d\lambda \tag{7.35}$$

Then the chain length is

$$\nu = \frac{3}{2\pi l^3 [R]} \tag{7.36}$$

The average sweep of a hydrogen atom in polyethylene estimated by equation (7.36) is 1.2 nm at $\nu \approx 33$.

Photoradical chains evolve in the neighbourhood of an initial radical. In connection with this, the size of the reaction zone (L) may be determined by the average distance of the displacement of free valence and the chain length: $L = l\sqrt{\nu}$. The products of photoradical reactions will therefore be distributed non-uniformly in the matrix. Thus, the irradiation of macroradicals in polyethylene by UV light can create a matrix zone of 4 nm in diameter where double bonds and cross-linkages resulting from reactions (7.32) and (7.33) are grouped. The local concentrations of products can be two to five times greater than those averaged. Such a non-uniform distribution of products of the radical reactions may drastically change the polymeric material properties, in particular, the mechanical strength.

Chain photoradical reactions provide additional possibilities for investigating the kinetic peculiarities of the solid phase reactions. They can be used as an efficient method for determining the distribution of radicals in their reactivity. The monitoring of the spatial distribution of radicals and the determination of parameters characterizing the efficiency of radical migrations permit an understanding of the mechanism for the influence of solid media on the kinetics of chemical reactions.

References

1. Frank J. and Rabinovitch E. (1934) *Trans. Faraday Soc.*, **30**, 120.
2. Meadows L.F. and Noyes R.M. (1960) *J. Am. Chem. Soc.*, **82**, 1872.
3. Booth D. and Noyes R.M. (1960) *J. Am. Chem. Soc.*, **82**, 1868.
4. Gurman V.S. and Pergushov V.I. (1981) *Chem. Phys.*, **55**, 131.
5. Cohen M.H. and Turnball D. (1959) *J. Chem. Phys.*, **31**, 1164.
6. Doolittle A.K. (1951) *J. Appl. Phys.*, **22**, 1471.
7. Mel'nikov M.Ya. (1982) *Chem. Phys. Lett*, **86**, 105.
8. Pergushov V.I. and Gurman V.S. (1981) *Doklady Akad. Nauk SSSR*, **259**, 163.
9. Anisimov V.M. and Karpukhin O.N. (1973) *Izv. Akad. Nauk SSSR*, 1914.
10. Anisimov V.M., Karpukhin O.N. and Mattuchi A.M. (1974) *Doklady Akad. Nauk SSSR*, **214**, 828.
11. Karpukhin O.N. (1978) *Uspekhi Khimii*, **47**, 1119.
12. Bystritskaya E.V. and Karpukhin O.N. (1975) *Doklady Akad. Nauk SSSR*, **221**, 1100.

13. Karpukhin O.N. and Kutcenova A.V. (1977) *Vysokomolek. Soed.*, **A19**, 1047.
14. Ranby R. and Rabek J.F. (1975) *Photodegradation, photooxidation and photostabilization of polymers*, London, New York, Sydney, Toronto: John Wiley & Sons, p. 35.
15. Zaitceva N.I., Poholok T.V., Pariyskii G.B. and Toptygin D.Ya (1976) *Doklady Akad. Nauk SSSR*, **229**, 906.
16. Poholok T.V., Zaitceva N.I., Pariyskii G.B. and Toptygin D.Ya. (1977) *Vysokomolek. Soed.*, **A19**, 2049.
17. Poholok T.V., Zaitceva N.I., Pariyskii G.B. and Toptygin D.Ya. (1980) *Vysokomolek. Soed.*, **A22**, 196.
18. Poholok T.V., Zaitceva N.I., Pariyskii G.B. and Toptygin D.Ya. (1982) *Vysokomolek. Soed.*, **A24**, 349.
19. Gamlen G.A. and Jordan D.O. (1953) *J. Chem. Soc.*, 1435.
20. Vorob'ev A.Kh. and Gurman V.S. (1979) *Kinetika i Kataliz*, **20**, 1439.
21. Vorob'ev A.Kh. and Gurman V.S. (1980) *Doklady Akad. Nauk SSSR*, **253**, 138.
22. Albrecht A.C. (1957) *J. Chem. Phys.*, **27**, 1413.
23. Albrecht A.C. (1961) *J. Molec. Spectrosc.*, **6**, 84.
24. Pergushov V.I., Bormot'ko O.N. and Gurman V.S. (1977) *Chem. Phys. Lett.*, **51**, 269.
25. Shida T. (1978) *J. Phys. Chem.*, **82**, 991.
26. Rumyantceva Yu.I., Anisimov V.M., Zhbankov R.G. and Karpukhin O.N. (1983) *Izv. Akad. Nauk SSSR, ser. Khimich.*, 935.
27. Mardaleishvili I.R., Davydov E.Ya. and Anisimov V.M. (1989) *Vysokomolek. Soed.*, **A31**, 27.
28. Shelimov B.N., Fok N.V. and Voevodskii V.V. (1964) *Kinetika i Kataliz*, **5**, 1008.
29. Klinshpont E.R. and Milinchuk V.K. (1973) *Vysokomolek. Soed.*, **B15**, 332.
30. Chervonenko V.S. and Pshezhetsky S.Ya. (1977) *Vysokomolek. Soed.*, **B19**, 783.
31. Vasilenko V.V., Klinshpont E.R., Milinchuk V.K. and Isakov L.I. (1980) *Vysokomolek. Soed.*, **A22**, 1770.
32. Seropegina E.N., Fok N.V. and Mel'nikov M.Ya. (1987) *Doklady Akad. Nauk SSSR*, **293**, 399.
33. Pergushov D.V. (1991) *Khimich. Fizika*, **10**, 1612.
34. Pergushov V.I. and Korol'kova M.L. (1992) *Khimich. Fizika*, **11**, 365.

KINETIC PECULIARITIES OF SOLID PHASE REACTIONS

E. Ya. Davydov, A. P. Vorotnikov, G. B. Pariyskii and **G. E. Zaikov**
N. M. Emanuel Institute of Biochemical Physics, Russian Academy of Sciences, Moscow, Russia

Much data has been collected from experiments on the kinetics of radical reactions in different solids, but to date, this has not been presented in book format in a thorough and comprehensive way. This book makes the experimental data accessible for all chemists involved in these reactions.

Various models of the tunnel atom transfer are analyzed in order to explain the kinetic isotope effect in solid phase reactions and photoinitiated radical reactions are inspected for the kinetic non-equivalence of particles and factors affecting their reactivity.

Topics covered include:

- kinetic description of reactions with dispersion particles in reactivity
- the influence of space-orientation factors on reactivity in cage reactions
- the influence of molecular dynamics on the kinetics of elementary reactions
- the effect of structural-physical modification on kinetics of cage radical reactions

ISBN 0-471-98374-8
9 780471 983743

JOHN WILEY & SONS
Chichester · New York · Weinheim · Brisbane · Singapore · Toronto